CHARACTERIZATION OF EPITAXIALLY GROWN III-V NANOSTRUCTURES BY ELECTRON MICROSCOPY

Yusuf Eren Suyolcu

Master of Science Thesis

Advanced Technologies Program - Nanotechnology

January 2014

This thesis study was supported in part by The Scientific and Technological Research Council of Turkey (TUBITAK) under the Grant No. 111T335 and by Anadolu University Scientific Research Projects under the project BAP-1205F083.

ANADOLU ÜNİVERSİTESİ

JÜRİ VE ENSTİTÜ ONAYI

Yusuf Eren SUYOLCU'nun **"Characterization of Epitaxially Grown III-V Nanostructures by Electron Microscopy"** başlıklı **İleri Teknolojiler** Anabilim Dalı **Nanoteknoloji** Bilim Dalındaki, Yüksek Lisans Tezi 19.12.2013 tarihinde, aşağıdaki jüri tarafından Anadolu Üniversitesi Lisansüstü Eğitim-Öğretim ve Sınav Yönetmeliğinin ilgili maddeleri uyarınca değerlendirilerek kabul edilmiştir.

	Adı-Soyadı	**İmza**
Üye (Tez Danışmanı)	**: Doç. Dr. Bülent Aslan**	………………
Üye	**: Doç. Dr. Uğur Serincan**	………………
Üye	**: Yard. Doç. Dr. Hilmi Yurdakul**	………………

Anadolu Üniversitesi Fen Bilimleri Enstitüsü Yönetim Kurulu'nun ……………… tarih ve ………… sayılı kararıyla onaylanmıştır.

Enstitü Müdürü

ANADOLU ÜNİVERSİTESİ

ÖZET

Yüksek Lisans Tezi

EPİTAKSİYEL OLARAK BÜYÜTÜLEN III-V NANOYAPILARIN ELEKTRON MİKROSKOPİ İLE KARAKTERİZASYONU

Yusuf Eren SUYOLCU

Anadolu Üniversitesi

Fen Bilimleri Enstitüsü

İleri Teknolojiler Programı – Nanoteknoloji

Danışman: Doç. Dr. Bülent ASLAN

İkinci Danışman: Prof. Dr. Servet TURAN

2014, 106 sayfa

Epitaksiyel olarak büyütülen III-V grubu yarıiletken nanoyapılar elektron mikroskopi teknikleri ile araştırılmıştır. Özellikle, kızılötesi fotoalgılayıcı olarak tasarlanan InAs/GaSb tip-II süperörgü (SL) ve kendiliğinden oluşan InAs/GaAs kuantum nokta (QD) yapılar taramalı elektron mikroskobu (SEM), geçirimli elektron mikroskobu (TEM) ve taramalı geçirimli elektron mikroskobu (STEM) ile incelenmiştir. Bu çalışmada kullanılan yapılar, moleküler demet epitaksi (MBE) ile büyütülmüş ve tabaka kalınlıkları, arayüz özellikleri, yüzey kaliteleri gibi yapısal özellikleri ve bileşimsel özellikleri bakımından kapsamlı olarak karakterize edilmiştir. Aynı görüntüleme teknikleri GaSb epikatmanların yüzey karakterizasyonu ve AlSb kuantum noktaların gözlenmesi için de kullanılmıştır. Elde edilen sonuçlar, farklı koşullar altında büyütülen epikatmanların yüzeylerinde görülen istenmeyen özelliklerin ve kusurların uygun eylemler uygulandığında önlenebileceğini göstermiştir. Ayrıca, bu çalışmanın önemli bir kısmı çalışılan malzeme sistemleri için etkin, tekrarlanabilir ve güvenilir bir yan-kesit numune hazırlama reçetesi geliştirilmesine adanmıştır.

Anahtar Kelimeler: III-V nanoyapılar, MBE, Yan kesit numune hazırlama, TEM, STEM, SEM

ANADOLU ÜNİVERSİTESİ

ABSTRACT

Master of Science Thesis

CHARACTERIZATION OF EPITAXIALLY GROWN III-V NANOSTRUCTURES BY ELECTRON MICROSCOPY

Yusuf Eren SUYOLCU

Anadolu University

Graduate School of Science

Advanced Technologies Program – Nanotechnology

Supervisor: Assoc. Prof. Dr. Bülent ASLAN

Co-Supervisor: Prof. Dr. Servet TURAN

2014, 106 pages

Epitaxially grown III-V group semiconductor nanostructures have been investigated by means of electron microscopy techniques. Particularly, InAs/GaSb type-II superlattice (SL) structures designed as infrared photodetector and InAs/GaAs self-assembled quantum dots (QDs) have been analysed by scanning electron microscopy (SEM), transmission electron microscopy (TEM) and scanning transmission electron microscopy (STEM) techniques. Structures used in this study were grown by molecular beam epitaxy (MBE) and extensively characterized for their structural properties such as layer thicknesses, interface properties, surface qualities and compositional properties. The same imaging techniques have also been used for surface characterization of GaSb epilayers and observation of both InAs and AlSb QDs. The acquired results have shown that undesired features and defects evidenced on the surfaces of the epilayers grown under different conditions can be avoided once proper actions are taken. Also, a significant amount of work in this study has been devoted to develop an effective, reproducible and reliable cross-section sample preparation recipe for the studied material systems.

Keywords: III-V nanostructures, MBE, Cross-section Sample Preparation, TEM, STEM, SEM

ANADOLU ÜNİVERSİTESİ

ACKNOWLEDGMENTS

I would like to thank to my dignified supervisor Assoc. Prof. Dr. Bulent Aslan for his guidance and valuable supports since 2010. His kindness, goodwill and respectability will always be remembered with pleasure. I would also like to thank him for his enthusiastic support as a friend.

I also would like to thank my co-supervisor Prof. Dr. Servet Turan for his guidance, experienced approach and suggestions and also fatherly behaviours.

I really appreciate my honorary advisor Assoc. Prof. Dr. Uğur Serincan, not only for his guidance but also his sincerity and friendly behaviours.

Nanoboyut Research Laboratory family: Bülent Arıkan, Burcu Arpapay, Güven Korkmaz, Ayşe Şevik, Seval Şahin, Mehmet Erkuş, Melih Korkmaz and Serkan Ulukut from Electron Microscopy Group: Thank you all for your sharing and friendship. Tuğçe Karakulak; thank you very much for your help at the beginning of this journey. And… The Oscar goes to Pınar Kaya… If she was not there, everything would be more difficult, more unpleasant and also more insufferable. Thank you for everything…

Special thanks to my flatmates, my friends, my brothers; Emin Yagcıoğlu, Ö. Faruk Erol, T. Efe Turan and Samet Özdemir; "just" for everything.

Finally, I would like to thank my family for supporting me in all circumstances. My father was always behind me, my mother was always with me and my sister was always close to me. Without them and their support without expecting anything in return, I would not have had opportunity to perform this study.

Y. Eren Suyolcu

January, 2014

ANADOLU ÜNİVERSİTESİ

TABLE OF CONTENTS

Page

ÖZET i
ABSTRACT ii
ACKNOWLEDGMENTS iii
TABLE OF CONTENTS iv
LIST OF FIGURES vi
LIST OF TABLES xi
LIST OF ABBREVIATIONS xii

1. INTRODUCTION **1**

2. III-V GROUP NANOSTRUCTURES **4**
2.1. InAs/GaSb Type-II Superlattices 5
2.1.1. 6.1 Å Family and Their Band Alignments 5
2.1.2. Effect of the Layer Thicknesses 8
2.2. InAs/GaAs Self-assembled Quantum Dots 10
2.3. Aim of the Study 12

3. EXPERIMENTAL PROCEDURES **14**
3.1. MBE Grown Structures 14
3.2. Sample Preparation for Transmission Electron Microscopy 16
3.3. Sample Preparation for Scanning Electron Microscopy 24
3.4. SEM, TEM and STEM Investigations 25

4. RESULTS & DISCUSSION **30**
4.1. Thickness Determination by Scanning Electron Microscopy 30
4.2. Characterization of GaSb Epilayers 35
4.2.1. Surface Characterization with Scanning Electron Microscopy 36

ANADOLU ÜNİVERSİTESİ

4.2.2. Back scattered Electron Imaging & EDX Line Analyses 43
4.3. Characterization of InAs/GaSb Type-II Superlattices 50
4.3.1. Optimization of Sample Preparation Method for TEM.................50
4.3.2. TEM-BF Imaging 55
4.3.3. HRTEM Imaging...62
4.3.4. STEM – HAADF Imaging 67
4.3.5. STEM – EDX Analyses 70
4.3.6. EFTEM Study 76
4.4. Investigation of GaSb Epilayer on GaAs substrate................ 78
4.5. Observation of InAs Self-assembled Quantum Dots on/in GaAs.............83
4.5.1. Surface Characterization with Scanning Electron Microscopy.. .84
4.5.2. TEM-BF and HRTEM Imaging...90
4.5.3. STEM Imaging... 93

5. CONCLUSION 97

REFERENCES 100

ANADOLU ÜNİVERSİTESİ

LIST OF FIGURES

Page

2.1 III-V group semiconductors and their compounds 4
2.2 The energy gap versus the lattice constant of InAs, GaSb, and AlSb compared with other semiconductors (left) and InAs, GaSb, and AlSb energy band lineups (right) 6
2.3 Schematic illustration of the energy band alignment in the nearly lattice-matched InAs/GaSb/AlSb material system 7
2.4 Schematic illustration of an InAs/Ga(In)Sb type-II broken-gap superlattice. 8
2.5 Effect of the GaSb barrier on the CB level. Thin GaSb layer results to a stronger wavefunction overlap 9
2.6 An illustration of the broadening of the CB as a function of GaSb thickness 10
2.7 Illustration of different growth modes: (a) 2 dimensional layer-by-layer growth: Frank-van der Merwe, (b) island growth in 3 dimension: Volmer-Weber, (c) 3 dimensional island growth following layer-by layer growth: Stranski-Krastanov 11
3.1 A schematic representation of the first step in cross-section sample preparation. Images of b) cleaved and c) glued pieces 18
3.2 The views of the sample (a) before and (b) after slicing. (c) One of the slices picked up for later steps. 19
3.3 The cutting process with ultrasonic disc cutter: sample gets 3mm disc after the operation. (a) Disc cutter, (b) during the operation, (c) sample after the operation. 20
3.4 The view of a) the disc grinder and b) the specimen on the holder after polishing 21
3.5 The view of the specimen after gluing copper grid. The surface of the sample seen in the figure is the polished side 22

ANADOLU ÜNİVERSİTESİ

Page

3.6 The view of a) the dimpling machine and the specimen on the holder b) before and c) after dimpling. 23

3.7 The schematic representation of a standard dimpled TEM sample from the crosssection. Blue arrows show the direct Ar beam onto the sample and red arrows show the shadowed edges. 23

3.8 Electron – atom interactions: SEM (left) and TEM (right) 25

3.9 The signals and the techniques in which they are used 26

3.10 An illustration of HRTEM image formation 27

3.11 An illustration of STEM detectors....................28

4.1 The cross-section images of a) YES-01 and b) YES-02 32

4.2 The cross-section images of a) YES-03 b) YES-04 and c) YES-05 34

4.3 The surface images of the samples a) YES-06, b) YES-07 and c) YES-08 grown with different Sb fluxes. The images were taken in the same magnification for easy comparison 37

4.4 The surface imagess of the samples with different types of defects: a) YES-09, b) YES-10, and c) YES-11 38

4.5 The surface images of sample YES-14 taken with a) SE detector b) in-lens detector 41

4.6 An image of the region between etched and unetched surface of sample YES-07 taken with in-lens detector. Two parts are zoomed into show the image quality 42

4.7 An image taken to reveal the difference between in-lens (upper half) and SE (lower half) detectors (YES-12)… 43

4.8 The back scattered images of samples a) YES-13, b) YES-06, c) YES-11 44

4.9 SEM-EDX line analysis results of YES-13 46

4.10 SEM-EDX line analysis results of YES-06 47

4.11 SEM-EDX line analysis results of YES-11 48

4.12 The ratio of the Sb signal to Ga signal for the samples YES-13, YES-06 and YES-11. 49

4.13 TEM images taken from a) improperly and b) properly prepared samples from type-II SL structure. 51

ANADOLU ÜNİVERSİTESİ

4.14 The images of thicker (left) and thinner (right) samples after ultrasonic disc cutting Thicker sample was not cut while the thinner sample was cracked during the process.. 52
4.15 Example images of a) a sample with epoxy spread, and (b) a successively glued sample onto the copper grid. The red arrow in (a) indicates the clear opening where there is no epoxy 53
4.16 Samples with different dimple radius. Processes were performed with different weights: a) 37 g b) 32 g c) 27 g d) 22 g 54
4.17 The latest improved specimen preparation stages 55
4.18 TEM-BF images of the sample YES-16 at a) lower and b) higher magnifications. 56
4.19 TEM-BF images of the sample YES-15 at a) lower and b) higher magnifications 57
4.20 TEM-BF images of the sample YES-17 at a) lower and b) higher magnifications 58
4.21 TEM-BF images of the sample YES-17 at a) lower and b) higher magnifications 59
4.22 Linear defects on a) upper piece and b) lower piece of InAs/GaSb SL (YES-18). The red arrows show the linear defects 61
4.23 The HRTEM images of the samples a) YES-16 and b) YES-15. 63
4.24 The HRTEM images of the samples a) YES-17 and b) YES-18 64
4.25 High resolution x-ray rocking curve around GaSb (004) of InAs/GaSb superlattice structure. 66
4.26 HRTEM images processed with Wiener filtering with variable noise reduction ratios: (a) no filtering, (b) 3X, (c) 6X, (d) 10X 67
4.27 STEM-HAADF images of samples a) YES-16 and b) YES-15.. 68
4.28 STEM-HAADF images of samples a) YES-17 and b) YES-18 69
4.29 STEM-EDX line analysis spectras of a) YES-16 b) YES-15 c) YES-17 d) YES-18 71
4.30 STEM-EDX Line analysis spectra of the sample YES-16 72
4.31 STEM-EDX Line analysis spectra of the sample YES-15 72
4.32 STEM-EDX Line analysis spectra of the sample YES-17 73

ANADOLU ÜNİVERSİTESİ

4.33 STEM-EDX Line analysis spectra of the sample YES-18 73
4.34 STEM-HAADF image of sample YES-17. STEM-EDX spot analyses were performed at the indicated points (YES-17) 74
4.35 STEM-EDX point analyses spectras of Point 1 (top) and Point 2 (bottom) 75
4.36 Three window elemental maps: a) the map of Sb M4,5 edge with 527 eV energy loss, b) the map of In M4,5 edge with 443.1 eV energy loss In c) the unified map of both In and Sb elements 77
4.37 TEM-BF images of AlSb QDs with two different magnifications. 79
4.38 HRTEM images of AlSb QDs at different magnifications. 80
4.39 STEM-HAADF image of sample YES-19: GaSb epilayer grown on GaAs substrate...81
4.40 STEM-EDX spectra of sample YES-19: GaSb epilayer grown on GaAs substrate...82
4.41 STEM-EDX line analysis of sample YES-19: GaSb epilayer grown on GaAs substrate..82
4.42 The surface images of sample YES-19 taken with in-lens detector. No clear defects observed. 83
4.43 Secondary electron image of sample YES-21 85
4.44 Image of sample YES-21 taken with in-lens detector 85
4.45 SEM images of a) YES-20, b) YES-21, c) YES-22, d) YES-23, e) YES-24 samples 86
4.46 SEM image of InAs QDs (YES-22) 89
4.47 TEM-BF image of sample YES-22. The white arrow indicates the out of focus, the black arrow shows the space between the sample and the epoxy, and the red arrows indicate the location of the buried QDs. 90
4.48 TEM-BF image of sample YES-22 showing four uncapped surface QDs 91
4.49 Cross sectional HRTEM image shows two uncapped surface InAs QDs (YES-22) 92
4.50 Cross sectional HRTEM image of an InAs QD (YES-22). The red arrows indicate the strain field caused by the irregularity of atomic packing...93

ANADOLU ÜNİVERSİTESİ

4.51 a) STEM-BF and b) STEM-ADF images of InAs QDs (YES-22). 94
4.52 a) STEM-BF and b) STEM-ADF images of InAs QDs. The red arrows show the QDs. 95

ANADOLU ÜNİVERSİTESİ

LIST OF TABLES

Page

Table 3.1 List of samples used in this study..15
Table 4.1 Targeted and measured thicknesses of InAs1-xSbx epilayers grown on GaSb substrates … 33
Table 4.2 Measured FWHM values of sample YES-06 and YES-11 ………. ..50
Table 4.3 The results of high resolution x-ray rocking curve analysis for each sample…………… 66
Table 4.4 Quantitative results of STEM-EDX point analyses from the sample YES-17 75
Table 4.5 Number of QDs per area extracted from the images..........................89

ANADOLU ÜNİVERSİTESİ

LIST OF ABBREVIATIONS

ADF : Annular Dark Field

AlSb : Aluminium Antimonide

AlGaAs : Aluminium Gallium Arsenide

AlGaN : Aluminium Gallium Nitride

AlGaAsSb : Aluminium Gallium Arsenide Antimonide

As : Arsenic

BF : Bright Field

BS : Back Scattered

CB : Conduction Band

Cu : Copper

EBSD : Electron Back Scattered Diffraction

EDS : Energy Dispersive Spectrometer

EDX : Energy Dispersive X-ray

EFTEM : Energy Filtering Transmission Electron Microscope

EELS : Electron Energy Loss Spectrometer

FEG : Field Emission Gun

Ga : Gallium

GaAs : Gallium Arsenide

GaSb : Gallium Antimonide

GaInAsSb : Gallium Indium Arsenide Antimonide

HAADF : High Angle Annular Dark Field

HRTEM : High Resolution Transmission Electron Microscopy

In : Indium

ANADOLU ÜNİVERSİTESİ

InAs : Indium Arsenide

InAsSb : Indium Arsenide Antimonide

LPE : Liquid Phase Epitaxy

MBE : Molecular Beam Epitaxy

ML : Monolayer

N : Nitrogen

P : Phosphorus

QD : Quantum Dot

SE : Secondary Electron

SEM : Scanning Electron Microscopy

SK : Stranski-Krastanov

SL : Superlattice

STEM : Scanning Transmission Electron Microscopy

TEM : Transmission Electron Microscopy

VLM : Visible Light Microscope

ANADOLU ÜNİVERSİTESİ

1. INTRODUCTION

The III-V group semiconductors are the compounds of group III and group V elements [1, 2]. These material systems have important characteristics that are suitable for many high-speed electronic and optoelectronic applications especially in medical field, military services, telecommunications, and automatic control systems. Realization of their compounds (binary, ternary or quaternary etc.) for device applications, mostly require epitaxial growth techniques such as molecular beam epitaxy (MBE) [3, 4]. The same material system can easily be designed/used for variety of optoelectronic devices such as light emitting diodes, lasers, photovoltaic cells, photodetectors, and charged coupled imaging devices by simply changing the order and the thicknesses of the layers. The MBE grown III-V nanostructures designed particularly for infrared detection are of great importance in recent years' technologies. Among those InAs/GaSb superlattices [5] and InAs/GaAs quantum dots [6, 7] have attracted a lot of interest because of their anticipated advantages. Superlattices are periodic structures of very thin layers of the order of 2-3 nm and quantum dots are disc shaped lumps of ~2 nm in height and ~20 nm in diameter in average. These structures can therefore only be investigated directly by electron microscopy techniques and that constitutes the main framework of this thesis.

InAs/GaSb based type-II SL structures are formed by the multiple repetitions of consecutive InAs and GaSb layers. These structures are mainly used for detecting infrared light in a wide range (3-30 μm) due to their bandgap tunability [8]. Many years after it is first proposed [9], InAs/GaSb type-II SLs have become a very promising material system for the third generation infrared detector technology [10-13] whose application areas have been increasing steadily. Even though the lattice parameters of InAs (6.0585 Å) and GaSb (6.0959 Å) are very close to each other, their consecutive growth as thin layers causes strain accumulation in the entire structure. This may then lead to misfit dislocations and defect formation in the structure especially when the number of the repeat (i.e. period number) is big. Fortunately, the lattice mismatch can be minimized by

ANADOLU ÜNİVERSİTESİ

engineering the interfaces between InAs and GaSb layers which is known to have a profound effect on the device performance [14-16]. To minimize the stress formation in the structure, a layer of different material consisting of the same atoms such as GaAs and InSb is intentionally introduced as an interface between InAs and GaSb layers [8, 17]. The thickness of such interface layers are in the order of 0-1 monolayer (ML). It is particularly known that the use of InSb at InAs-GaSb transition improves not only the crystal quality of the SL but also the device performance [8, 20-22].

Self-assembled InAs QDs in the GaAs matrix is the most widely studied material system in QD structures. Because of the ~7% lattice mismatch between InAs and GaAs (6.0584 Å and 5.65325 Å, respectively) crystals [23] after a critical thickness is reached the InAs crystal relaxes and aggregates to form lumps called *quantum dots*. These QDs confine electrons in three dimensions at discrete the energy levels within the dot as in the case of real atoms [6, 24]. QDs are very versatile in their properties by nature; their size, shape, density, strain and material compositions can be controlled and changed for their expediency. Changes in all these parameters modify the energy spacing between bound energy levels and therefore it is possible to obtain a very broad range of operating spectra [24].

The characterization of these semiconductor nanostructures by using electron microscopy techniques is of vital importance. Since the defects in the crystal, individual layer thicknesses, and intermixing at the interfaces are crucial especially for InAs/GaSb type-II SL structures, the following electron microscopy techniques are used for their characterizations: (i) transmission electron microscopy bright field (TEM-BF) imaging technique – to examine the microstructure and the structural quality [18, 25-27] (ii) high resolution transmission electron microscopy (HRTEM) – to investigate the layer thicknesses, to examine the packing of atoms at the interfaces and to confirm the structural quality [28-33] and (iii) scanning transmission electron microscopy (STEM) [34-38] – to distinguish the compositional differences between the layers. STEM imaging techniques are of great significance particularly for the observation of the

ANADOLU ÜNİVERSİTESİ

buried QDs [39-41] with favour on the contrast in the images when compared to TEM imaging techniques [42].

It is also known that the epitaxial growth of high quality electronic and optoelectronic devices requires the use of high quality substrates and an atomically smooth, defect-free buffer layers. High quality buffer layers are necessary to separate device layers from the substrate surface where parasitic electron gases can form [43]. They also remove the impurities, smooth the growth surface for subsequent device layers, and reduce macroscopic defect densities that can for example reduce the yield of arrays of devices [43]. Surface morphology is therefore a critical first-pass consideration of epi-wafer quality. Any anomalies resulting from the GaSb substrate quality or from the growth process will generate rough surfaces and/or high defect densities that can in turn degrade the fabricated devices' Figures of merit parameters [44]. On the other hand, the use of GaAs substrates as an alternative to lattice matched GaSb substrates is a common practice to grow type-II superlattice structures on GaAs substrates [45]. Their good crystal qualities and less expensive prices have created a persistent demand [17]; however, the large lattice mismatch (~7%) between the substrate and the layer increases the possibility of having high defect densities due to rather difficult growth conditions. Since the defects can also appear on the surface, it is also important to investigate the surfaces especially after the growth of a buffer layer. One possible method for surface analyses is to use a scanning electron microscope and its capabilities.

This thesis is mainly focuses on the characterization of the MBE grown III-V nanostructures by different electron microscopy techniques. This chapter is intended to draw a general picture about the subject. In the second chapter, the development and the physics of the studied nanostructures are briefly given. In chapter 3, MBE grown structures, sample preparation methods for electron microscopy and the electron microscopy techniques are discussed. The following chapter (chapter 4) is dedicated to the experimental results and discussions. Finally, the conclusion is presented in chapter 5.

ANADOLU ÜNİVERSİTESİ

2. III-V GROUP NANOSTRUCTURES

The III-V group semiconductors are the compounds of group III and group V elements of the periodic table. As illustrated in Figure 2.1, group III elements are indium (In), gallium (Ga), aluminium (Al) and group V elements are nitrogen (N), arsenic (As), phosphorus (P) and antimony (Sb). Their binary, ternary and quaternary compounds such as InAs, GaAs, GaSb, AlGaAs, AlGaN, InAsSb, AlGaAsSb, GaInAsSb are some common III-V semiconductors [1, 2].

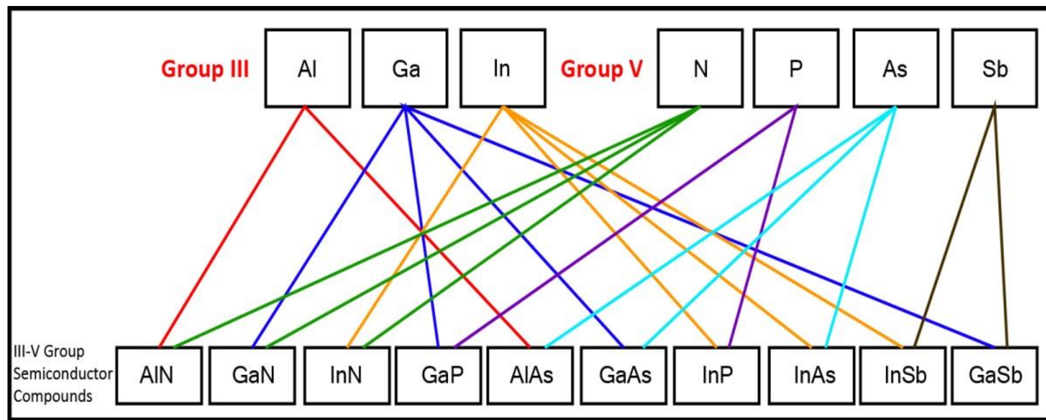

Figure 2.1 III-V group semiconductors and their compounds [2]

The III–V group semiconductor systems are potentially of great importance for many high speed electronic and optoelectronic devices and mostly require epitaxial growth techniques such as liquid phase epitaxy (LPE) and MBE. Demonstrations of a continuous wave laser diode operated at room temperature and a high electron mobility transistor from GaAs/$Al_xGa_{1-x}As$ heterostructures grown by LPE and MBE, respectively, are just the two examples showing the importance of III-V epitaxy in the history of semiconductors [3]. Development of fundamental and material sciences and technology for the semiconductors resulted in indispensable use heterostructures in today's opto-electronic technology. Electron confinement in such structures and the manifestation of quantum-size effects especially in optical spectra of III-V semiconductor heterostructures led to

ANADOLU ÜNİVERSİTESİ

the discovery of many physical effects and inventions. Today, the III-V group alloys are vital materials for optoelectronic devices such as light emitting diodes, laser diodes and photodetectors, as well as for electronic transport devices such as field effect transistors, high electron mobility transistors and heterojunction bipolar transistors [4].

In this chapter, we mainly focus on two different nanostructures grown by MBE: (i) InAs/GaSb type-II superlattices and (ii) InAs/GaAs self-assembled quantum dots.

2.1. InAs/GaSb Type-II Superlattices

Superlattice studies were first started in 1970 by the work of Esaki and Tsu [46]. In general, a *superlattice* is defined as a periodic structure of alternating very thin layers of two (or more) semiconductor materials with different bandgaps. Since the thicknesses of the constituent layers are generally in 2-5 nm range (~6-15 ML), lattice constant of the superlattice structure is determined not by the individual lattice constants of the layers but by the periodicity of the structure. Therefore, the new energy bands are formed within both conduction and valence bands that defines the “new” bandgap of the structure. This energy gap (i.e. bandgap) depends mainly on the individual layer thicknesses and slightly on the interface compositions [6, 7].

2.1.1. 6.1 Å Family and Their Band Alignments

Materials known as the 6.1 Å family has a significant place in III-V semiconductor compounds and their technology. It constitutes nearly lattice-matched semiconductors InAs (a = 6.0584 Å), GaSb (a = 6.0959 Å) and AlSb (a = 6.1355 Å) (see Figure 2.2) [47]. The small lattice mismatch of the family to GaSb substrates enables high quality growths with low density of defects and

ANADOLU ÜNİVERSİTESİ

dislocations [6]. Together with their alloys InSb, GaAs and AlSb, the 6.1 Å semiconductors provide a great degree of versatility in designing heterostructures for opto-electronic applications due to the diverse nature of their band alignments.

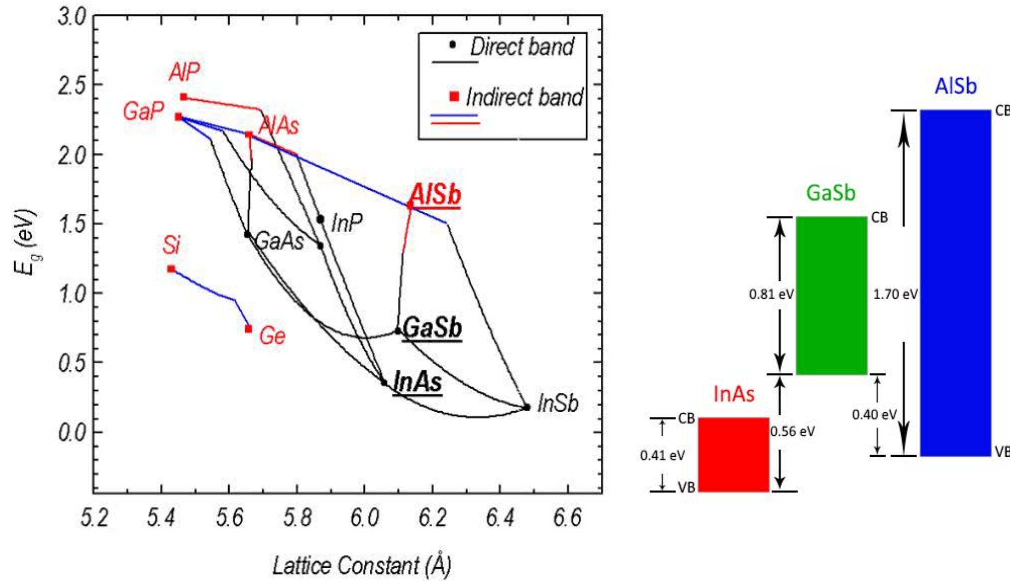

Figure 2.2 The energy gap versus the lattice constant of InAs, GaSb, and AlSb compared with other semiconductors (left). InAs, GaSb, and AlSb energy band lineups (right) [6].

Depending on the bandgap energies and their positions with respect to one another, it is possible to have three types of alignment for 6.1 Å family as shown in Figure 2.3. In type-I (nested) band alignment, the conduction and valence band edges of GaSb lie within the bandgap of AlSb and a potential for both electrons and holes are forms. The heterojunctions between InAs and the other two members benefit from the unique features of the type-II band alignment [7]: On one hand, InAs/AlSb junction forms a type-II staggered line up where the conduction band (CB) of InAs is slightly above the valence band of AlSb. The high energy gap of AlSb leads to an exceptionally large CB offset of about 1.45 eV, enabling the realization of very deep quantum wells. On the other hand, the heterojunction between InAs and GaSb leads to the broken gap line up where the CB of InAs is about 0.15 eV lower than the valence band of GaSb [6].

ANADOLU ÜNİVERSİTESİ

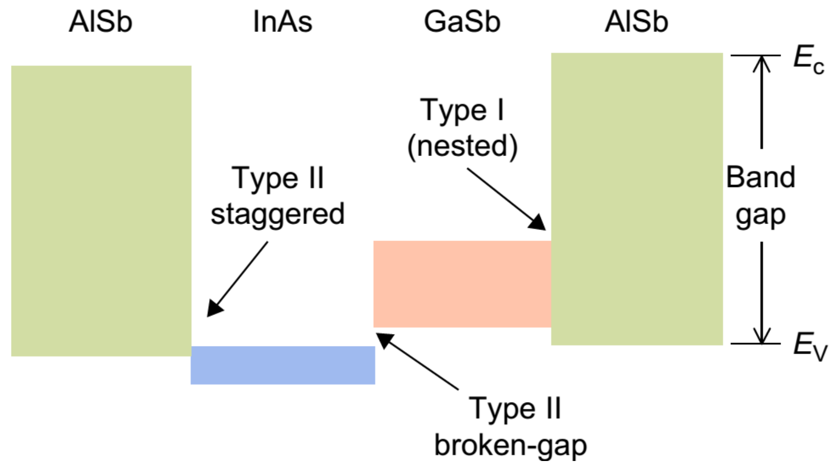

Figure 2.3 Schematic illustration of the energy band alignment in the nearly lattice-matched InAs/GaSb/AlSb material system [7]

In the case of InAs/GaSb type-II SL structures, the wavefunctions of the lowest conduction subband and the highest valance subband are localized in InAs and GaSb layers, respectively as shown in Figure 2.4. This means that electrons and holes are localized in spatially different places (i.e. InAs and GaSb layers, respectively). It is then possible to control the interaction between localized electrons by way of changing potential barrier thickness. On the other hand, if the number of periods forming the superlattice is large then the superlattice behaves like semimetal but if the superlattice period is shortened, the quantization effects are enhanced causing a transition from a semi-metal to a narrow gap semiconductor [5, 6, 47]. These fundamental properties make InAs/GaSb superlattice structures convenient for infrared detection: their bandgaps can be made arbitrarily small by bandgap engineering [8] and they are more suitable to band-to-band tunnelling in comparison to bulk material [6]. Moreover, they have decreased Auger recombination values due to the localization of electrons and holes in physically different locations [48, 49]. Effective mass of the electrons are small enough to have high carrier mobility and diffusion but big enough to reduce the tunnel and Auger currents in the structure [7].

ANADOLU ÜNİVERSİTESİ

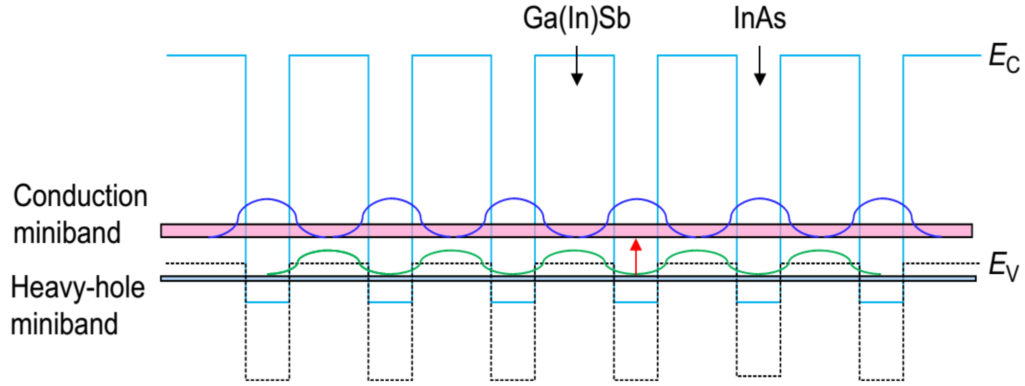

Figure 2.4 Schematic illustration of an InAs/Ga(In)Sb type-II broken-gap superlattice [7]

2.1.2. Effect of the Layer Thicknesses

As mentioned, electrons and holes are confined spatially in different layers of InAs/GaSb type-II SLs structure. The electronic band structure of the SL is identified by the energy level of electrons and holes in the quantum wells and through the interaction between the carriers in adjacent wells [6]. The local confinements of carriers and energy levels depend on the thicknesses of the adjacent layers. In other words, layer thicknesses control the separation of the confined states [8]. In InAs/GaSb type-II SLs, it has been experimentally proved that it is possible to tune the effective bandgap from 40 meV to more than 400 meV (3 to 30 μm) by just changing the consecutive layer thicknesses [19, 50, 51].

Effect of the InAs Layer

The InAs layer, in which the electrons are confined, is a quantum well in one period of the SL (see Figure 2.4 and/or Figure 2.5). It is known that the energy level of a particle in a quantum well is inversely proportional to its effective mass and the square of the well width [6]. The position of the CB edge for InAs/GaSb SLs changes rapidly with InAs layer thickness due to the small electron effective mass [8]. When the InAs layer thickness is reduced, the CB edge is pushed up to higher energies due to the stronger confinement, and vice

ANADOLU ÜNİVERSİTESİ

versa. On the other hand, in an extreme case for very thick InAs layer, it is possible to have the CB energy is as low as the valence band and even lower. Therefore, electrons can directly tunnel from one well to another via the valance band of the GaSb barrier, thus the superlattice starts to behave as a semimetal [6]. Thus, for a given GaSb thickness, it is necessary to use thicker InAs layers for long wave detection. For instance, ~5-10 ML InAs is used for mid-wave infrared and ~10-20 ML InAs is used for long-wave infrared applications [52, 53].

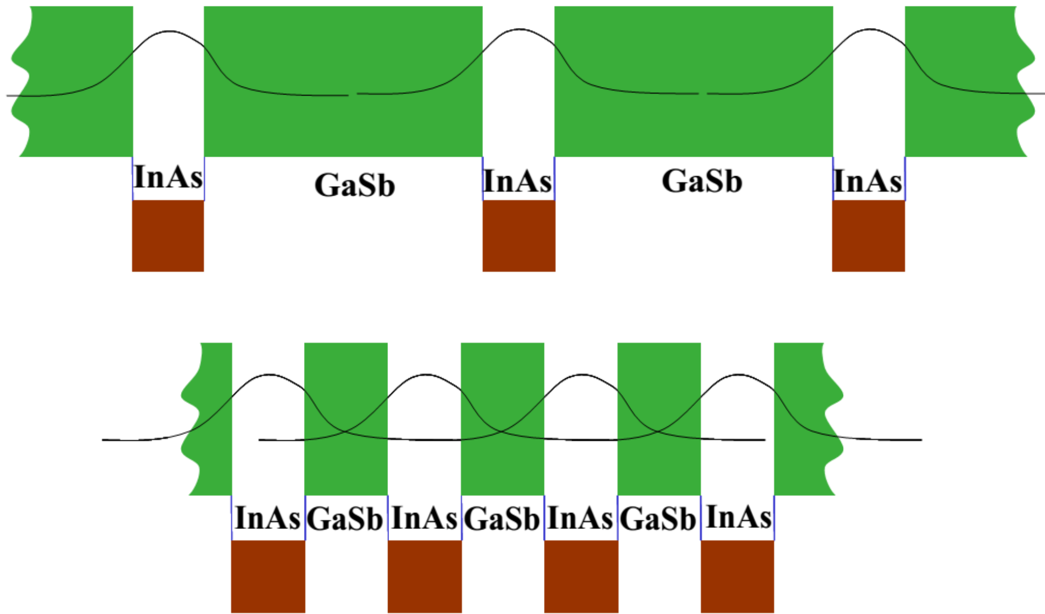

Figure 2.5 Effect of the GaSb barrier on the CB level. Thin GaSb layer results to a stronger wavefunction overlap [6].

Effect of the GaSb Layer

The GaSb layer in the SL forms a quantum well for holes and it also behaves as a barrier for electrons localized in the InAs layers. Since the effective mass of the holes in the valence band is much heavier than that of electrons, the dependence of the energy on the well width becomes much weaker. The energy level of holes with respect to the bottom of the well is normally very small and remains almost unchanged for GaSb layer thicknesses more than ~5 ML (~1.5 nm) [6]. However, the bandgap of the SL is affected by the GaSb layer thickness

ANADOLU ÜNİVERSİTESİ

through the superposition of the electron wavefunctions in the CB: The thinner the GaSb barrier thickness, the more the effect of the superposition (Figure 2.5). Similar to the formation of bulk band structures from discrete atomic levels, the CB of SL is the broadening of individual energy levels of electrons in InAs wells due to the interaction between wells. Since the interaction is determined by the distance between the InAs wells, in the case of thick GaSb layers the electron wavefunctions cannot overlap. As in the case of thinner GaSb layers, electron wavefunctions overlap and broadens the miniband as indicated in Figure 2.6 [6]. This pushes the lowest conduction level downward, closer to the constant valence level and thus the energy gap becomes smaller.

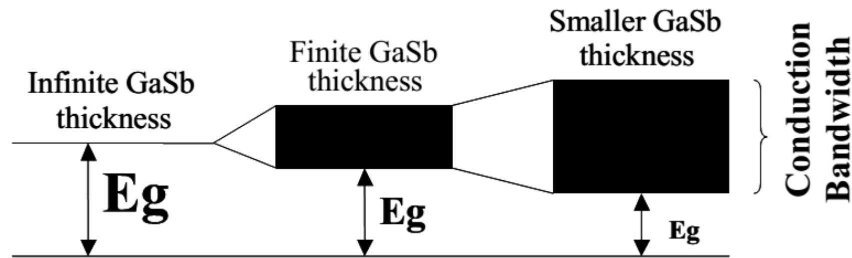

Figure 2.6 An illustration of the broadening of the CB as a function of GaSb thickness [6]

2.2. InAs/GaAs Self-Assembled Quantum Dots

In recent years, with the ability to grow self-assembled quantum dots (QDs) by epitaxial methods, scientists have been showing a growing interest in understanding their nature not only from the fundamental physics perspective but also from their applications point of view. Their atom-like energy levels and some anticipated advantages (especially over quantum well structures) such as long carrier lifetimes, lower threshold currents, higher gain mechanisms etc. make them convenient for many different applications [24]. QDs are very versatile in their properties by nature; their size, shape, density, strain and material composition can be changed for their expediency. These modify the energy

ANADOLU ÜNİVERSİTESİ

spacing between bound energy levels and therefore it is possible to obtain a very broad range of operating spectra [24]. Even though there are several ways to form quantum dots, only those having size confinement in all spatial directions by self-assembly will briefly be mentioned here.

The most widely studied material system in self-assembled QD structures are InAs QDs in the GaAs matrix. There is ~7% lattice mismatch between InAs and GaAs (6.0584 Å and 5.65325 Å, respectively) crystals [23]. Because of the lattice mismatch, after a critical thickness is reached the InAs crystal relaxes and aggregates to form lumps called *quantum dots*. This is known as Stranski-Krastanov (SK) growth [54]. Note that there is a direct correspondence between the growth mode and the film morphology, which gives the structural properties such as perfection, flatness and interface abruptness of the layers [55]. There are there classical growth modes as schematically shown in Figure 2.7. Depending on the materials to be grown, the growth can be realized layer-by-layer up to a certain thickness and then three dimensional islands are formed to release strain energy caused by the lattice mismatch between the epilayer and the substrate. This growth mode (SK) has been the most widely used approach for fabricating epitaxial QDs [23].

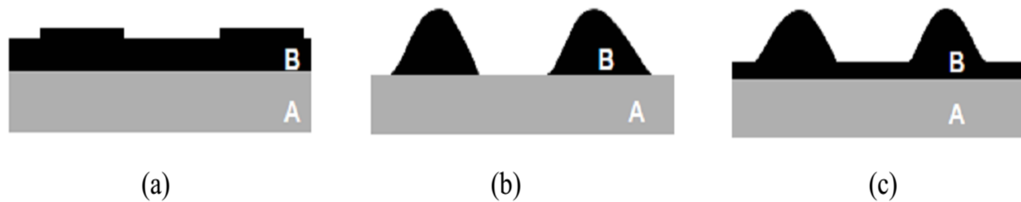

Figure 2.7 Illustration of different growth modes: (a) 2 dimensional layer-by-layer growth: Frank-van der Merwe, (b) island growth in 3 dimension: Volmer-Weber, (c) 3 dimensional island growth following layer-by layer growth: Stranski-Krastanov [55]

The electronic shell structure and the level separations of InAs/GaAs self-assembled QDs are determined by the dot size and shape [56-58]. In general, these self-assembled QDs are wide in the in-plane direction (~20 nm) and narrow in the growth direction (~3 nm). Therefore, the strong confinement is in the

ANADOLU ÜNİVERSİTESİ

growth direction while the in-plane confinement is weak resulting in several levels in the dots [59]. Analogous to real atoms, the bound states are grouped into three shells: s, p, and d. Changing the size and the shape of the QDs, the position of these energy levels can be controlled: for smaller QDs the minimum energy is pushed up to higher values because of the higher confinement. Self-assembled QDs grown in SK growth mode tend to have pyramidal or lens-like shapes that are flattened in the growth plane. The in-plane asymmetry in QD's shape leads non-degenerate energy levels in the dot. Note that the shape of the QD is not as easily controlled as the QD size [54].

The QD density in SK growth is determined by the QD nucleation process and subsequent ripening. Most growth experiments have shown that decreasing the growth temperature can increase the quantum dot density [6, 60]. Since the QDs are formed by self-assembly there is a Gaussian distribution of the size of the coherent dots causing non-uniformity in many aspects. Fortunately for device applications, the strain profile of the SK QDs results in preferential growth such that the cap layer returns to a flat surface once the QDs have been completely covered, which facilitates the stacking of more dot layers on top. For the stacking of dots the layer-to-layer spacing is important because below a certain thickness the strain field of the buried dot layer will cause the QDs in subsequent layers to vertically align with the dots below [6]. The standard deviation in size for SK grown QDs is around 10% [6].

2.3. Aim of the Study

In the case of InAs/GaSb superlattice devices, it is possible to tune its operating range in the electromagnetic spectra by changing the individual layer thicknesses. Successively and repeatedly grown very thin (~3 nm) layers of InAs and GaSb increases the importance of the effect of the interfaces of 1-2 ML to the performance. Therefore, it is critical not only to investigate the growth quality of the layers but also to examine the interfaces between the layers and the structural defects in the interfaces. As in the case of InAs/GaAs quantum dot structures, the

ANADOLU ÜNİVERSİTESİ

shape, size, density and the uniformity of the dots determine both the properties and the performance of the devices. It is therefore equally important to structurally characterize the MBE grown quantum dot layers. One of the most appropriate techniques to use for the investigations of such nanostructures is electron microscopy since it gives direct information about the structures. However, for reliable analyses, especially in TEM characterizations, it is crucial to have a well-prepared specimen that is suitable for the chosen technique.

The objective of this thesis is to investigate epitaxially grown III-V nanostructures, particularly multi-layered InAs/GaSb superlattice and InAs/GaAs quantum dot structures, by using both SEM and TEM techniques for their structural properties such as layer thicknesses, interface properties, surface qualities and surface and defect characterizations. It is therefore aimed to develop a cross-section sample preparation recipe for our material systems for more effective, reproducible and reliable analyses. As a consequence of these studies, it is also intended to have better understanding about the structures and to provide a feedback for the growth optimization in the MBE system.

.

ANADOLU ÜNİVERSİTESİ

3. EXPERIMENTAL PROCEDURES

In this chapter structures of the MBE grown samples whose characterization results are given in chapter 4 will be described briefly. Then the main cross section TEM sample preparation steps for III-V group semiconductors will be explained. Most of these sample preparation steps are commonly used in similar studies for many years [61]. It is however not a simple task to control and reproduce good quality TEM specimen with high efficiency and throughput. And finally, electron microscopy techniques used in the investigation of the samples are mentioned. As in the case of sample preparation, most of the electron microscopy characterization techniques are extensively used in many different areas of research. Note that it is not aimed in this chapter to describe the fundamentals of the techniques; it summarises some of the important points with brief explanations. Their details can be found in many textbooks [42, 62].

The entire process of MBE grown III-V group semiconductor samples' preparation and their characterization by electron microscopy had been started in our laboratories with another MSc thesis [63]. The sample preparation procedures have been perfected and optimized throughout the present thesis. In addition, some of the studies such as high resolution TEM are applied for the first time in this thesis in our laboratories.

3.1. MBE Grown Structures

The samples investigated in this thesis can be collected in four main groups; GaSb epilayers, InAsSb epilayers, InAs/GaSb type-II SL structures and InAs QDs. All the samples were grown on GaSb and/or GaAs substrates by molecular beam epitaxy (MBE, Veeco Gen20 solid-source) in Nanoboyut Research Laboratory, Anadolu University. List of the samples whose characterization results are presented in this thesis are given in Table 3.1. Since it

ANADOLU ÜNİVERSİTESİ

is not in the scope of this thesis, limited details about the structures are given throughout the thesis but further information can be obtained by following the references given.

Table 3.1 List of samples used in this study

Sample Code	Structure
YES-01	InAs/GaSb Multilayer
YES-02	InAs/GaSb Multilayer
YES-03	$InAs_{1-x}Sb_x$ Epilayer
YES-04	$InAs_{1-x}Sb_x$ Epilayer
YES-05	$InAs_{1-x}Sb_x$ Epilayer
YES-06	GaSb Epilayer
YES-07	GaSb Epilayer
YES-08	GaSb Epilayer
YES-09	GaSb Epilayer
YES-10	GaSb Epilayer
YES-11	GaSb Epilayer
YES-12	GaSb Epilayer
YES-13	GaSb Epilayer
YES-14	InAs/GaSb Type-II SL
YES-15	InAs/GaSb Type-II SL
YES-16	InAs/GaSb Type-II SL
YES-17	InAs/GaSb Type-II SL
YES-18	InAs/GaSb Type-II SL
YES-19	GaSb Epilayer on GaAs
YES-20	InAs QDs
YES-21	InAs QDs
YES-22	InAs QDs
YES-23	InAs QDs
YES-24	InAs QDs

The studied epilayers were grown for both growth condition optimization and growth rate determination for the MBE system. Each sample in the set of InAs/GaSb type-II SL structures investigated in this study has 140 period of InAs and GaSb layers followed by a 20 nm InAs top layer. Since they are designed to

ANADOLU ÜNİVERSİTESİ

be infrared detectors for a systematic study, their individual layer thicknesses were kept constant but the interfaces were modified: each period contains 9 ML InAs and 9 ML GaSb with InSb-like strain balancing interfaces [10]. In another set of samples whose electron microscopy characterizations are given in this thesis consist one buried, one surface InAs quantum dots in/on GaAs matrix element. Additionally, a structure having an AlSb quantum dot layer used as a transition interface from GaAs to GaSb was investigated.

3.2. Sample Preparation for Transmission Electron Microscopy

For electron microscopy characterizations, especially with TEM, it is known that the thickness of the samples directly affects the analysis. Depending on the technique to be performed, samples' thicknesses may differ from one another and therefore different sample preparation procedures may be followed. For instance, in some diffraction techniques (e.g. Kikuchi diffraction and convergent-beam electron diffraction) relatively thicker samples are preferred compared to high resolution studies [42]. Thus, for electron microscopy investigations, efficient sample preparation recipes must be adapted based on both the type of the sample and the method chosen for analyses. Within the scope of this study, an adapted sample preparation recipe has been improved for the aforementioned material systems for more effective and reproducible analyses specifically for transmission electron microscopy techniques.

Because of the soft and brittle characteristics of GaSb substrate and the fact that the sample to be studied (i.e. specimen) should be very thin (<100 nm) for reliable analyses, the sample preparation procedure is very important. For the structures investigated in this study it is crucial to prepare the optimal cross-sectional TEM specimens to identify the individual very thin layers of InAs and GaSb in superlattice structures and small quantum dot features in others. The conventional cross-sectional TEM sample preparation process has been modified for the studied structures and for the equipment used in the processes. Method is

ANADOLU ÜNİVERSİTESİ

slightly different in comparison to conventional method and it will not be deceptive to emphasize that TEM sample preparation process is challenging and relatively time consuming. Therefore, in this study, it is aimed to improve an efficient cross-sectional TEM sample preparation recipe for MBE grown structures. The recipe adapted for cross-section TEM sample preparation has the following stages: cleaving the substrate and gluing pieces face to face, slicing the glued sample into strips, cutting a 3 mm disc from a strip, grinding and polishing the 3 mm disc, gluing the polished disc on a grid, dimpling, and finally ion milling. Details of each step are given below.

Cleaving & Gluing

Two pieces from the sample to be characterized and four pieces from Si substrates are cleaved approximately on the same sizes. Because of their durable nature, Si pieces are used as reinforcement. The use of the same size (both width and length) pieces easies the consequent step, i.e. diamond wire slicing. Pieces are then glued together in a way that the epilayers on the sample pieces are facing each other as indicated in Figure 3.1. This allows more space to be characterized cross-sectionally and increases the chance of finding a better place on the sample for analysis. For gluing, several types of polymer (often called “glue” for such preparation techniques) can be used. In this study, a high temperature resisting epoxy (M-Bond 610) was used. Gluing the pieces provides more physical resistance to such soft and brittle samples and eases the consequent mechanical steps.

ANADOLU ÜNİVERSİTESİ

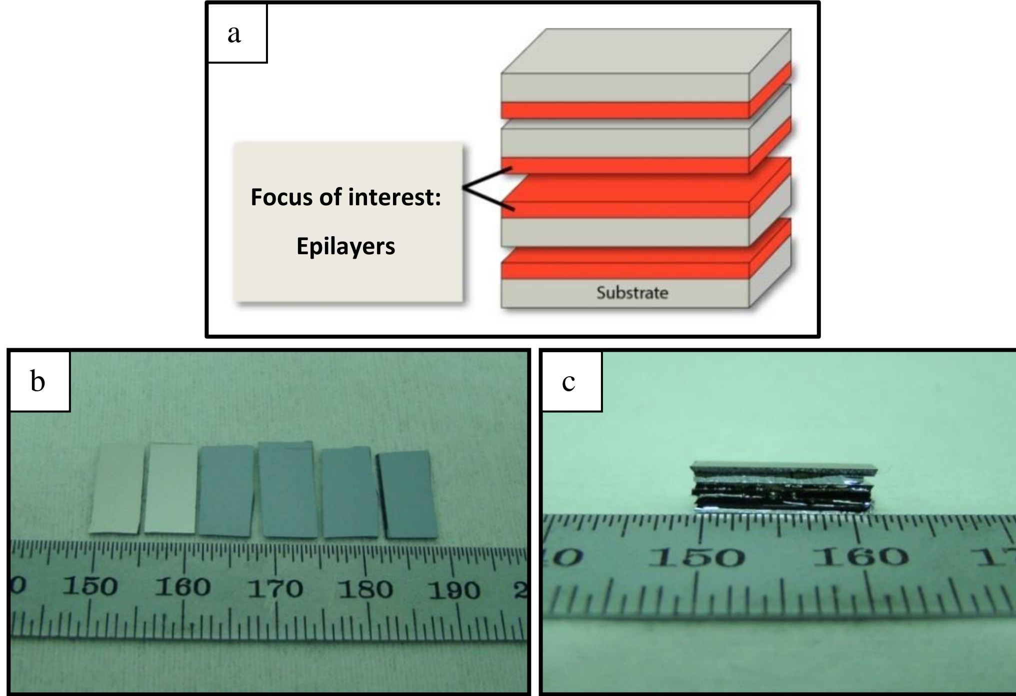

Figure 3.1 a) A schematic representation of the first step in cross-section sample preparation. Images of b) cleaved and c) glued pieces.

Slicing

The glued pieces are then sliced with diamond wire saw (Well3242) into strips of approximately equal thicknesses. Representative pictures of the sample before and after slicing are presented in Figure 3.2. One of the good looking sliced pieces is then picked for the next step, ultrasonic disc cutting.

ANADOLU ÜNİVERSİTESİ

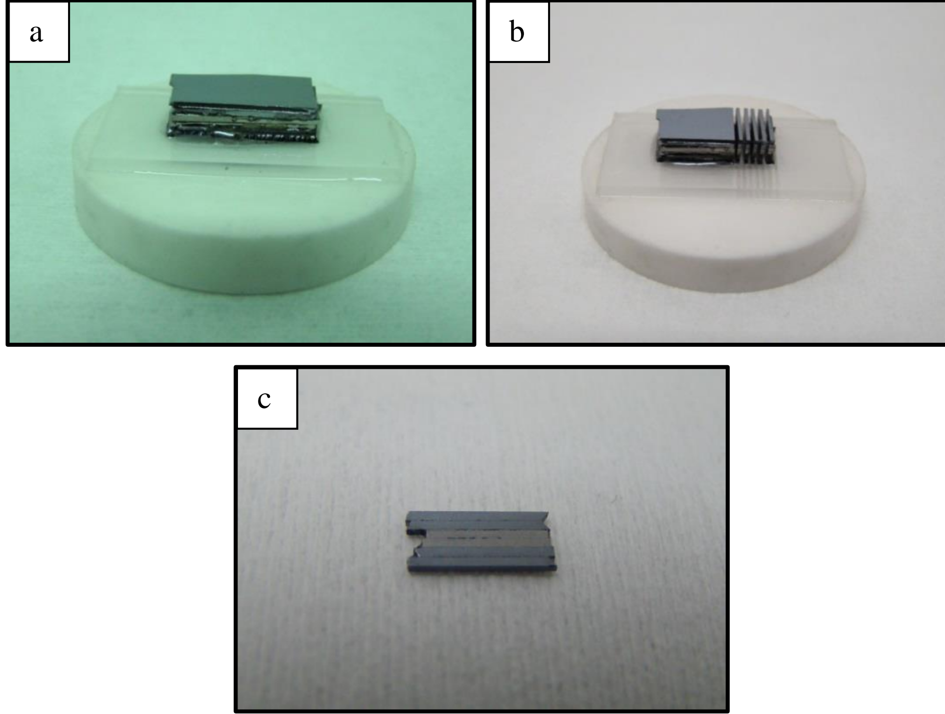

Figure 3.2 The views of the sample (a) before and (b) after slicing. (c) One of the slices picked up for later steps.

Cutting 3mm disc

Because of the TEM holders' designs, samples are required to be as 3mm diameter discs [64]. Therefore, the specimens have to be cut as 3mm discs from the sliced pieces. For this purpose, an ultrasonic disc cutter (South Bay Technology 380) was used. The chosen strip is cautiously attached onto the holder of ultrasonic disc cutter with wax then the cutting tip is aligned so as to the sample pieces (epilayers) are at the centre. After the two drops of lubricant are dripped on the sample, the cutting process is finalized. Note that in this study samples were thinned down to the thickness of ~250 μm before the cutting process for better results. The views of ultrasonic disc cutter and a sample after cut as 3 mm disc are presented in Figure 3.3.

ANADOLU ÜNİVERSİTESİ

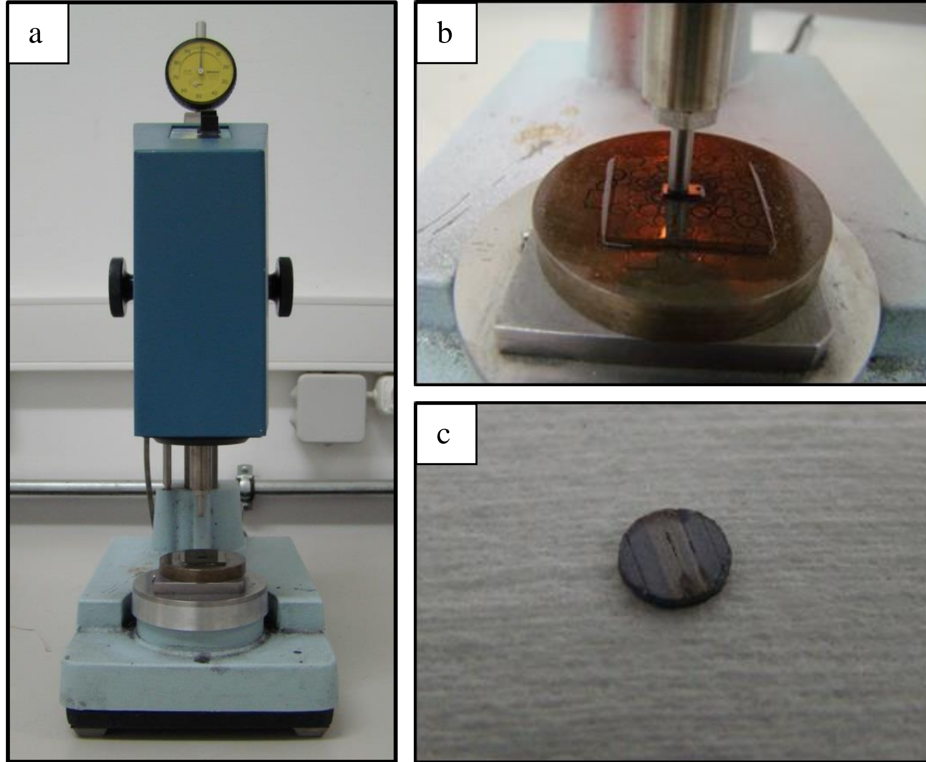

Figure 3.3 The cutting process with ultrasonic disc cutter: sample gets 3mm disc after the operation. (a) Disc cutter, (b) during the operation, (c) sample after the operation.

Grinding and Polishing

It is an accepted fact that during the TEM sample preparation processes, samples must be thinned meticulously. Therefore, this step has a special importance in the entire process. Grinding is the most commonly used technique to reduce the thickness of the samples. Throughout this study, grinding and polishing steps are carried out by using a disc grinder (Gatan Disc Grinder Model 623) with lapping films as abrasives. The specimen of a 3 mm disc is thinned and polished from one side by using lapping films having different sized diamond particles embedded on them. The particle sizes on the lapping films used in the process are 30-15-9-6-3-1-0.5 and sometimes 0.1 μm, respectively. The lapping films with bigger diamond particles are mainly used for coarse material removal. As the sample gets thinner, lapping films with smaller particle sizes are used for fine polishing. After the specimen is thinned down to a particular thickness (<150 μm), the process has to be carried on with increased care. The surface is then

ANADOLU ÜNİVERSİTESİ

polished carefully with lapping films of smallest sizes for smooth and bright surface. The view of the disc grinder and the specimen after polishing are presented in Figure 3.4.

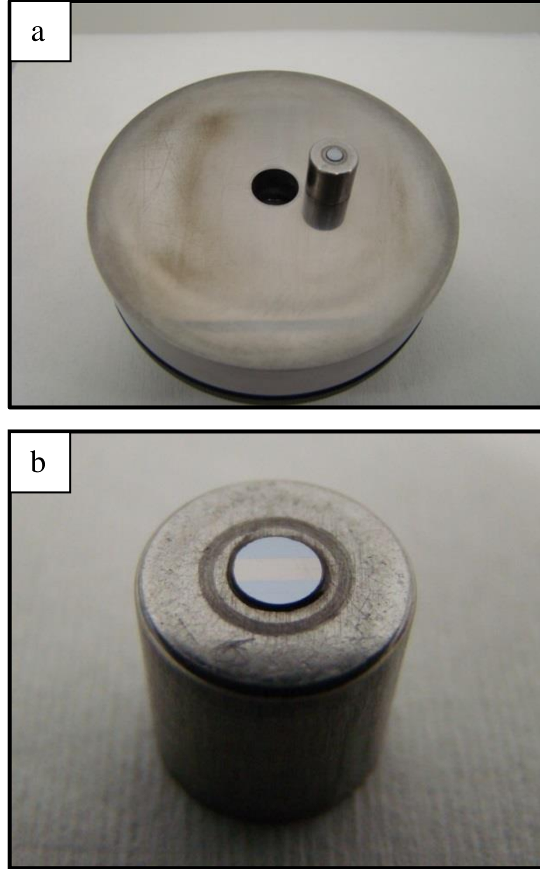

Figure 3.4 The view of a) the disc grinder and b) the specimen on the holder after polishing.

Gluing the Polished Disc on a Grid

After polishing, a copper support grid is glued onto the polished side with the high temperature resisting epoxy as seen in Figure 3.5. The use of copper grid provides physical endurance and reduces the risk of damaging the sample. At the end of this step the sample is also thinned from the unpolished side to a total sample thickness of about 40 µm and this surface is the polished too.

ANADOLU ÜNİVERSİTESİ

Figure 3.5 The view of the specimen after gluing copper grid. The surface of the sample seen in the figure is the polished side.

Dimpling

Dimpling process is generally carried out for soft and brittle samples to prevent sample from being crashed if further physical thinning is applied. Below the thickness of ~40 µm it is quite difficult to continue thinning the samples with parallel thinning. With dimpling, it is aimed to thin the sample further down for ion milling. The general procedure of dimpling is as follows: Specimen is placed onto the holder and an abrasive paste is spread onto the surface. Owing to the turning disc and the base rotation, a dimple is formed on the surface. The process is continued until the thickness of the sample at the centre is reduced to ~20 µm. Making the final thickness smaller reduces the exposure time in ion milling. The views of dimpling machine and the specimen after dimpling are presented in Figure 3.6.

ANADOLU ÜNİVERSİTESİ

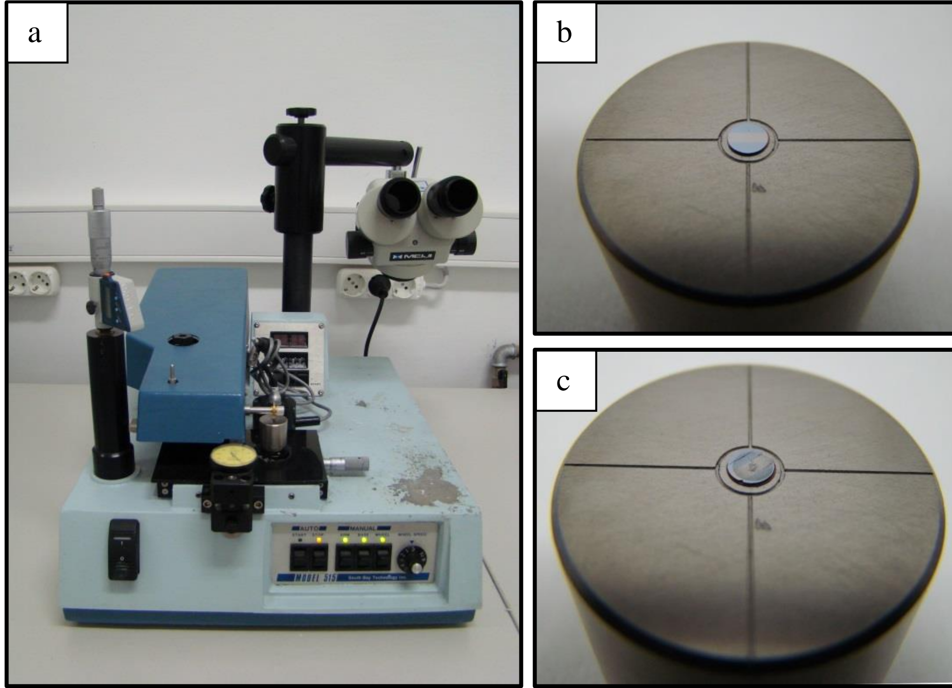

Figure 3.6 The view of a) the dimpling machine and the specimen on the holder b) before and c) after dimpling.

Additionally, the geometry of a dimpled sample limits the milling angle in the consequent step because of the shadow effect as illustrated in Figure 3.7. As the thickness difference between the edge and the centre of the sample after the dimpling process increases, the angle limitation becomes an issue that should be taken care of. Another concern in this stage is the fact that at minimum angles, material from the sample edge may be milled and re-deposited onto the centre of the dimple in ion milling operation. Therefore, proper precautions should be taken.

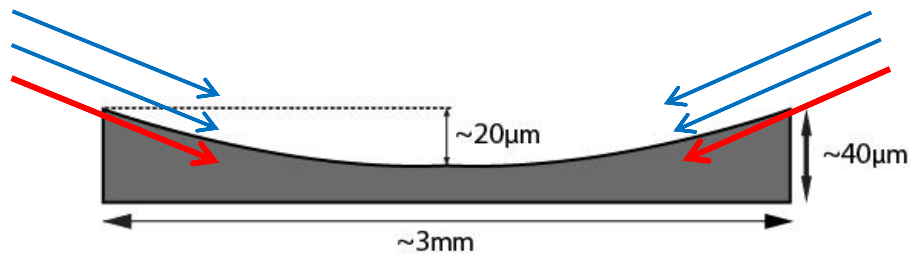

Figure 3.7 The schematic representation of a standard dimpled TEM sample from the cross-section. Blue arrows show the direct Ar beam onto the sample and red arrows show the shadowed edges.

ANADOLU ÜNİVERSİTESİ

Ion Milling

Ion milling is used to thin samples down to the level of electron transparency after the final mechanical thinning processes. The technique consists of bombarding the sample's surface with energetic Ar ions that will sputter atoms from the surface [61]. The sputtering process is continued until the centre thickness of the sample is thin enough (<100 nm) for TEM analyses.

The ion milling process starts with relatively high voltages (~7 kV; this increases the energy of the Ar ions) and high angle of incidence (~10º). The ion beam penetration into the specimen is minimized by lowering the accelerating voltage and lowering the angle of incidence. Once a hole is created through the sample in the process, the angle and the accelerating voltage are continuously decreased to 4º and 4 kV, respectively. Ion beam thinner BAL-TEC RES 101 was used in this study.

3.3. Sample Preparation for Scanning Electron Microscopy

Although new and high-technology techniques such as cross-polishing are available for SEM sample preparation, the conventional method is the most common one. This technique has four main stages: cutting/sectioning, mounting, grinding and polishing and if necessary coating. The most important step is polishing where the use of appropriate solutions or fine abrasives has a critical importance. Note that some materials do not require any special sample preparation methods for SEM analyses; they can be investigated as is.

In this thesis, the samples studied for surface investigations did not require any preparation procedures for SEM analyses. But for the samples investigated in cross-section a shorter procedure suchlike TEM sample preparation method was carried out. For the analyses, the wafers are cleaved approximately on the same sizes, then glued face to face and finally polished with the help of the lapping films.

ANADOLU ÜNİVERSİTESİ

3.4. SEM, TEM and STEM Investigations

In order to investigate the microstructures of different types of materials in atomic scale, the use of particles smaller than the atoms are required. In electron microscopy, high energy electrons produced by a source (electron gun) collide with the atoms of the sample piece. As a result of these interactions (i.e. between the material and the electron beam) different types of signals are originated [42]. Based on the nature of these signals, various techniques and different types of electron microscopes have been developed. It is therefore crucial to comprehend the interactions between the electrons and the atoms of the sample for proper interpretation of the images, spectras or diffraction patterns. The interactions between the electrons and the atoms are illustrated in Figure 3.8.

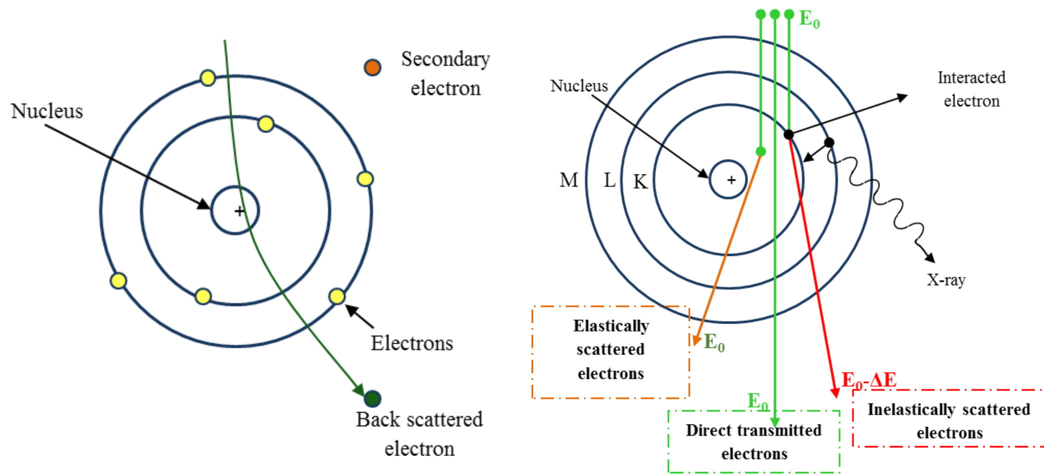

Figure 3.8 Electron – atom interactions: SEM (left) and TEM (right) [63]

The analyses of the MBE grown nanostructures used in this thesis were carried out by varying electron microscopy techniques for different investigations. In some of the investigations, a Schottky emitter field emission gun SEM (Zeiss SUPRA 50 VP) equipped with In-Lens, back scattered (BS), electron back scattered diffraction (EBSD) (Oxford) and energy dispersive X-ray (EDX) (Oxford) detectors are used. All the SEM investigations were performed at an

ANADOLU ÜNİVERSİTESİ

accelerating voltage of 20 kV and with 30 µm aperture. Surfaces of the samples were investigated by using In-Lens detector with relatively short working distances (~4 mm) and for the EDX analyses the working distance was kept constant at 8 mm.

In the TEM investigations, 200 kV field emission TEM (JEOL™ JEM-2100F) equipped with STEM high angle annular dark field (STEM-HAADF) detector (Model 3000, Fischione), parallel electron energy loss spectrometer (EELS) and energy filter (Gatan™ GIF Tridiem), and energy dispersive spectrometer (EDS) (JEOL™ JED-2300T) were operated. In TEM, high energy electrons emitted from an electron gun are directed to the sample where the interactions take place and different types of signals are produced. The nature of these signals and the corresponding techniques are shown in Figure 3.9.

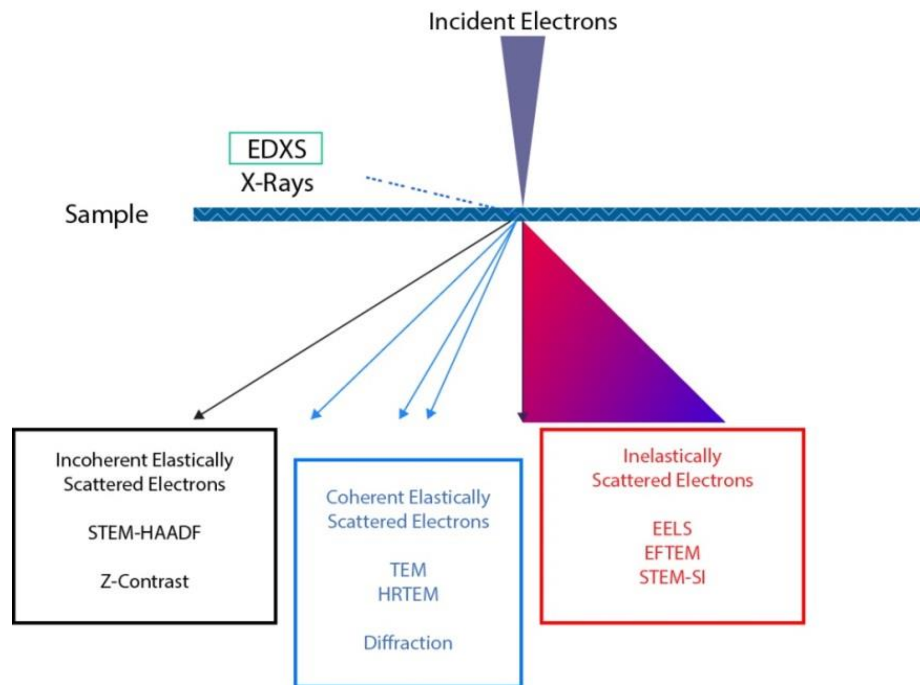

Figure 3.9 The signals and the techniques in which they are used [63]

TEM-BF imaging technique, in which directly transmitted electrons are selected by inserting the objective aperture into the back focal plane of the

ANADOLU ÜNİVERSİTESİ

objective lens, was used to determine the overall microstructural consistency and the structural quality of the MBE grown samples.

HRTEM imaging technique was used to investigate individual InAs/GaSb layers, AlSb QDs and InAs QDs for the purpose of examining the crystal qualities and also the structural defects. In this technique, the phase difference between the transmitted electrons produces high resolution of lattice and structure images for crystalline materials [42]. The directly transmitted beam (center beam in Figure 3.10) is required to provide a reference phase of the electron wavefront. High resolution images are the interference patterns obtained from the phase relationships of diffracted and directly transmitted beams (see Figure 3.10) [62].

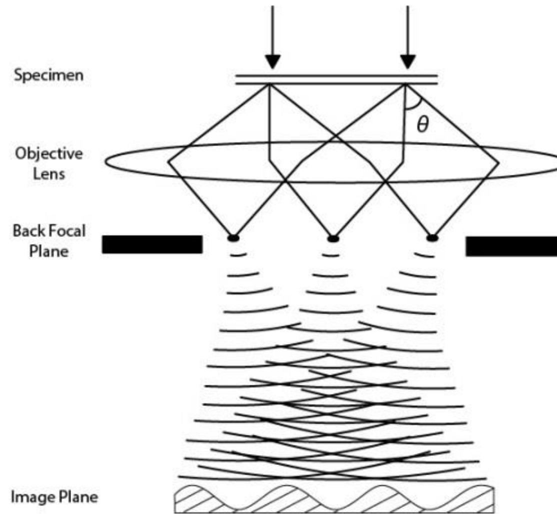

Figure 3.10 An illustration of HRTEM image formation

Scanning transmission electron microscope (STEM) has similar functions with SEM but transmitted electrons are also used and considerably better resolution is achieved [65]. Although apertures are used to select the directly transmitted or diffracted electrons to form images in TEM, special detectors collect the signals and use them to form images in STEM. Thus, no lens is used to form images and the imaging lens related degradation in the image quality is prevented [42]. The illustration of the STEM detectors is given in Figure 3.11.

ANADOLU ÜNİVERSİTESİ

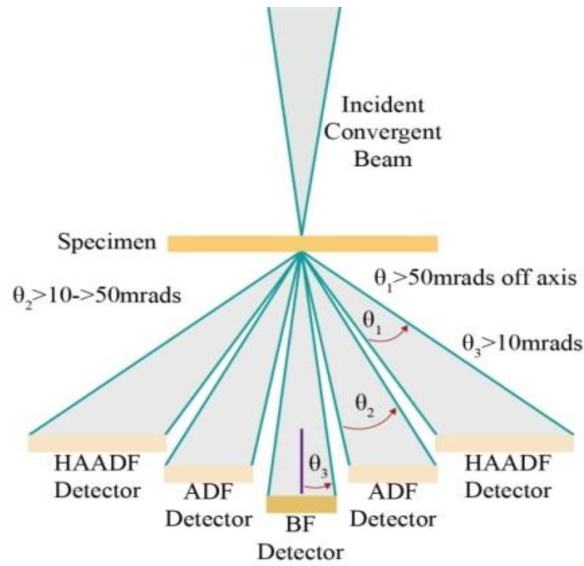

Figure 3.11 An illustration of STEM detectors [42]

Unlike HRTEM technique, images are formed from *incoherent* elastically scattered electrons in STEM-HAADF. While the interferences and phase differences are the major subjects for imaging in HRTEM, they are not relevant in STEM-HAADF. Each atom can be regarded as individual scatterer because there is no constructive or destructive interference between the phases of wavefunctions emanated from different atoms [62]. In STEM, for DF imaging, an annular detector surrounding the BF detector is used to pick up all the scattered electrons. This detector is called annular dark field (ADF) detector and the process is called ADF imaging. Another detector is called HAADF detector that collects electrons scattered to higher angles and similarly the process is known as HAADF imaging (see Figure 3.11). In HAADF (also known as Z-contrast) imaging technique, which is related to the atomic weight of the elements under investigation, Rutherford scattering effects are maximized and diffraction contrast effects are smoothed out [42]. STEM-BF, STEM-ADF and STEM-HAADF imaging techniques were carried out for the investigations of the structures throughout this study.

EDX is an analytical technique used for chemical analyses of a sample. When the electrons interact with the atoms, one possible outcome is x-ray

ANADOLU ÜNİVERSİTESİ

excitation and each element has characteristic x-ray excitation energies defined by its electronic structure [66]. STEM-EDX technique was used for examining elemental distributions of the structures.

In energy filtered transmission electron microscopy (EFTEM) technique the inelastic electrons caused the background are shifted and the quality of the images and the diffraction patterns are enhanced [65]. Inelastic scattering results in both a loss of energy and a change in momentum, which in the case of inner shell ionization is characteristic of the element in the sample. EFTEM three-window elemental mapping technique was used for one of the InAs/GaSb type-II SL samples.

Further information about TEM and SEM techniques can be found in “Transmission Electron Microscopy: A Textbook for Materials Science” by Williams and Carter [42] and in “Scanning Electron Microscopy and X-Ray Microanalysis” by Joseph Goldstein [66].

ANADOLU ÜNİVERSİTESİ

4. RESULTS & DISCUSSION

In this chapter it is aimed to present and discuss the characterization results of the studied MBE grown nanostructures. First, the results of thickness measurements on the epilayers to assist the growth rate determinations will be given. The surface characterization results and EDX analyses of GaSb epilayers obtained by SEM techniques will then be discussed briefly. The optimized cross-section sample preparation method for TEM analyses and the steps of the procedure that is slightly different in comparison to the conventional methods will be mentioned prior to the findings of InAs/GaSb type-II SL structures' investigations. The InAs/GaSb type-II SL structures were characterized by using different TEM and STEM techniques. In the next section, after the importance of growing GaSb epilayers on GaAs substrates is mentioned, the investigations of the structure proposed for this purpose will be presented. In those structures, the formation of AlSb QDs serving as an interface layer between the GaAs substrate and the GaSb buffer layer were observed: The structure was investigated via TEM, STEM, and SEM imaging techniques. In the last section the observations of InAs/GaAs self-assembled quantum dots will be presented and discussed.

4.1. Thickness Determination by Scanning Electron Microscopy

In most of the devices used in today's opto-electronic technologies very thin layers and/or features in nanoscale are responsible for their properties as in the cases of InAs/GaSb SL and InAs/GaAs QDs investigated in this thesis. The epitaxial systems like MBE provide accuracy in the atomic scale in material growth but the precise thickness determination is required for epilayers after growth. For the purpose, SEM imaging techniques can be used as an unrefined thickness determination tool for especially relatively thick layers and the results give feedback to the growth. So, two samples specifically grown for coarse growth rate determination were characterized by SEM images. The systematically

ANADOLU ÜNİVERSİTESİ

changed InAs and GaSb layer thicknesses in multiple-repeat sample were measured from their cross-sections. The images taken from both samples by using in-lens detector are shown in Figure 4.1.

For each sample, compositionally different layers were distinguished by using the in-lens detector owing to its sensitivity to contrast effects [66]. The thicknesses of each layer were measured and indicated on the images shown in Figure 4.1. These thickness values were then correlated with the time used for the corresponding layer in the growth process to calculate the growth rate. This is an approximate determination and better accuracy requires different techniques and further studies. Details of the growth rate calculations are not given here since it is not in the scope of the thesis. The bright vertical line on the left side of the image (Figure 4.1a) is an artifact caused by the sample preparation: it is neither a defect nor a thin epitaxial layer. It is attributed to a topographical edge created at the interface. The same effect with less notable brightness is also observed in the image (Figure 4.1b) in more than one interface.

ANADOLU ÜNİVERSİTESİ

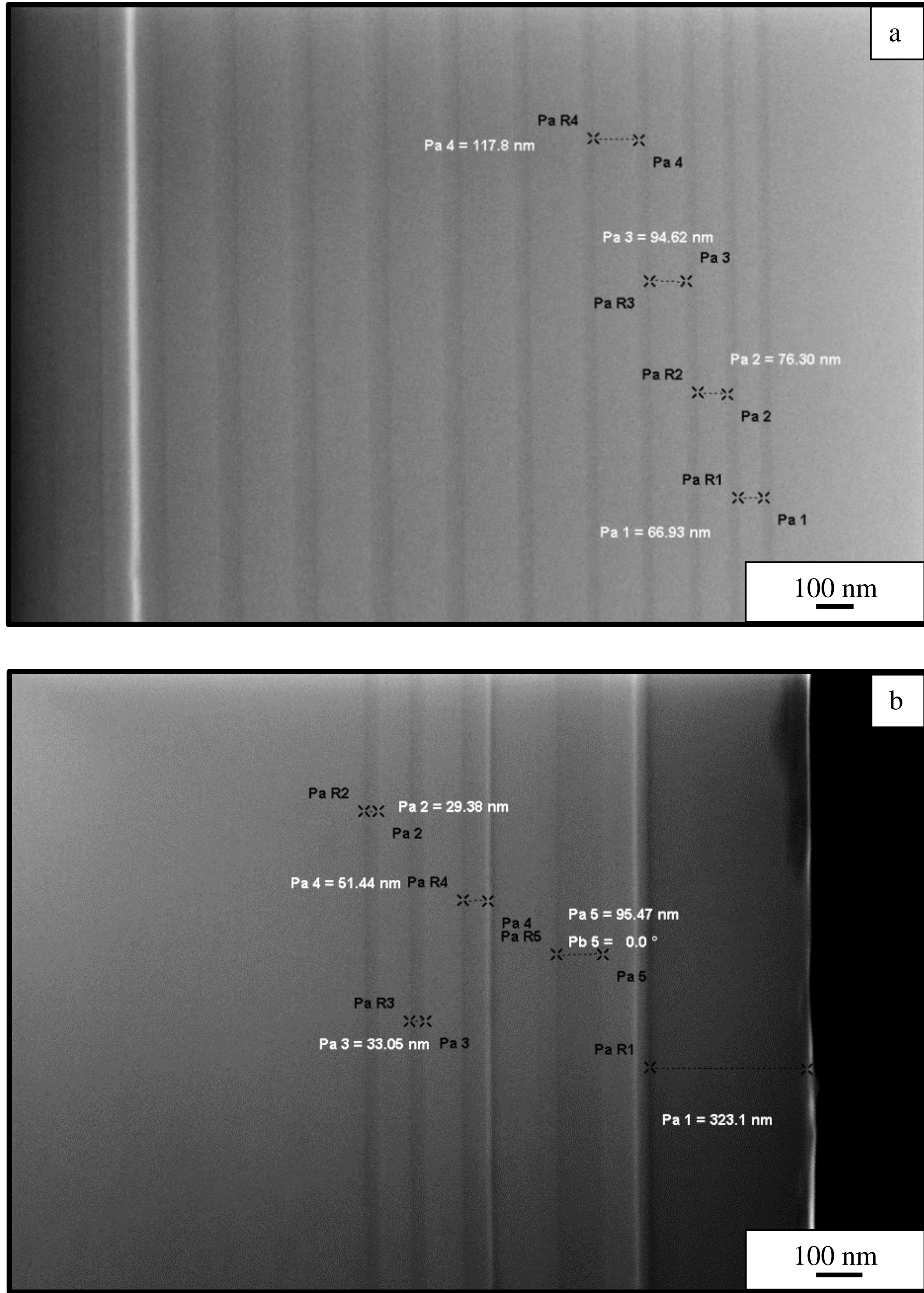

Figure 4.1 The cross-section images of a) YES-01 and b) YES-02

ANADOLU ÜNİVERSİTESİ

In a similar approach layer thicknesses for three different ternary compound $InAs_{1-x}Sb_x$ epilayers were measured. The images taken with the in-lens detector from each sample and the measured layer thicknesses are indicated on the images presented in Figure 4.2. The targeted and the measured values for the epilayer thicknesses are given in Table 4.1. Although the measured values are in very good agreement with the targeted thickness values for samples YES-03 and YES-05, there is around 20 nm difference for sample YES-04. Since all the samples had been grown under similar conditions, one possible explanation for this difference is that the sample had been mounted on the holder with an angle. This leads to a reading of the projected layer thickness rather than the real value. The spherical particles seen on the images are not related with the grown structures, they are contaminations coming from the epoxy used for gluing the substrates (see Figure 4.2).

Table 4.1 Targeted and measured thicknesses of $InAs_{1-x}Sb_x$ epilayers grown on GaSb substrates

Sample	Targeted Epilayer Thicknesses	Measured Epilayer Thicknesses
YES-03	592 nm	~590 nm
YES-04	567 nm	~545 nm
YES-05	555 nm	~555 nm

ANADOLU ÜNİVERSİTESİ

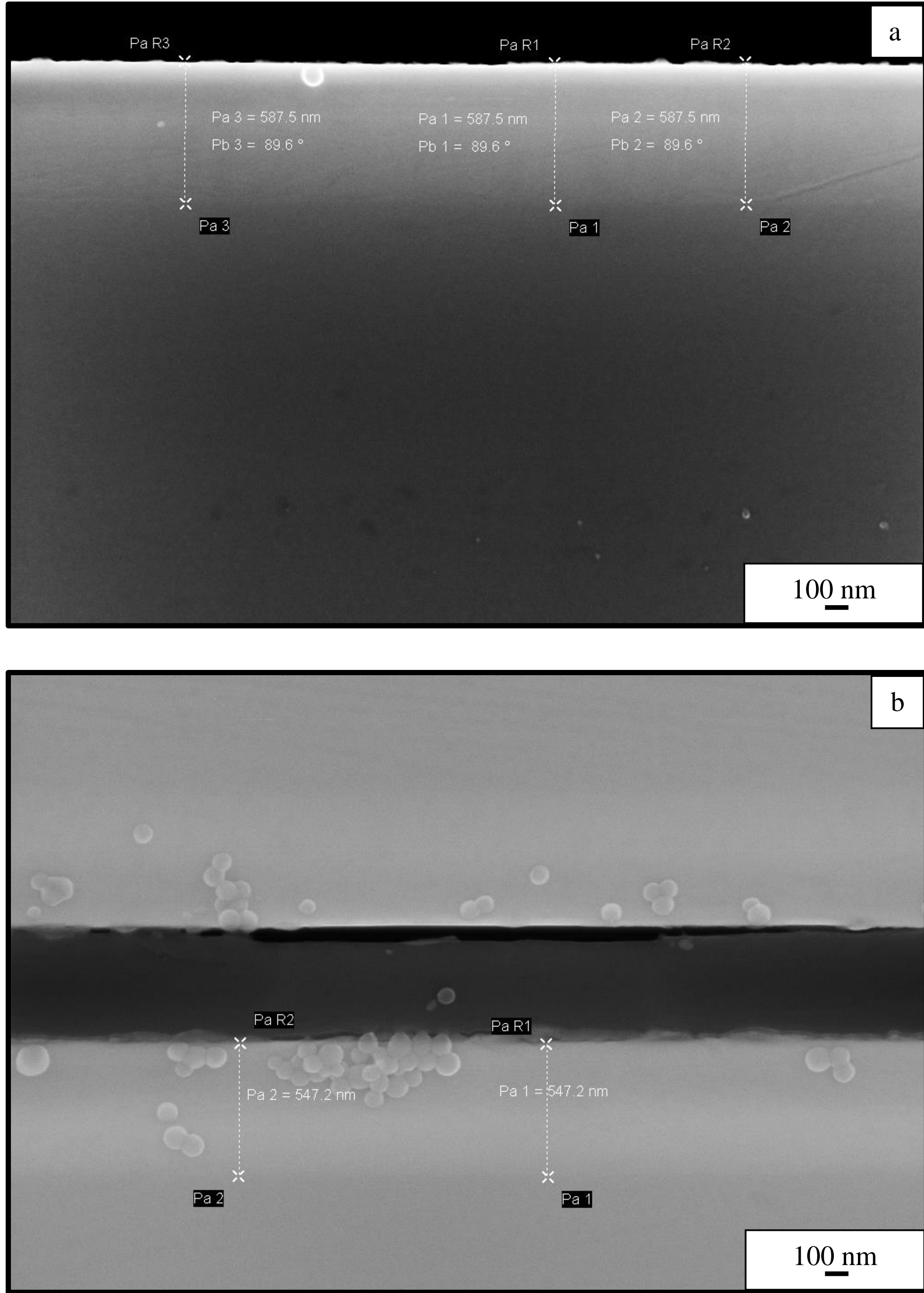

Figure 4.2 The cross-section images of a) YES-03, b) YES-04 and c) YES-05

ANADOLU ÜNİVERSİTESİ

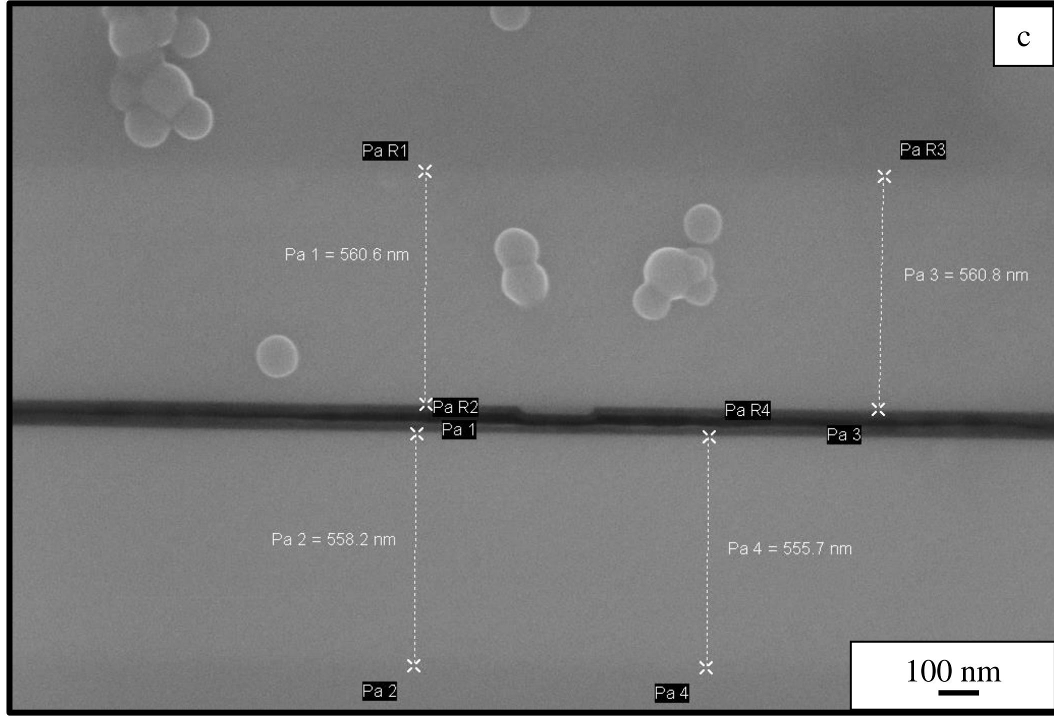

Figure 4.2 (Cont.) The cross-section images of a) YES-03 b) YES-04 and c) YES-05

4.2. Characterization of GaSb Epilayers

In epitaxially grown structures, the active layers are almost always grown on a buffer layer which is used to smooth the surface of the substrate. As for high quality InAs/GaSb SL structures it is particularly important to have a good quality GaSb epilayer on which the entire SL structure is grown. After the growth of earliest GaSb epilayers in our laboratory, it was realize that the surfaces are not smooth and shiny as they should be. For better understanding, the samples' surfaces were investigated by secondary electron (SE) imaging techniques; both conventional secondary electron detector and "in-lens" detector are used. Back scattered electron (BSE) imaging technique and EDX analyses were also performed for further characterization of the samples. SEM analyses provided a feedback for growth process and finally GaSb epilayers were grown with smooth surfaces.

ANADOLU ÜNİVERSİTESİ

In the following sections, SEM analyses of a set of samples grown under different conditions will be collectively discussed. However, the details of the growth conditions and the actions taken to perfect the surfaces will not be discussed since it is not in the scope of this thesis. A study dedicated to surface characterization of GaSb epilayer and growth optimization can be found elsewhere [67].

4.2.1. Surface Characterization with Scanning Electron Microscopy

Secondary electrons are the electrons that escape from the sample with energies below 50 eV. The yield of SEs emitted after the interaction of the primary electrons with the sample can even be higher than 1. Therefore, SEs are the most generated and the most widely used imaging signals in scanning electron microscopy, especially for morphologic and/or topographic investigations [68].

The surface morphologies of the GaSb epilayers were investigated by SEM and the images taken by using SE detector and in-lens detector are shown in Figure 4.3 and Figure 4.4, respectively. The presented images revealed that some of the samples have terrace-like structures and some extra features on their surfaces as shown in Figure 4.3. Further investigations and analyses with other techniques have shown that this is a condensed layer of Sb with thicknesses depending on the growth conditions. Some of the analyses are given in the following section. Images from some other samples showed that they have different types of defects on their surfaces as seen in Figure 4.4. These images were taken by using in-lens detector for which the working distance was kept constant at 4 mm during the operations. It is concluded from the surface images that different growth conditions can create different undesired features on the surface which need to be avoided.

ANADOLU ÜNİVERSİTESİ

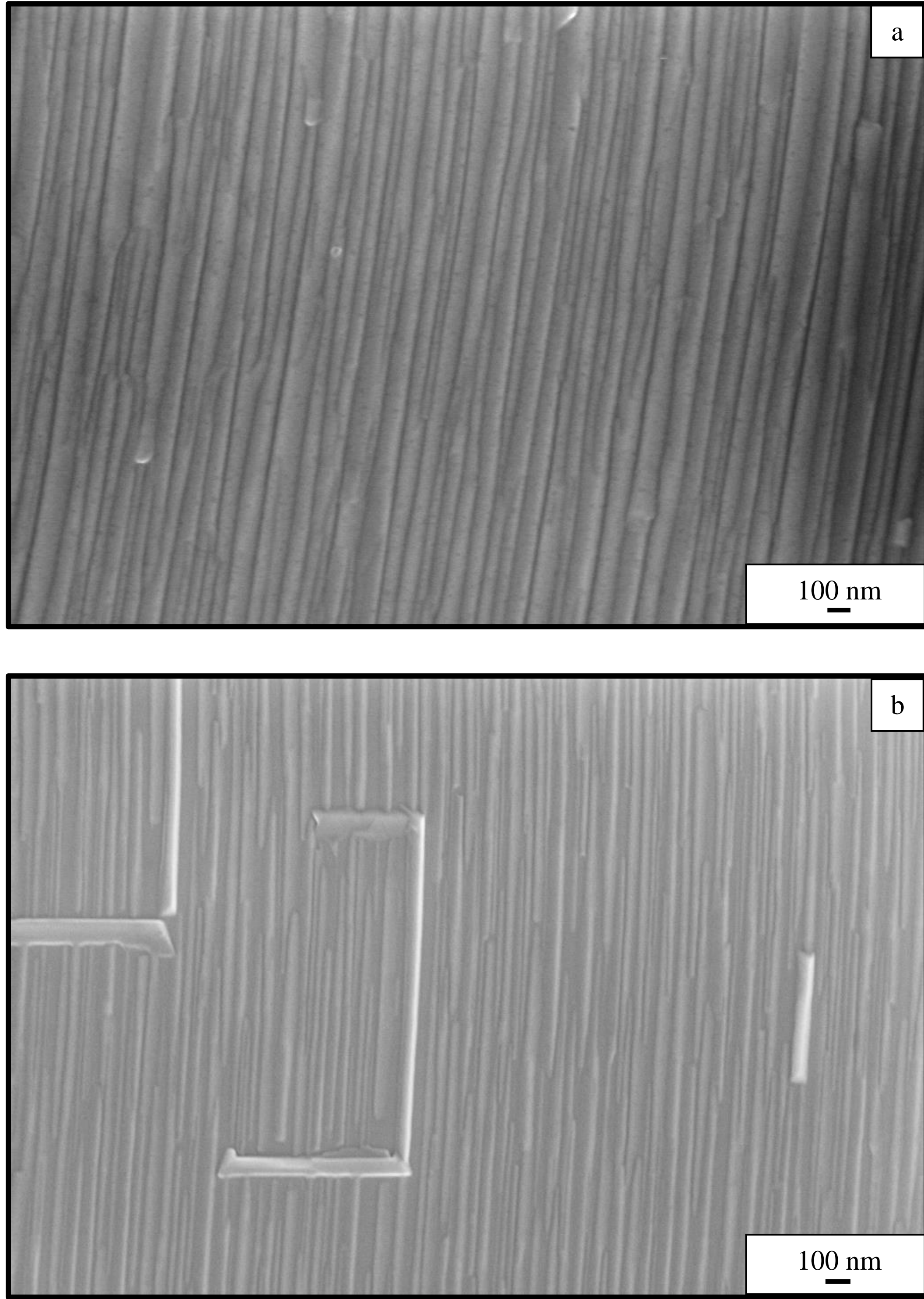

Figure 4.3 The surface images of the samples a) YES-06, b) YES-07, and c) YES-08 grown with different Sb fluxes. The images were taken in the same magnification for easy comparison.

ANADOLU ÜNİVERSİTESİ

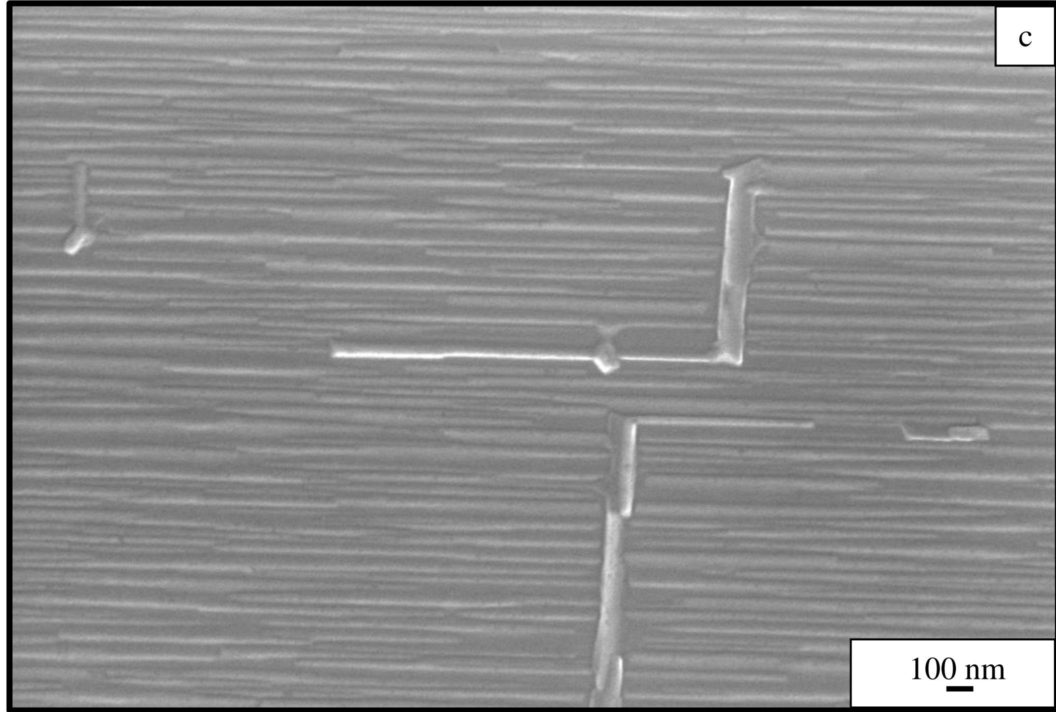

Figure 4.3 (Cont.) The surface images of the samples a) YES-06, b) YES-07, and c) YES-08 grown with different Sb fluxes. The images were taken in the same magnification for easy comparison.

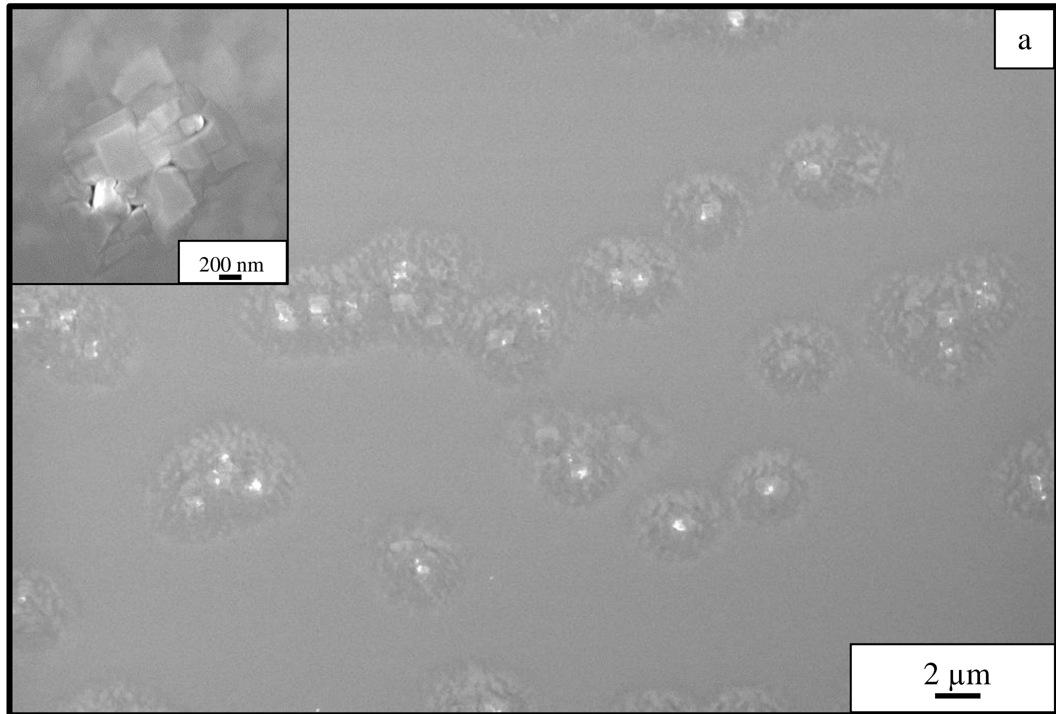

Figure 4.4 The surface images of the samples with different types of defects: a) YES-09, b) YES-10, and c) YES-11

ANADOLU ÜNİVERSİTESİ

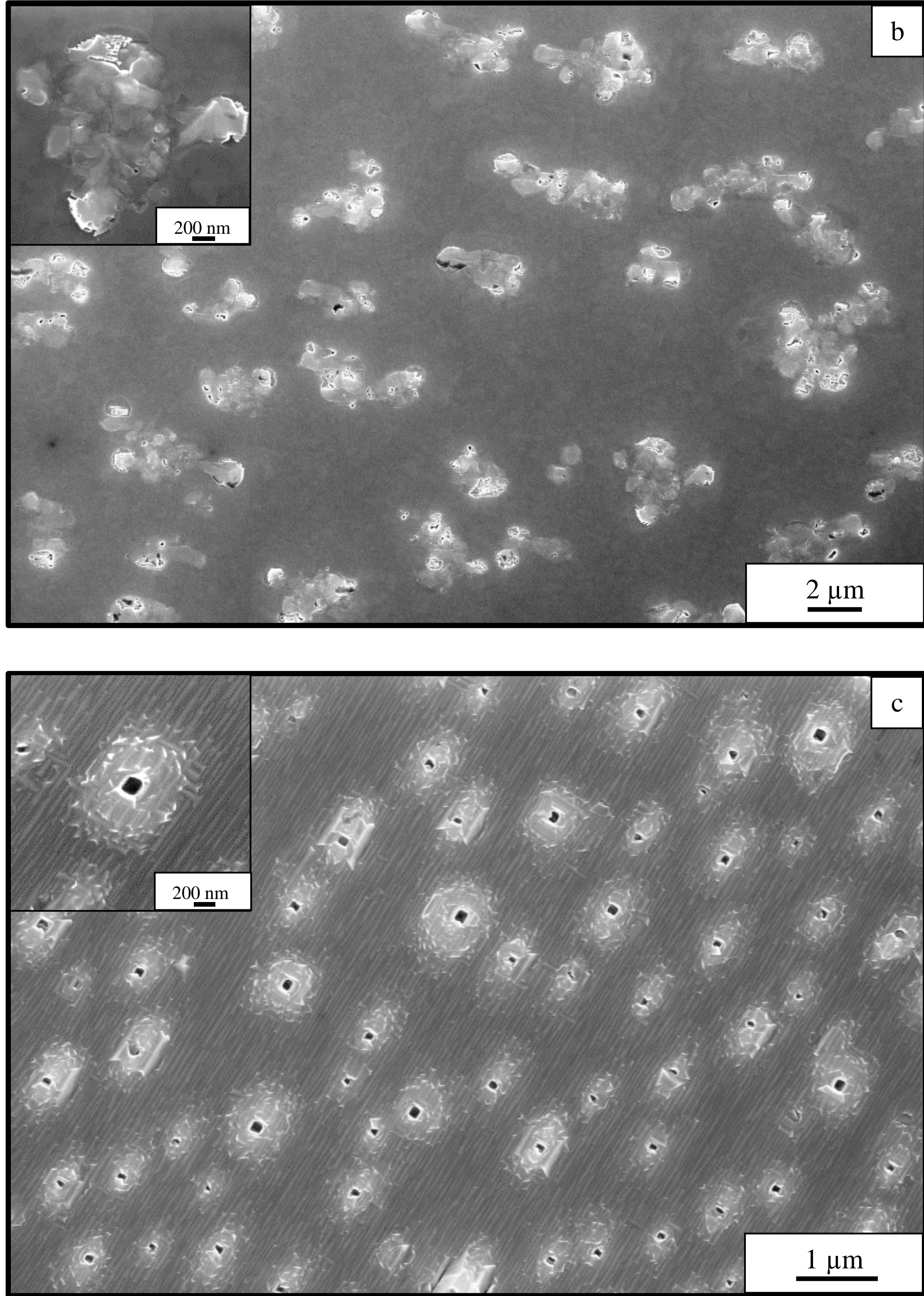

Figure 4.4 (Cont.) The surface images of the samples with different types of defects: a) YES-09, b) YES-10, and c) YES-11

ANADOLU ÜNİVERSİTESİ

Once the proper actions are taken after the analyses, GaSb epilayers with decent surface quality were grown. An SEM image taken by using SE detector from one of the samples is given in Figure 4.5a: it shows no special characters. As in Figure 4.5b, an SEM image taken by using in-lens detector from one of the InAs/GaSb SL structures grown on an optimized GaSb buffer is shown. The surface of this SL sample shows no undesired features either. The two images in Figure 4.5 are given for representative purposes such that the surface quality examined by SE imaging was confirmed with the in-lens detector. A specially designed high magnetic field low loss lenses and rotationally symmetric collection of electrons not only increase the collection efficiency but also allow operations at very short working distances [66]. Thus, at low voltages and small working distances, images with high contrast can be obtained by using an in-lens detector. In fact, an example image taken from the surface of the sample YES-07 after it was chemically etched is shown in Figure 4.6. Both very good contrast and resolution throughout the investigated region were obtained. The image was taken when the working distance was 4 mm. For the sake of visualization of the difference between conventional SE detector and in-lens detector images, an image was taken by changing the operating detector during the scan: the upper half of the image in Figure 4.7 was taken by using in-lens detector and it is then switched to SE detector for the lower half of the image. While the topographic information is dominant in the part of the image recorded by the conventional SE detector, information about morphology and the lateral differences are pronounced in the other half of the image taken by the in-lens detector. These differences arise from the fact that the in-lens detector is placed inside the electron column of the microscope.

ANADOLU ÜNİVERSİTESİ

Figure 4.5 The surface images of sample YES-14 taken with a) SE detector b) in-lens detector

ANADOLU ÜNİVERSİTESİ

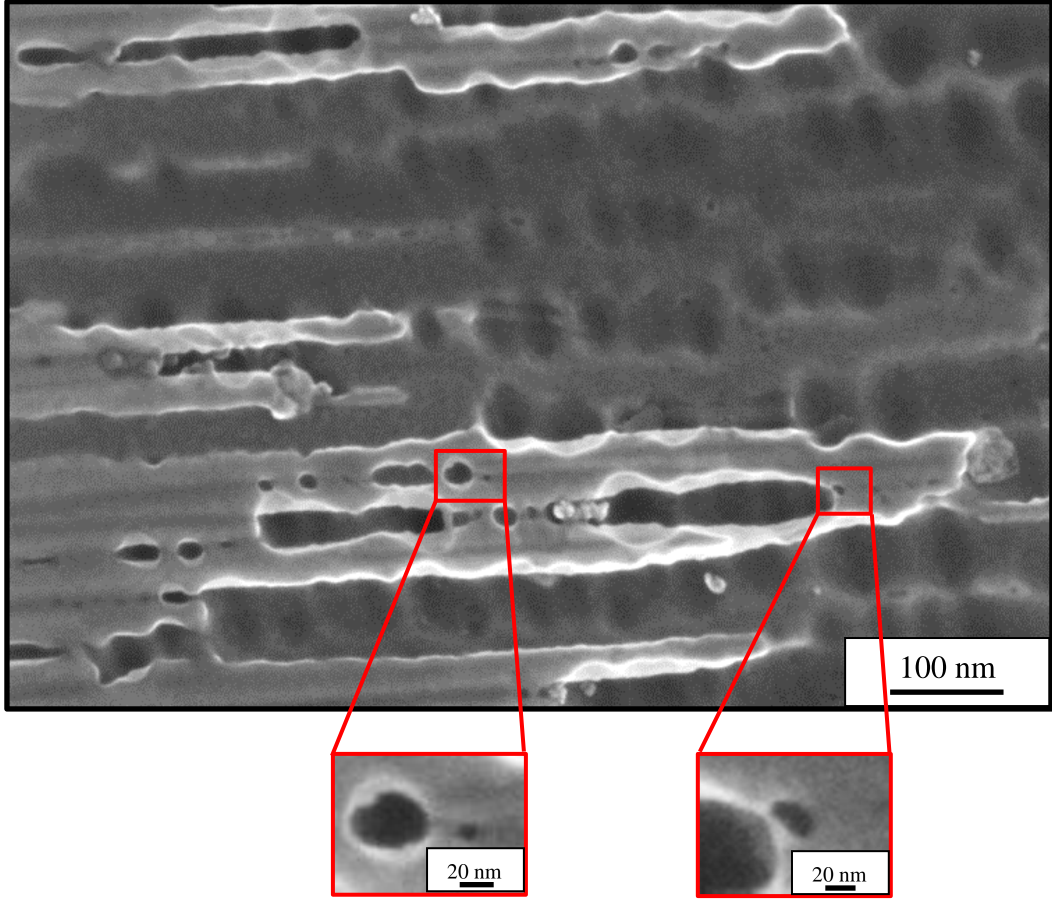

Figure 4.6 An image of the region between etched and unetched surface of sample YES-07 taken with in-lens detector. Two parts are zoomed in to show the image quality.

ANADOLU ÜNİVERSİTESİ

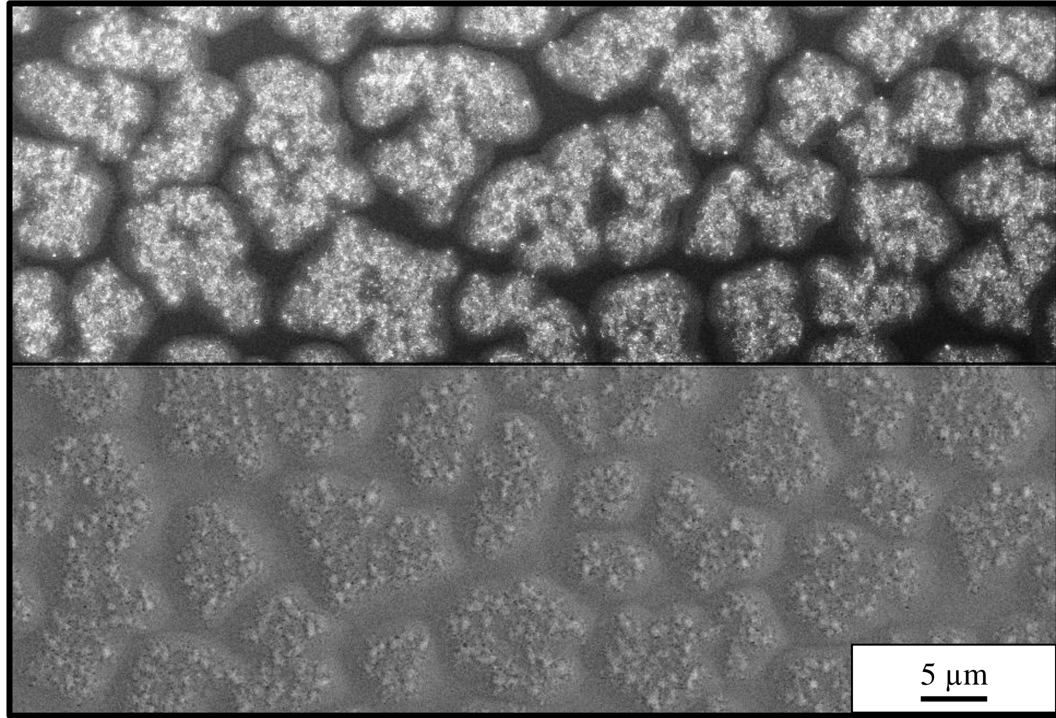

Figure 4.7 An image taken to reveal the difference between in-lens (upper half) and SE (lower half) detectors (YES-12)

4.2.2. Back scattered Electron Imaging & EDX Line Analyses

Back scattered electrons have an energy range from 50 eV up to the energies corresponding to the studied accelerating voltage of the SEM. A primary electron whose path is altered enough to have it leave the sample is referred to as a back scattered electron. The amount of BSEs generated in consequence of the electron-sample interaction depends on the atomic number of the sample [68]: heavy atoms with a high atomic number are stronger scatterers than light ones. Thus, BSE imaging technique is useful for investigating the samples containing different elements with the ability of providing contrast between them. That is, images with BSE contain compositional information.

As mentioned in the previous section, un-optimized growth conditions may cause Sb atoms to condensate on the surface. For the purpose of having complementary results samples were prepared for cross-section analyses and

ANADOLU ÜNİVERSİTESİ

investigated in SEM by EDX line analyses after taking the back scattered images. The aforementioned condensations give rise to the terrace-like structures with different thicknesses on the surfaces. Hence, it was aimed to measure the thickness of the condensation layer for each sample. The back scattered images shown in Figure 4.8 disclose an altered layer with different thicknesses on the top.

The back scattered imaging technique provided to image the condensation layers of the samples YES-13 and YES-06 thanks to the concentration differences. Hence, the thicknesses of the layers were measured from the surface and indicated on the images. The condensation layers containing more Sb seem brighter, because they scatter relatively more electrons, thus; more signals were collected by the detector. But for YES-11 which has the thinnest expected condensation layer could not be detected. In that case, for more information about the structures, SEM-EDX line analyses were carried out for each sample and the results are presented in Figures 4.9-4.11.

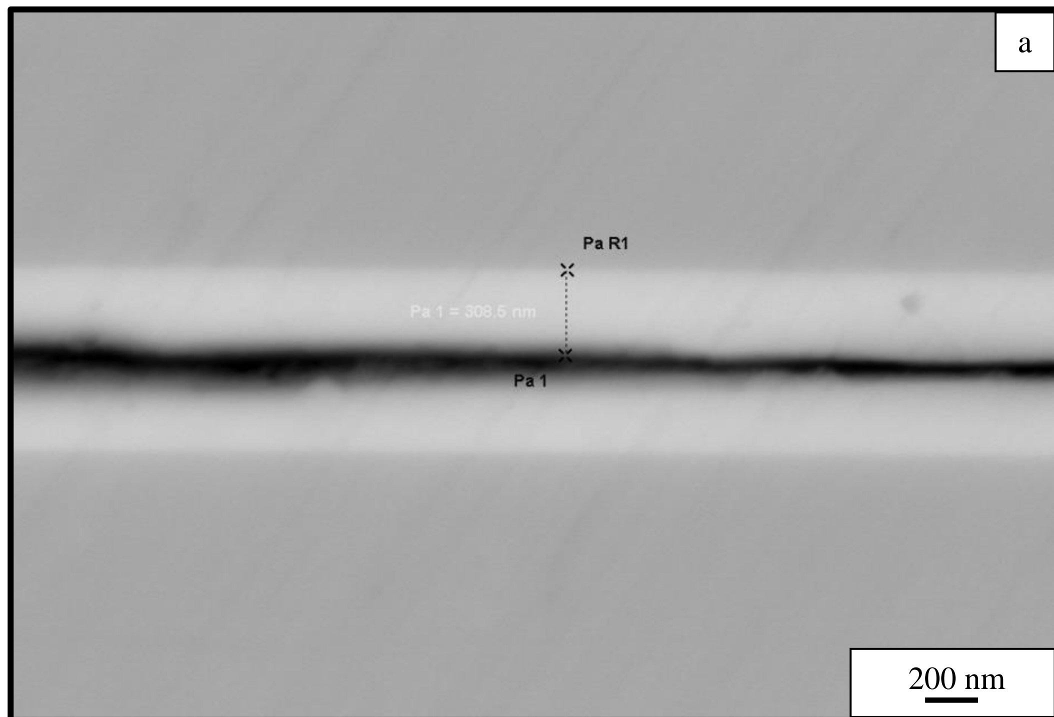

Figure 4.8 The back scattered images of samples a) YES-13, b) YES-06, and c) YES-11

ANADOLU ÜNİVERSİTESİ

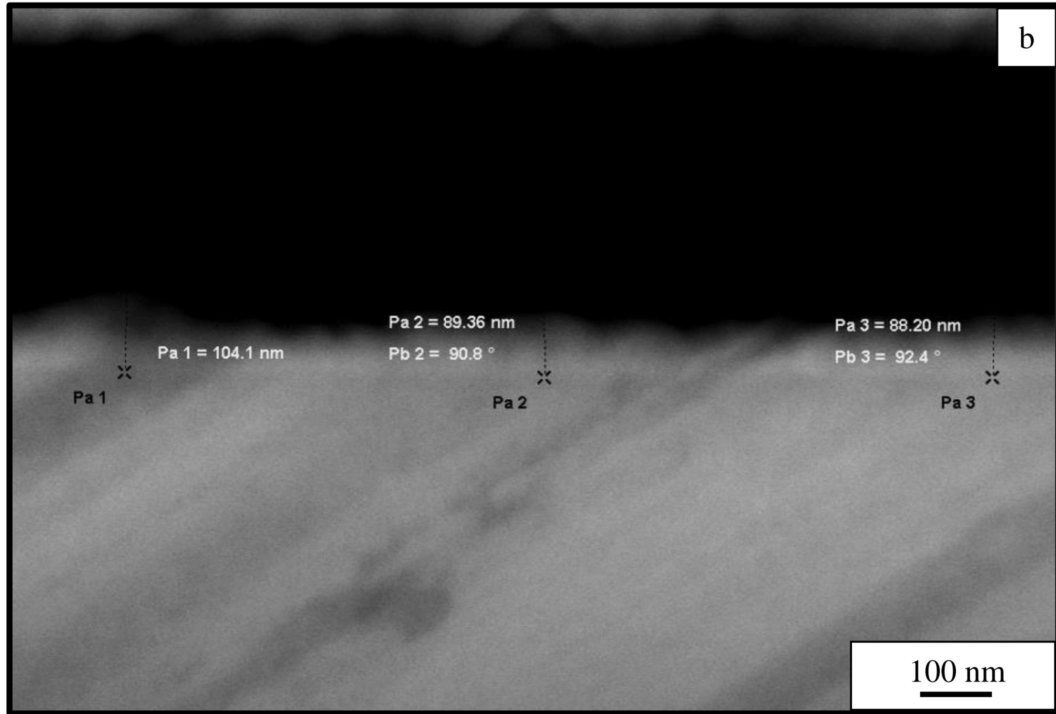

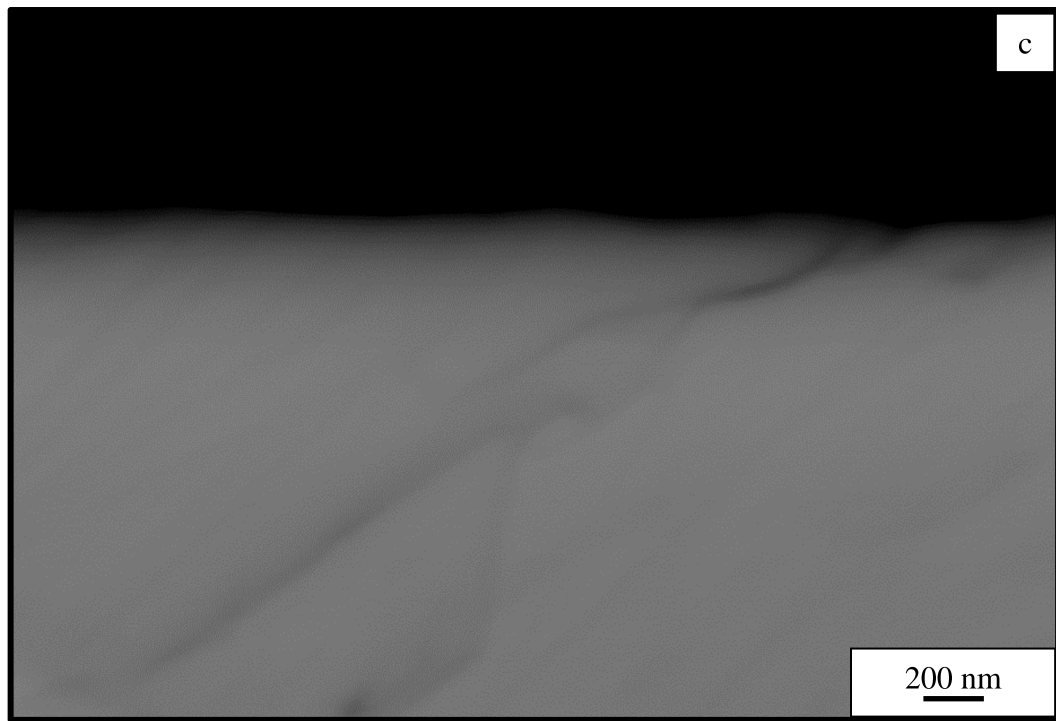

Figure 4.8 (Cont.) The back scattered images of samples a) YES-13, b) YES-06, and c) YES-11

ANADOLU ÜNİVERSİTESİ

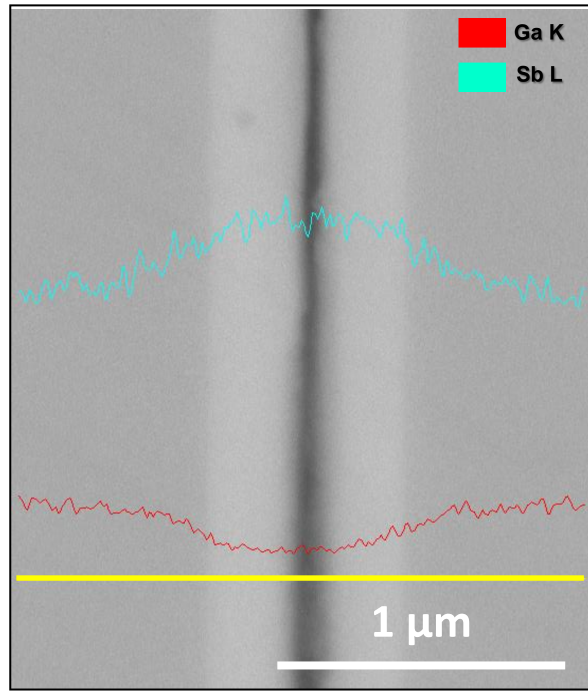

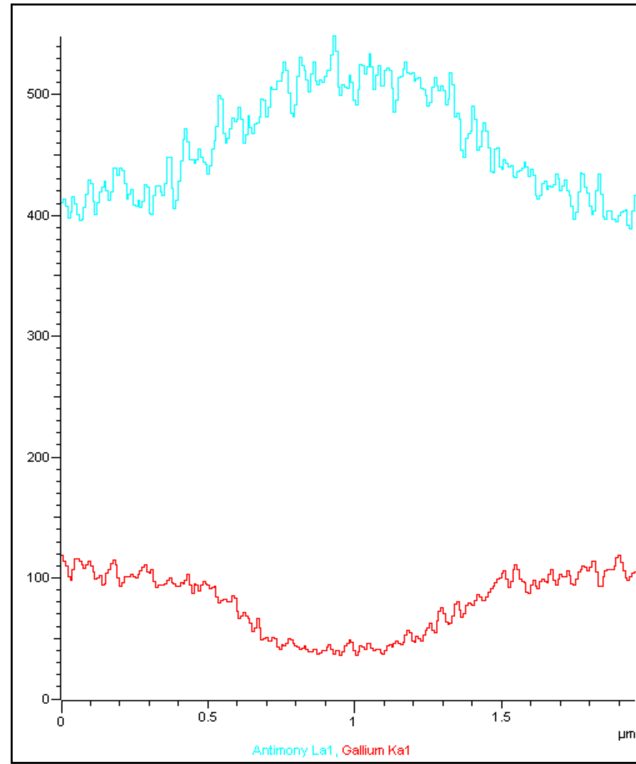

YES-13

Figure 4.9 SEM-EDX line analysis results for YES-13

ANADOLU ÜNİVERSİTESİ

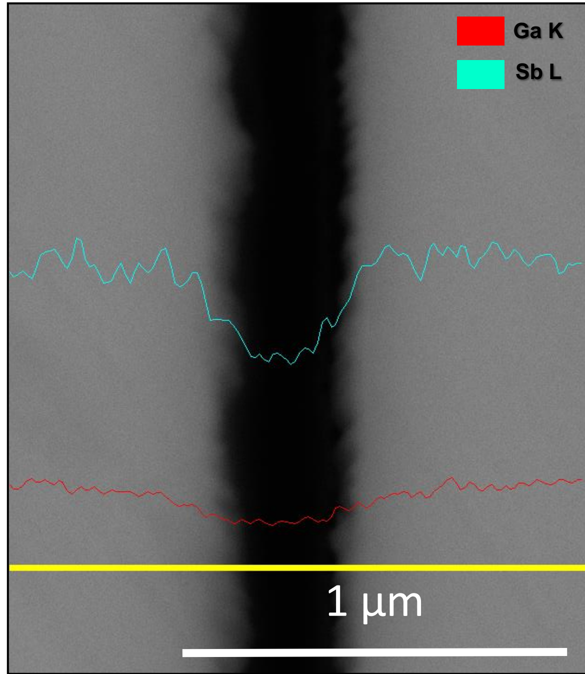

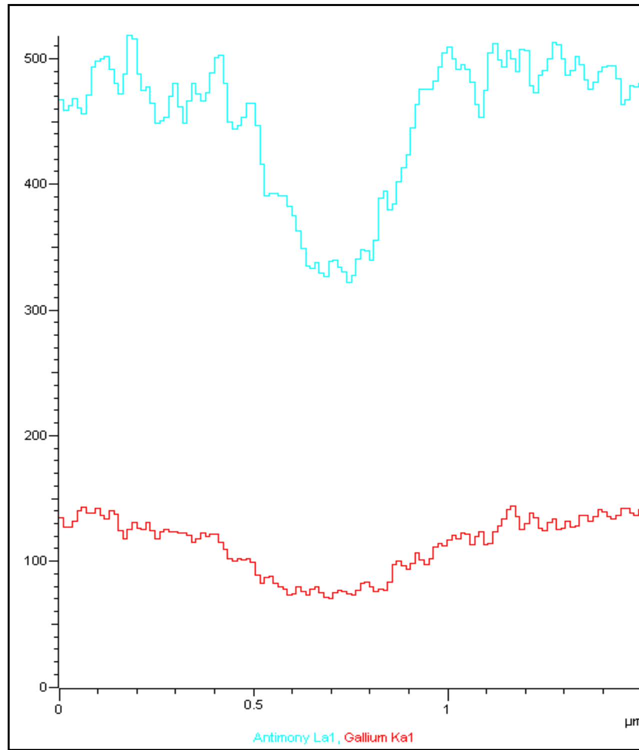

YES-06

Figure 4.10 SEM-EDX line analysis results for YES-06

ANADOLU ÜNİVERSİTESİ

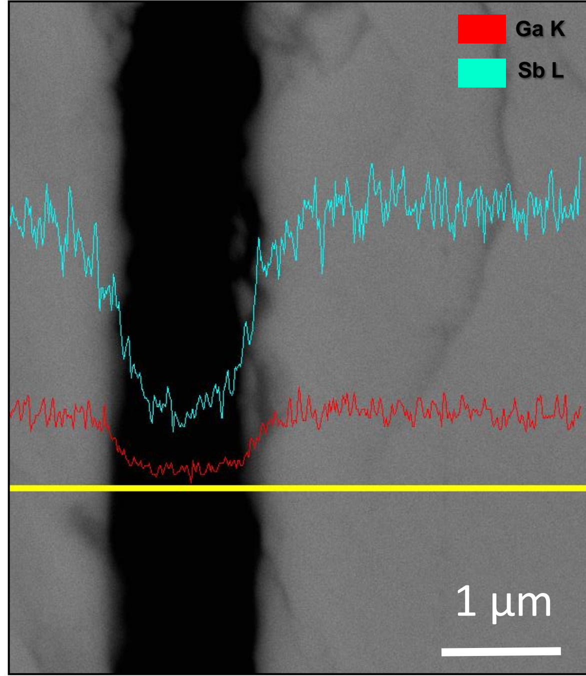

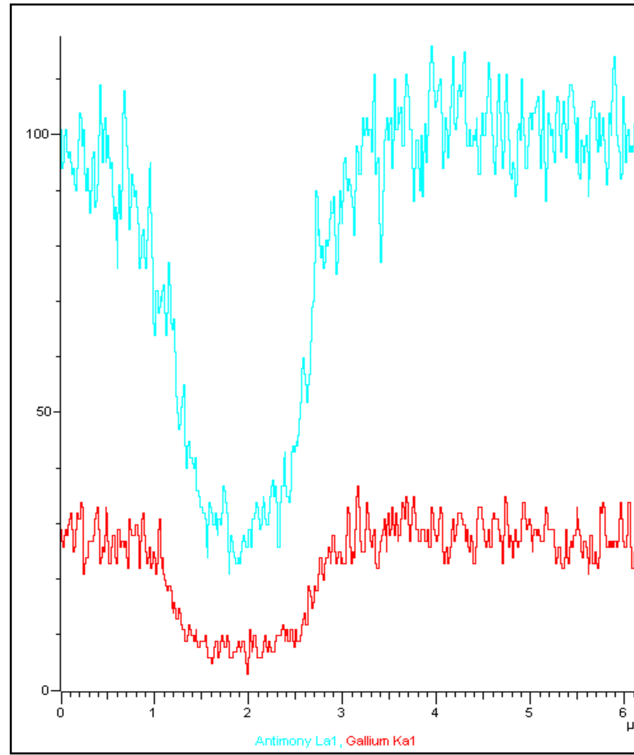

YES-11

Figure 4.11 SEM-EDX line analysis results for YES-11

ANADOLU ÜNİVERSİTESİ

The formation of the Sb layer is clearly evidenced for sample YES-13 by observing an increasing Sb signal towards the surface while the trend is opposite for Ga from the line analysis shown in Figure 4.9. Even though the interpretations of the line analyses are not as definite for other samples, the existence of an Sb layer it is still conclusive. So that, the ratio of the Sb signal to the Ga signal increases towards the surface. This ratio is shown for each sample in Figure 4.12 where the vertical dashed lines represent the centre of the gap between two glued pieces (see Figures 4.9 – 4.11). Since there is no material at the gap, both signals from Ga and Sb are reduced to a same level towards the centre of the graph. Additionally, the full width at half minimum (FWHM) of the well in the spectras for Sb is less than that for Ga as expected from samples having an extra Sb layer close to the surface. The approximate FWHM values for samples YES-06 and YES-11 are given in Table 4.2. For more definite results, different characterization techniques such as STEM-HAADF imaging should be carried out.

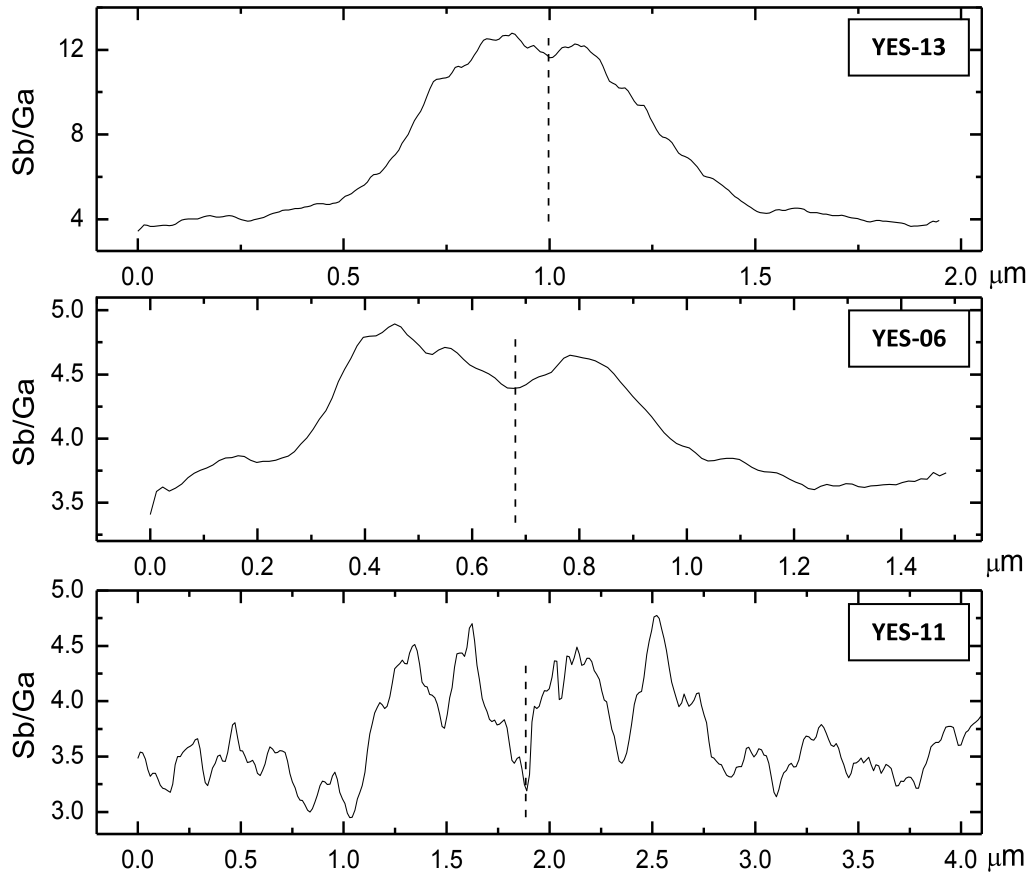

Figure 4.12 The ratio of the Sb signal to Ga signal for the samples YES-13, YES-06 and YES-11

ANADOLU ÜNİVERSİTESİ

Table 4.2 Measured FWHM values for samples YES-06 and YES-11

Sample	Sb	Ga
YES-06	~0.300 μm	~0.450 μm
YES-11	~1.400 μm	~1.500 μm

4.3. Characterization of InAs/GaSb Type-II Superlattices

As mentioned in the previous chapter, a set of InAs/GaSb SL structures designed for infrared detection were characterized with TEM techniques. In this set of samples individual layer thicknesses were kept constant but the interface (between InAs and GaSb) thicknesses were changed. After the sample preparation method was optimized for the structures, samples were comparatively characterized by (i) TEM-BF for overall microstructural consistency, (ii) HRTEM for interfaces and precise layer thicknesses, and (iii) by STEM for individual layer identification.

4.3.1. Optimization of Sample Preparation Method for TEM

One of the main difficulties for TEM analyses is the requirement of having well prepared samples. The required sample thickness (<100 nm) and specimen quality is crucial and directly influences the analyses. For the sake of visualization of the importance of sample preparation, TEM images taken from both improperly and properly prepared specimen of InAs/GaSb SLs are presented in Figure 4.13. As seen in the Figure, when the sample is not prepared neatly, no individual layers are observable.

ANADOLU ÜNİVERSİTESİ

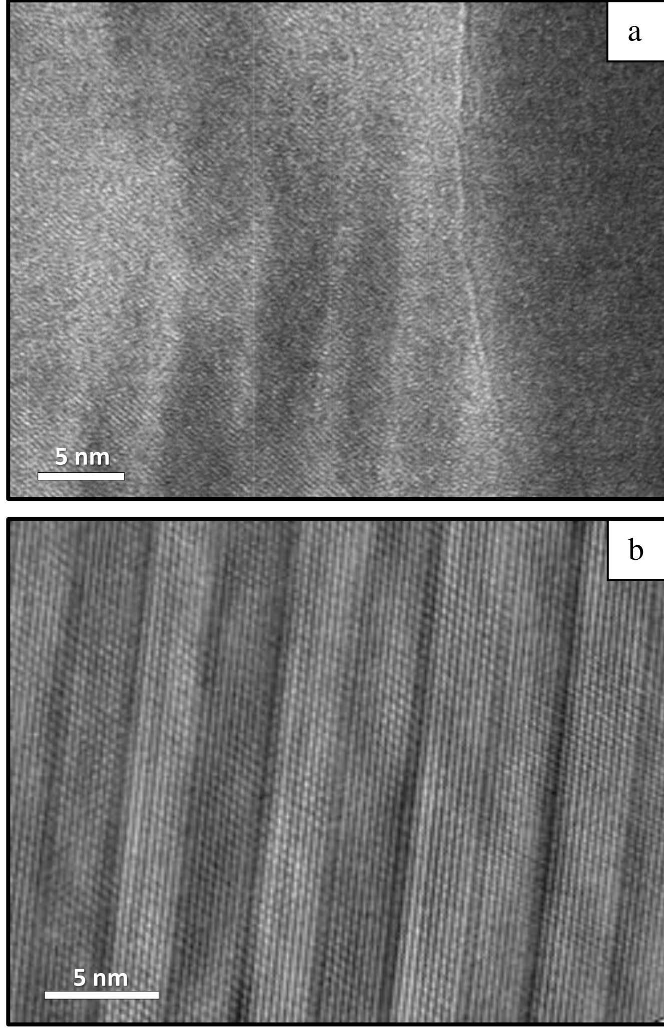

Figure 4.13 TEM images taken from a) improperly and b) properly prepared samples from type-II SL structure.

Through this thesis, adapted cross-sectional TEM sample preparation method was revised and parameters were optimized for our semiconductor nanostructures. A significant amount of time was spent during this improvements and an efficient with high success rate recipe was achieved. The noteworthy points are itemized below.

⇒ In diamond wire slicing optimum slicing thickness was determined as ~450μm in this study. For thinner strips, the probability of slicing without damaging the piece significantly decreases. On the other hand, the thicker pieces make the

ANADOLU ÜNİVERSİTESİ

mechanical thinning step longer and this leads to higher chance of damaging the sample.

⇒ It is preferable before ultrasonic disc cutting that the specimen (strip) is mechanically thinned to a certain value to make the cutting process safer for the piece. Because, if the strip is thicker, the cutting operation might not be accomplished as expected since it is more difficult to cut the sample successively. Another important point to take into consideration is that the specimen should not be thinner than 250µm. This may compromise the safety of the piece too since it becomes very fragile for possible damages. In the case that the strip is thinner, the probability of damaging increases. The visible light microscope (VLM) images of a thinner and a thicker sample are given in Figure 4.14.

Figure 4.14 The images of thicker (left) and thinner (right) samples after ultrasonic disc cutting. Thicker sample was not cut while the thinner sample was cracked during the process.

⇒ One should be careful in gluing the sample and the copper grid. The use of more than adequate epoxy causes the epoxy to spread on the sample's surface and leads to ineluctable contamination after the ion milling (the last step). Hence, the overmuch contamination comes from the sample not only complicates the analyses but also makes the results less reliable. An example VLM image of such case is presented in Figure 4.15a: the sample hole was formed after ion milling, but the residual epoxy created a thin film like an optically transparent membrane covering almost the entire opening. Only a small section of the sample hole has a

ANADOLU ÜNİVERSİTESİ

clear opening as seen from the image. If the gluing is carried out carefully and no epoxy is spread on the sample a clear opening over the entire sample hole is obtained after ion milling as shown in Figure 4.15b: no epoxy or contamination is visible on the sample after ion milling.

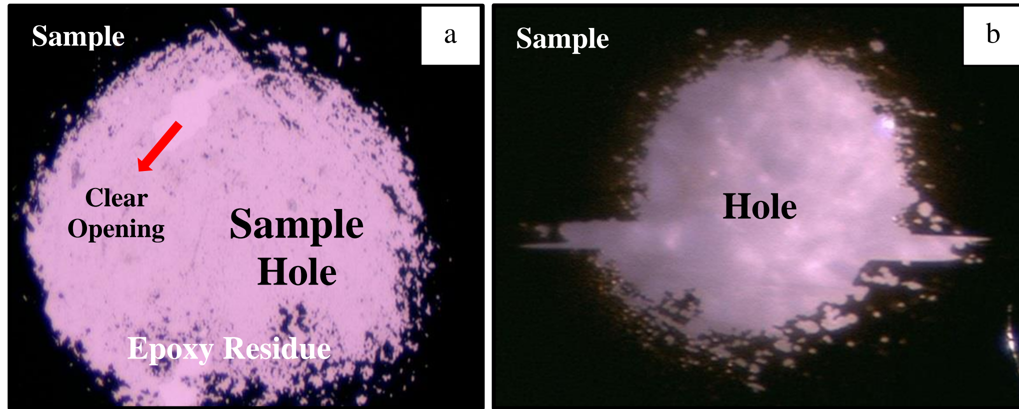

Figure 4.15 Example images of a) a sample with epoxy spread, and b) a successively glued sample onto the copper grid. The red arrow in (a) indicates the clear opening where there is no epoxy.

⇒ Through the practices it was experienced that the particle size of the diamonds on the lapping films seriously affects the durability of the sample during the thinning process. For our specific material system, when the thickness of the sample is less than ~150µm, the lapping film of particle size smaller than 9µm should be used otherwise the sample loses its physical endurance more and the abrasives having larger particle sizes damage the sample.

⇒ Dimpling parameters (weight and disc speed) were first optimized after many practices on dummy pieces: Correlation between the weight used and the dimple radius on the sample's surface was investigated. The increase in the weight makes the dimple radius larger and increases the probability of damaging the specimen during the process. The diameters of the samples are measured as 3.460 mm, 3.140 mm, 2.990 mm and 2.810 mm for the weights 37 g, 32 g, 27 g, and 22 g, respectively. The images of these unpolished dummies are presented in Figure 4.16.

ANADOLU ÜNİVERSİTESİ

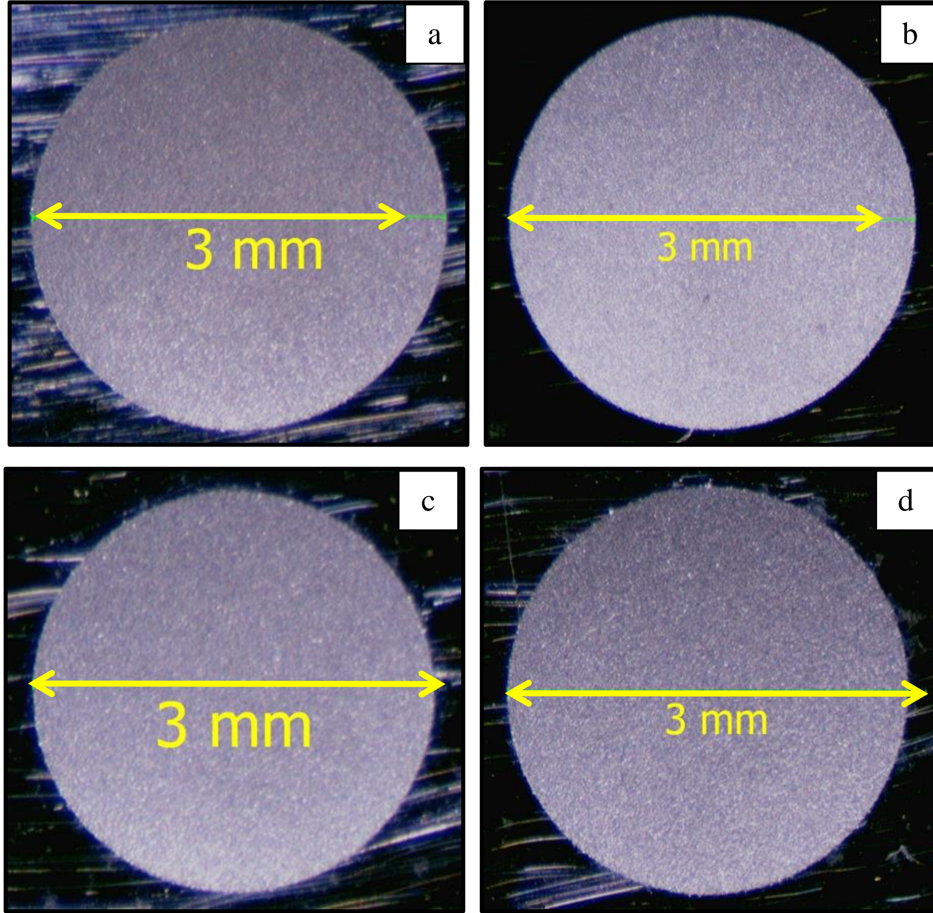

Figure 4.16 Samples with different dimple radius. Processes were performed with different weights: a) 37 g b) 32 g c) 27 g d) 22 g.

⇒ In ion milling stage, working at low energy induces fewer defects but makes the total thinning time longer. Once a hole is created through the sample, the angle and the accelerating voltage are continuously decreased down to 4º and 4 kV, respectively. Accelerating voltage of 3-7 keV and incident angle of 4º-10º were used as optimized ranges for our samples during the ion beam thinning operation.

The sample preparation studies are proceeded with many different parameters to optimize the recipe. As a result of these systematic studies, our starting recipe was revised and improved for better efficiency. In the latest version of our cross-section TEM sample preparation recipe "gluing the polished disc on a grid" and "dimpling" stages were removed from the process. This reduced the total time, and prevented the probable contaminations and the possible shadow

ANADOLU ÜNİVERSİTESİ

effects. The steps of the improved sample preparation method are summarized in Figure 4.17.

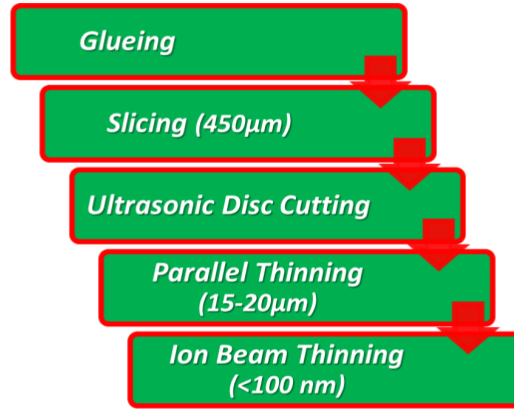

Figure 4.17 The latest improved specimen preparation stages

4.3.2. TEM - BF Imaging

Samples prepared from InAs/GaSb type-II SL structures with the modified sample preparation recipe for cross-section TEM analyses were first investigated with TEM-BF imaging technique mainly for their microstructural consistency and overall growth quality & accuracy. The periodic superlattice structure with a ~20 nm InAs cap layer for each sample is clearly demonstrated and representative images are presented in Figures 4.18-4.21.

ANADOLU ÜNİVERSİTESİ

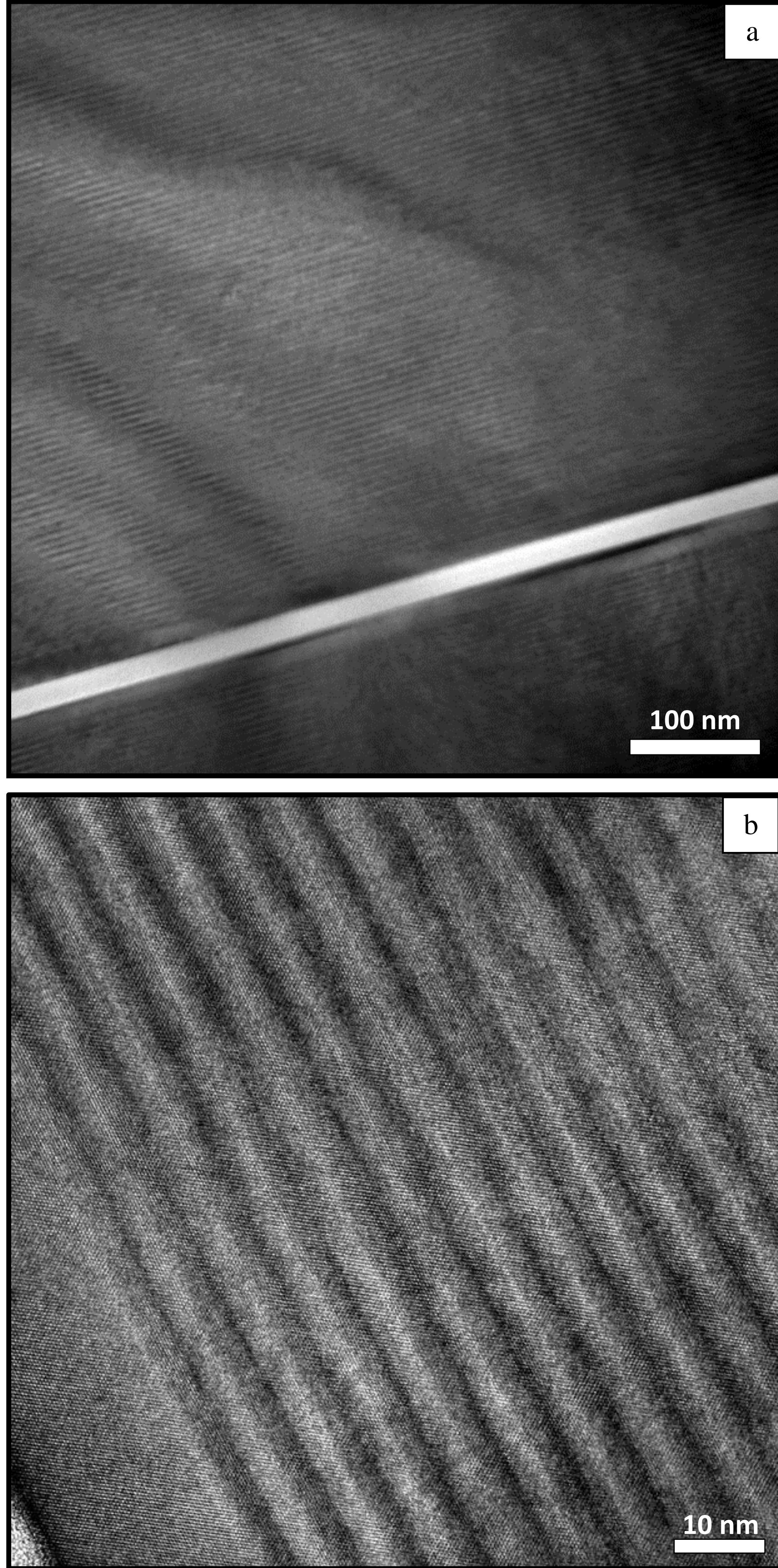

Figure 4.18 TEM-BF images of sample YES-16 at a) lower and b) higher magnifications.

ANADOLU ÜNİVERSİTESİ

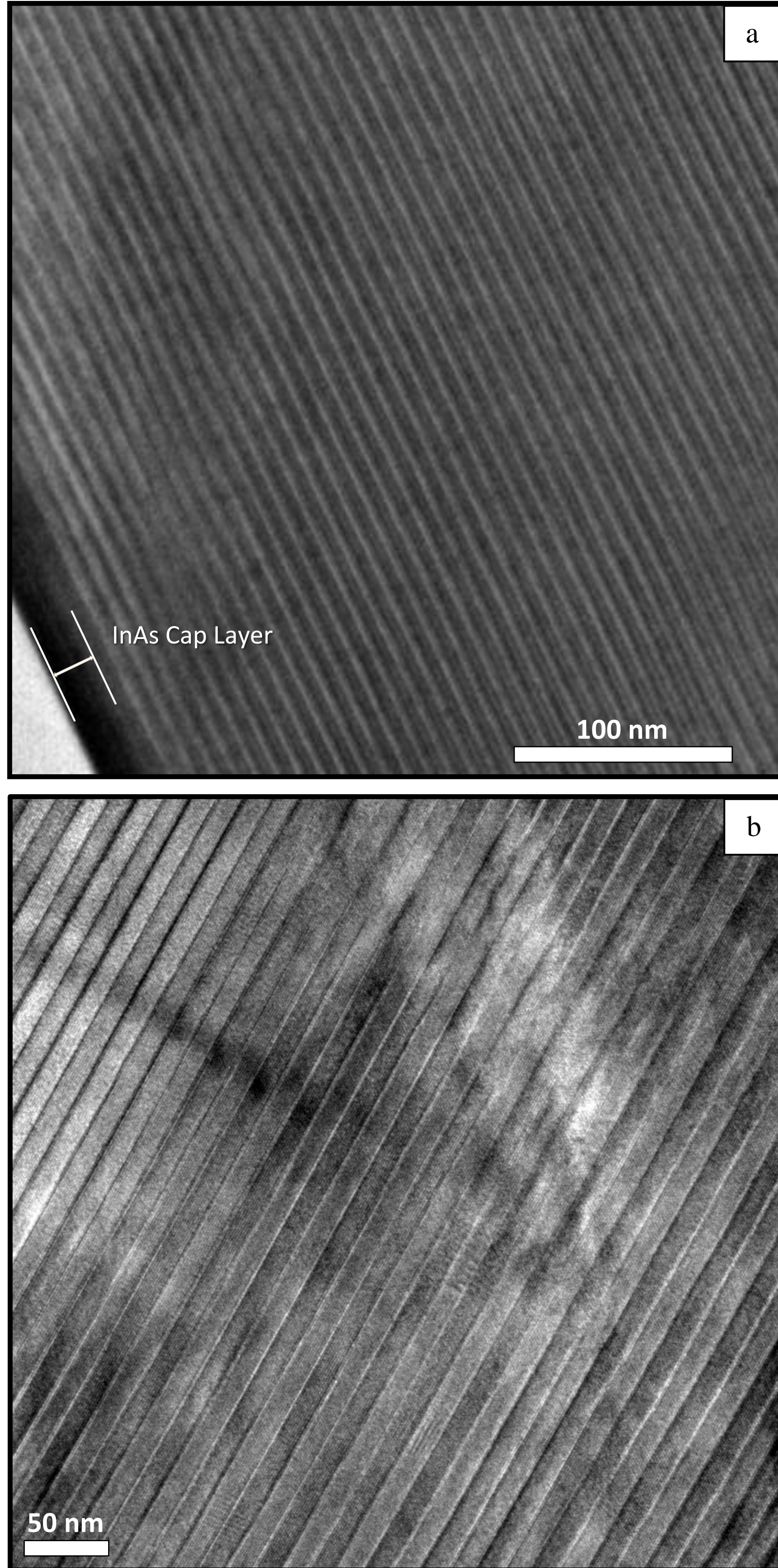

Figure 4.19 TEM-BF images of sample YES-15 at a) lower and b) higher magnifications.

ANADOLU ÜNİVERSİTESİ

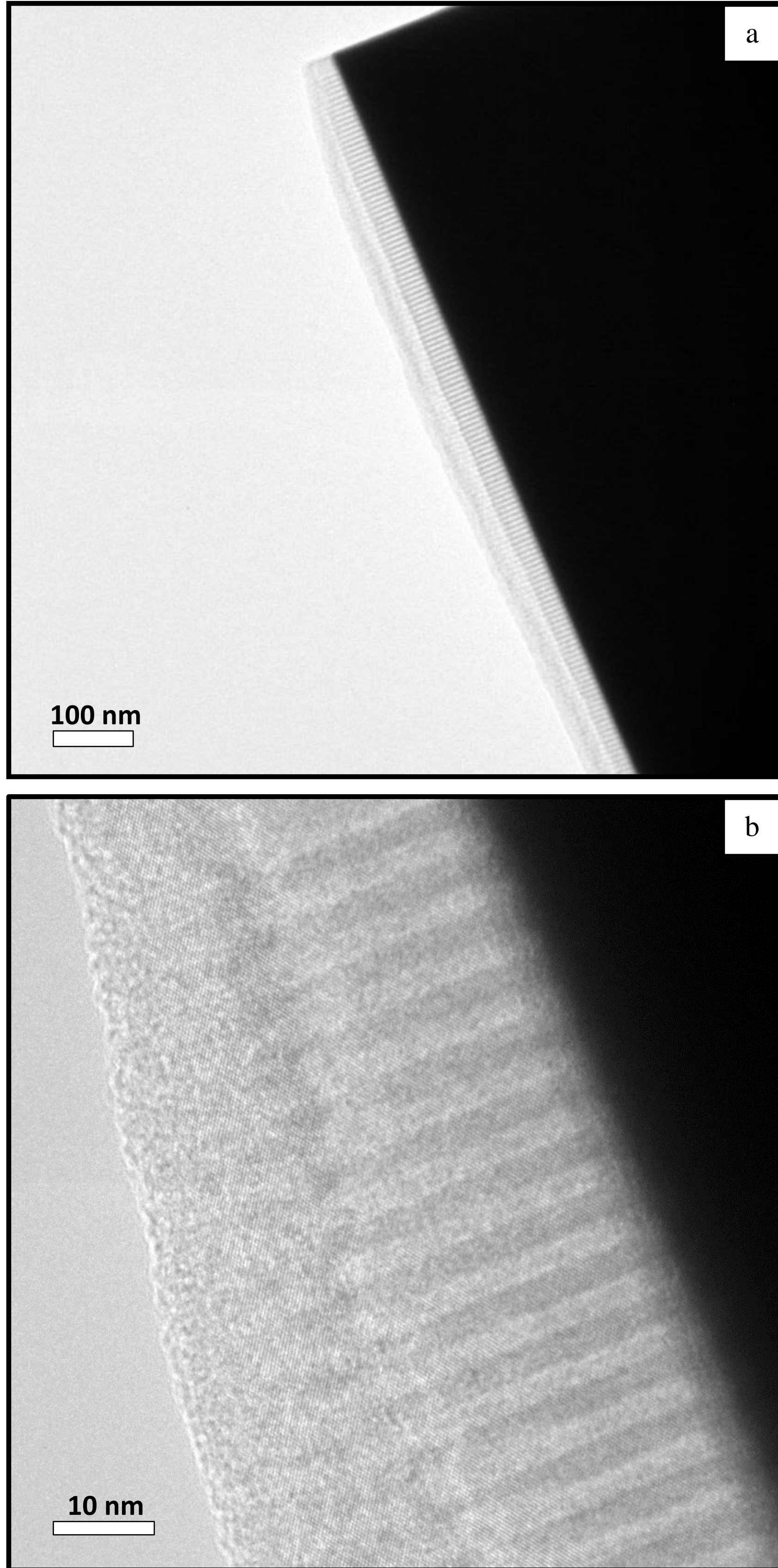

Figure 4.20 TEM-BF images of sample YES-17 at a) lower and b) higher magnifications.

ANADOLU ÜNİVERSİTESİ

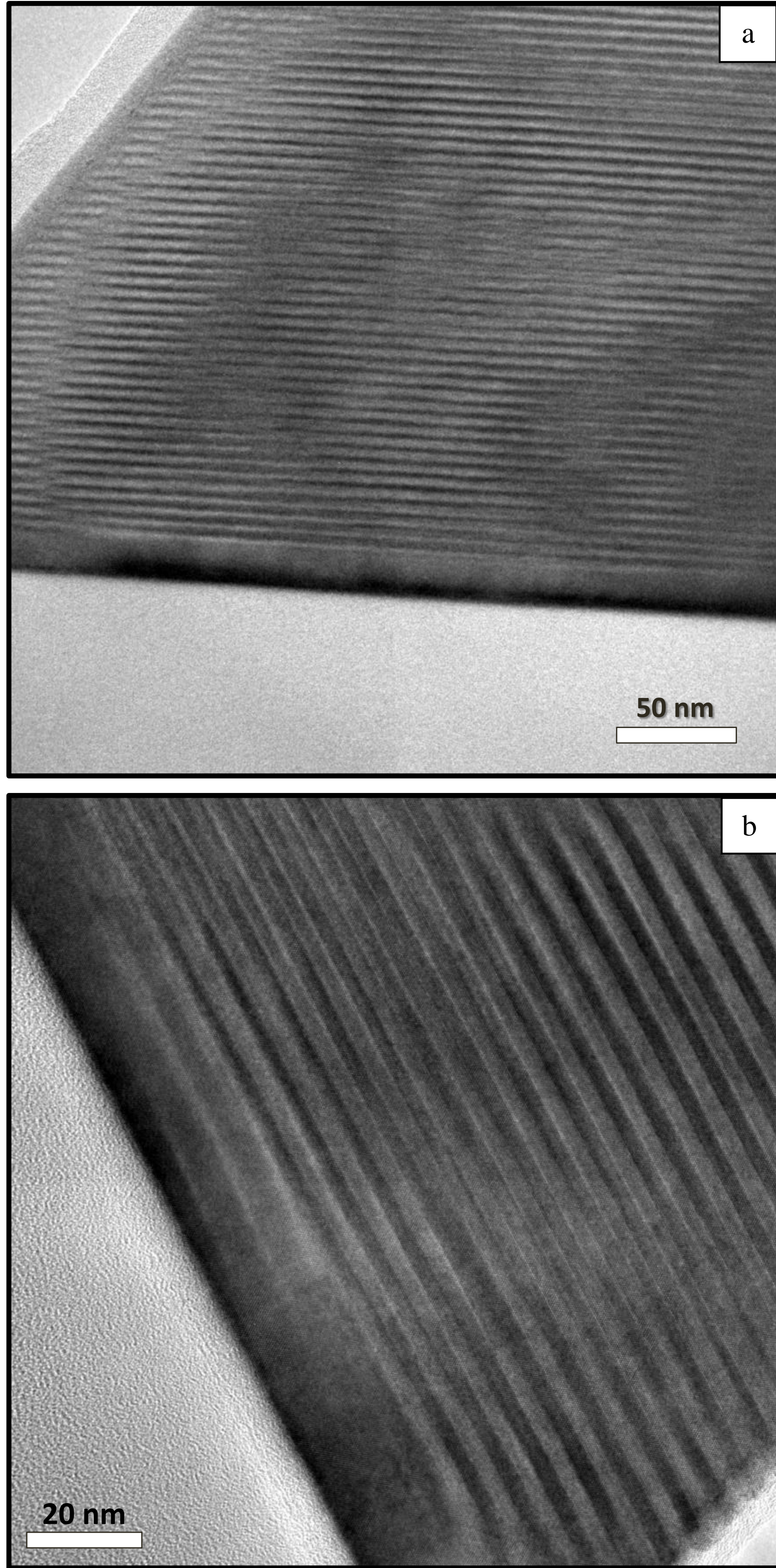

Figure 4.21 TEM-BF images of sample YES-18 at a) lower and b) higher magnifications.

ANADOLU ÜNİVERSİTESİ

In general, images revealed good crystalline quality with the absence of threading dislocations and almost no other visible defects. Within the accuracy of this technique, the observed individual layer thicknesses are in good agreement with the targeted thicknesses. Images in Figure 4.20 are particularly interesting because they were taken from the part of the sample where the thinning occurred parallel to the plane of layers not in the growth direction (i.e. perpendicular to the plane of layers) as in all other images. This caused sample and the images to be very uniform. The observed wave-like features in the contrast throughout the images in Figure 4.18a and Figure 4.21a are most probably the effect of the beam damage. In fact, this may also be caused by the sample preparation such that the uneven sample thicknesses in the investigated region results in such waviness in the images. So, they are not structural defects arising from the growth conditions. However, in one of the samples (YES-18) some linear defects were observed as presented in Figure 4.22. The nature of this effect is not clear but its existence was confirmed by the images taken from another piece. As mentioned in sample preparation section, two pieces of which the epitaxial layers are facing each other are prepared at once. Images from both pieces are shown in Figure 4.22a and 4.22b; features like linear defect are observable for both as indicated on the images with red arrows.

ANADOLU ÜNİVERSİTESİ

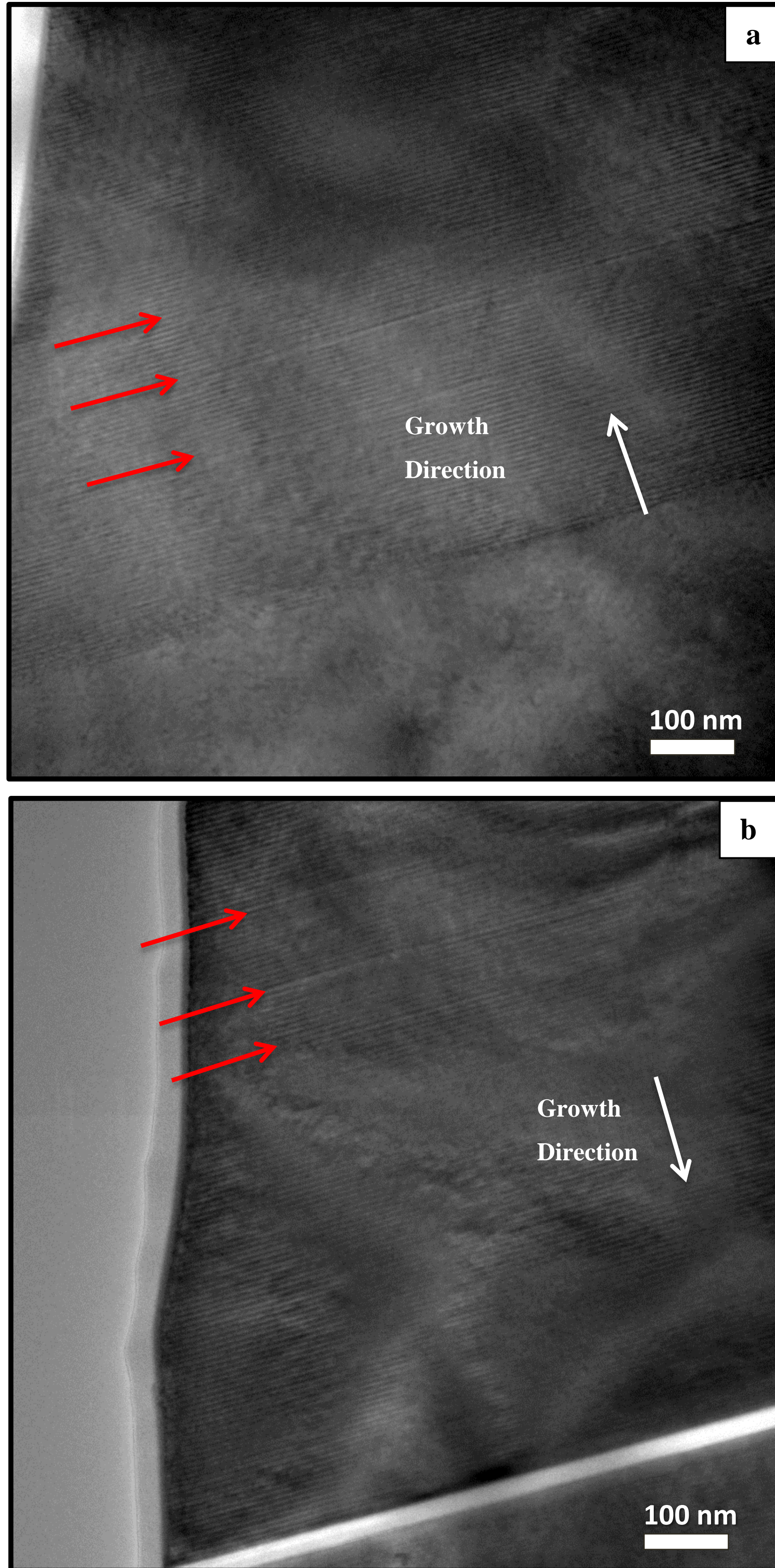

Figure 4.22 Linear defects on a) upper piece and b) lower piece of a superlattice structure (YES-18). The red arrows show the linear defects.

ANADOLU ÜNİVERSİTESİ

It is known that the contrast in TEM-BF images is created by the contribution of both the mass-thickness contrast and the diffraction in the structure: Thicker areas and the areas having bigger atomic mass appear in dark contrast [42]. For the structures studied, however, it is not possible to identify the consecutive layers as InAs or GaSb by using TEM-BF technique. The reasons are as follows: (1) The individual InAs and GaSb layer thicknesses are almost the same by design and therefore there is no visual identification point in the structures. (2) Total atomic mass of InAs (49+33=82) and GaSb (31+51=82) layers are equal therefore there is no region in the structure that can be atomically identified either. (3) Slight difference in the sample thickness throughout the surface may result in the observation of opposite contrast for the same layer depending on the location. In fact, this can be seen when the images (in Figure 4.19b for instance) are carefully investigated. (4) When the image is slightly out of focus, the contrast changes and also the interpretation ability on the layers weakens (see Figure 4.21b). In conclusion, it is safe to say that the interpretation of images is often obscured by the simultaneous occurrence of the contrast-forming events.

4.3.3. HRTEM Imaging

HRTEM has been extensively used for studying the interfaces between the successive layers in a superlattice structure. In this study, after the TEM-BF analyses, samples were investigated by using HRTEM technique for structural defects. A systematic set of SL structures with different InSb-like interface thicknesses for fixed InAs and GaSb layer thicknesses were characterized. Representative cross-sectional HRTEM images for the samples are shown in Figure 4.23 and Figure 4.24.

ANADOLU ÜNİVERSİTESİ

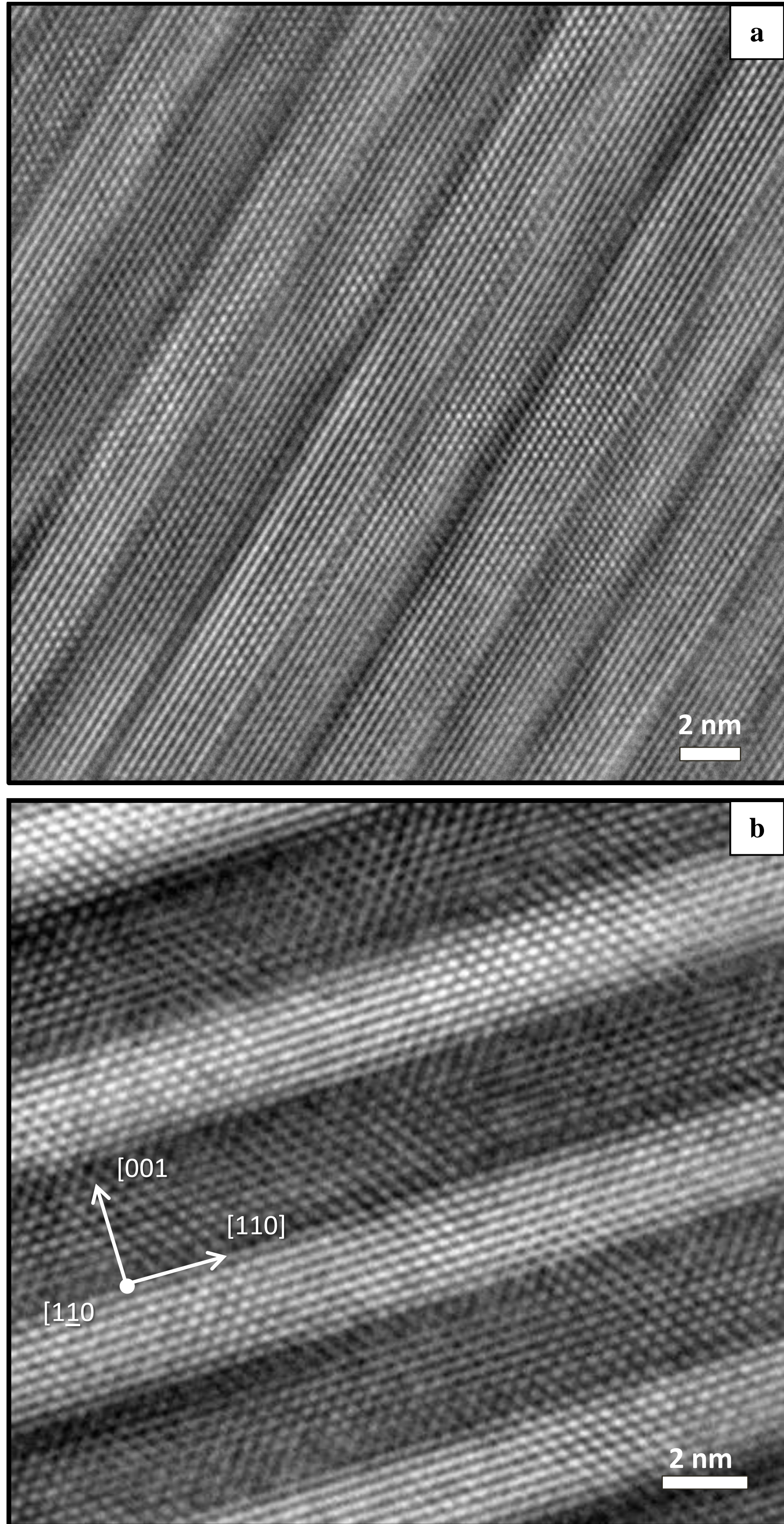

Figure 4.23 The HRTEM images of the samples a) YES-16 and b) YES-15.

ANADOLU ÜNİVERSİTESİ

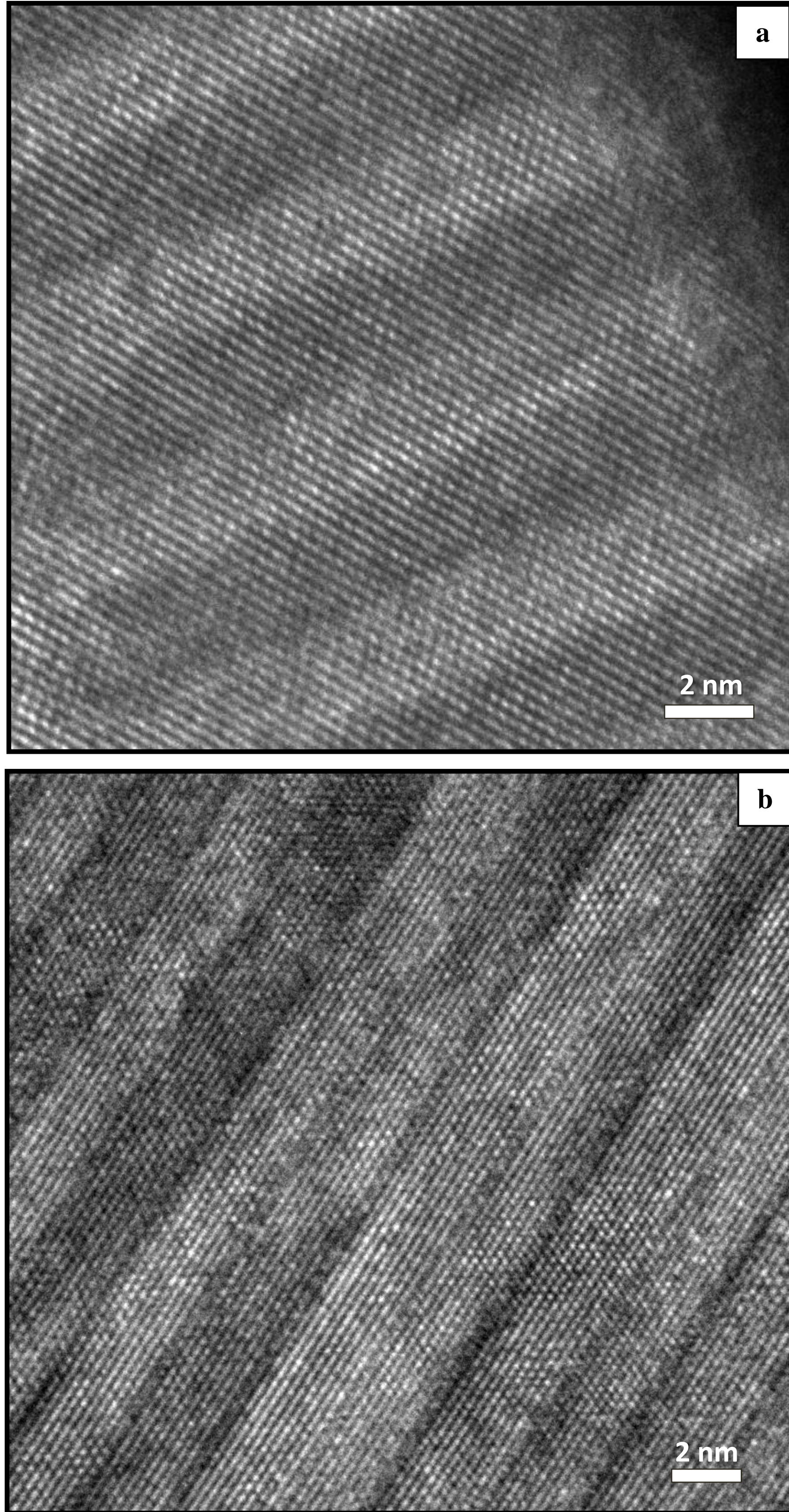

Figure 4.24 The HRTEM images of the samples a) YES-17 and b) YES-18

ANADOLU ÜNİVERSİTESİ

The cross-sectional high resolution images provided a condition to count the number of ML in each layer. Targeted layer thicknesses of 9 MLs for both InAs and GaSb layers were distinctly seen in high resolution images (see Figure 4.23). The structural qualities were evidenced with well-ordered lattice of atoms and well-defined InAs and GaSb individual layers were revealed. No evidence for any kind of defect such as dislocations was found.

The observed interfaces of the structures are very abrupt. But, they could not be examined in more detail because of the technical limitations of the microscope used in this study. The atoms at the interfaces could separately be seen with an "aberration corrected" TEM and thus even the sub-ML differences in the interfaces between the samples could be detected. The periodicity of the structures (total of one InAs layer, one GaSb layer and two interface thicknesses) was determined by high resolution x-ray rocking curve measurements performed around GaSb (004) symmetry axis with Panalytical X'Pert Pro MRD. A spectra obtained from one of the SL structures is shown in Figure 4.25 as an example. The sharp, well defined and long lasting (in angle) SL peaks around GaSb (004) substrate peak confirm high crystal quality. However, the periodicity that is extracted from the spacing between consecutive satellite peaks gives the total thickness of one period, but not the individual layer thicknesses. Nevertheless, the layer thicknesses for both InAs and GaSb layers had been confirmed by TEM analysis as 9 ML. It is therefore possible to extract the thickness of an InSb-like interface [8, 10]. Extracted SL periods and calculated interface thicknesses for the samples studied are summarized in Table 4.3. Note that no further details are given here since it is not within the scope of this thesis, but one can find the details elsewhere [10].

ANADOLU ÜNİVERSİTESİ

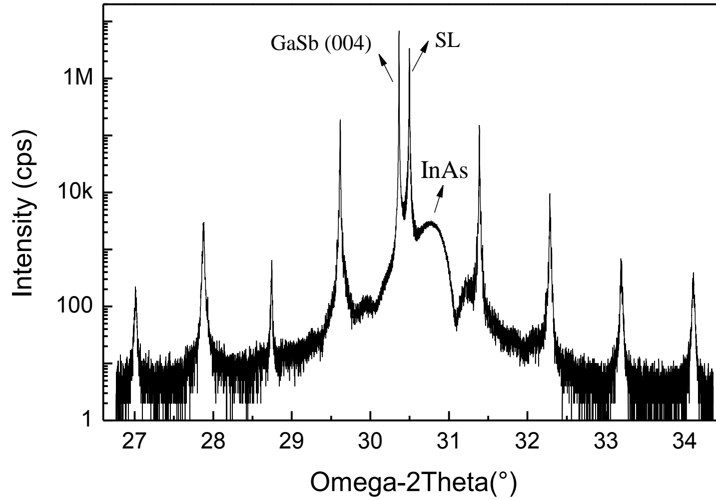

Figure 4.25 High resolution x-ray rocking curve around GaSb (004) of InAs/GaSb superlattice structure [10].

Table 4.3 The results of high resolution x-ray rocking curve analysis for each sample

Sample	SL period (Å)	Calculated Interface Thicknesses (ML)
YES-16	58.6 ± 0.1	0.60
YES-15	59.5 ± 0.1	0.74
YES-17	59.7 ± 0.1	0.77
YES-18	59.9 ± 0.1	0.80

Interpretation of the high resolution images is a momentous challenge. If the HRTEM analyses are done in a “noisy” room, the image quality degrades and interpreting becomes more difficult. For this reason, some signal processing techniques and/or computer simulations are used to make the interpretations easier. One of the common methods used for HRTEM images to get more accurate information by artificially removing the noise in the images is Wiener Filtering.

Examples of Wiener filtered HRTEM images are presented in Figure 4.26 where the filtering was applied for one of the images (from YES-17) with different noise reduction ratios: 3X, 6X and 10X. When it is applied for our images with proper noise reduction ratio, the interfaces were seen better with increased quality in

ANADOLU ÜNİVERSİTESİ

defining the positions of the atoms and their packing. However, one should be careful not to overdo the filtering; this results in very artificial looking images as in Figure 4.25d. For the noise filtering "EDM: Electron Direct Methods, Version 3.0" software was used.

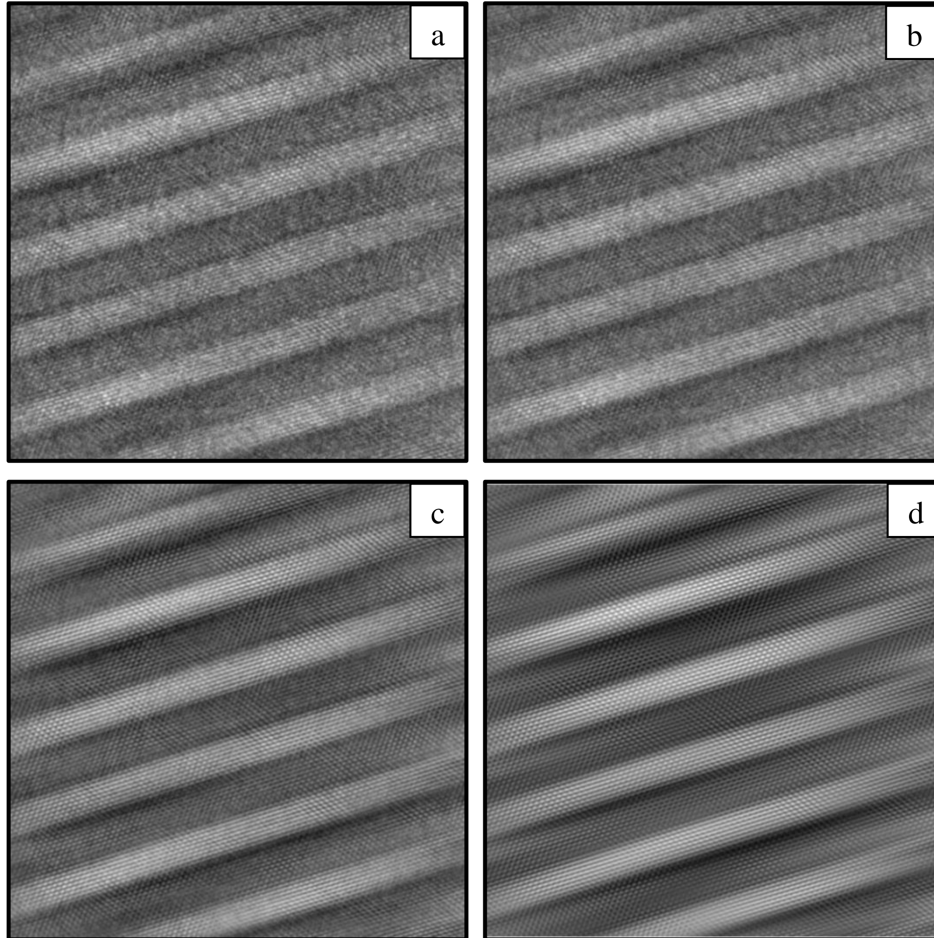

Figure 4.26 HRTEM images processed with Wiener filtering with variable noise reduction ratios: (a) no filtering, (b) 3X, (c) 6X, (d) 10X

4.3.4. STEM – HAADF Imaging

STEM-HAADF technique (Z-contrast imaging) is related to the atomic number contrast and used to examine the compositional differences in our samples. The images taken from the abovementioned set of SL samples are given below in Figure 4.27 and Figure 4.28.

ANADOLU ÜNİVERSİTESİ

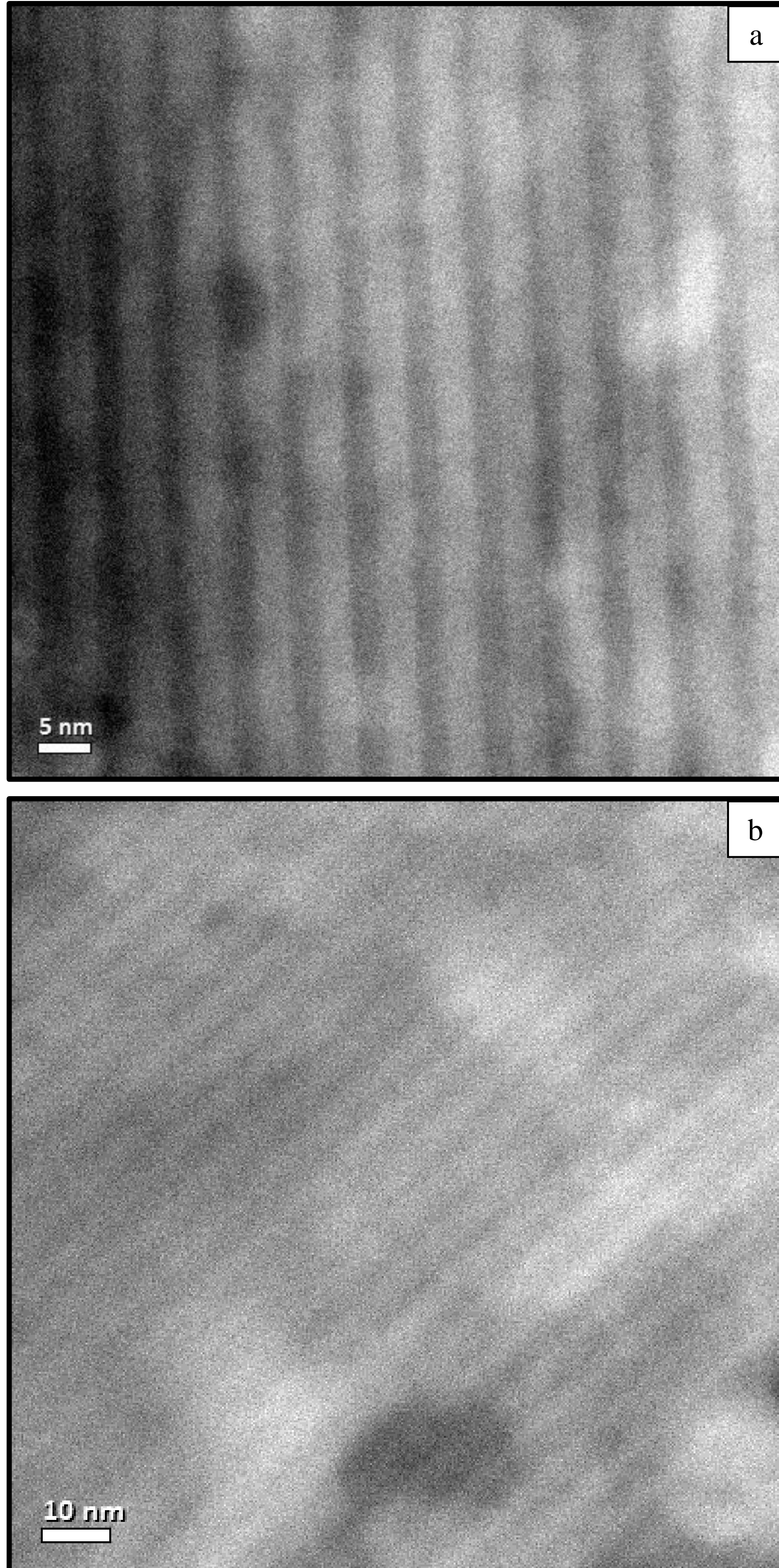

Figure 4.27 STEM-HAADF images of samples a) YES-16 and b) YES-15

ANADOLU ÜNİVERSİTESİ

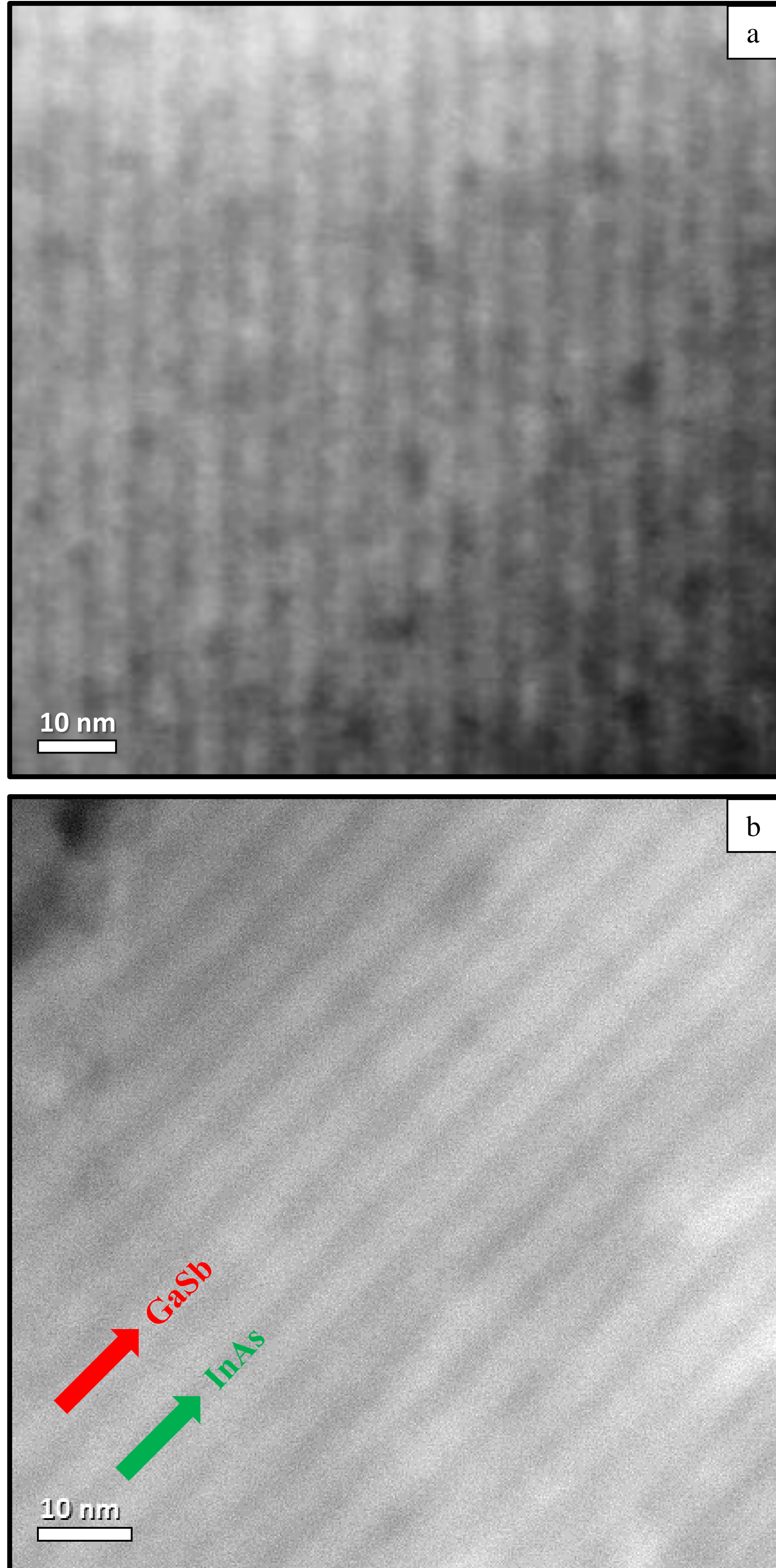

Figure 4.28 STEM-HAADF images of samples a) YES-17 and b) YES-18

ANADOLU ÜNİVERSİTESİ

The samples contain elements with different Z-values: Ga (Z: 31), Sb (Z: 51) and In (Z: 49), As (Z: 33). So that, the atomic contrast is sufficient to differentiate InAs and GaSb layers as labelled in Figure 4.28b. The dominant character of Sb having the highest atomic number of all made GaSb layer appear as bright in the TEM-BF images. This identification was also used for STEM-HAADF results.

4.3.5. STEM – EDX Analyses

The compositional analyses were carried out with STEM-EDX technique. It is mainly intended to verify the distribution of the containing elements. From the EDX line scan analyses performed in the growth direction (i.e. perpendicular to the observed layers) of such cross sectional samples; one would expect to differentiate the compositional changes between successive layers. The spectras obtained through the analyses are presented in Figure 4.29 and the images on which the results of the line scans are associated are presented in Figure 4.30 to Figure 4.33.

ANADOLU ÜNİVERSİTESİ

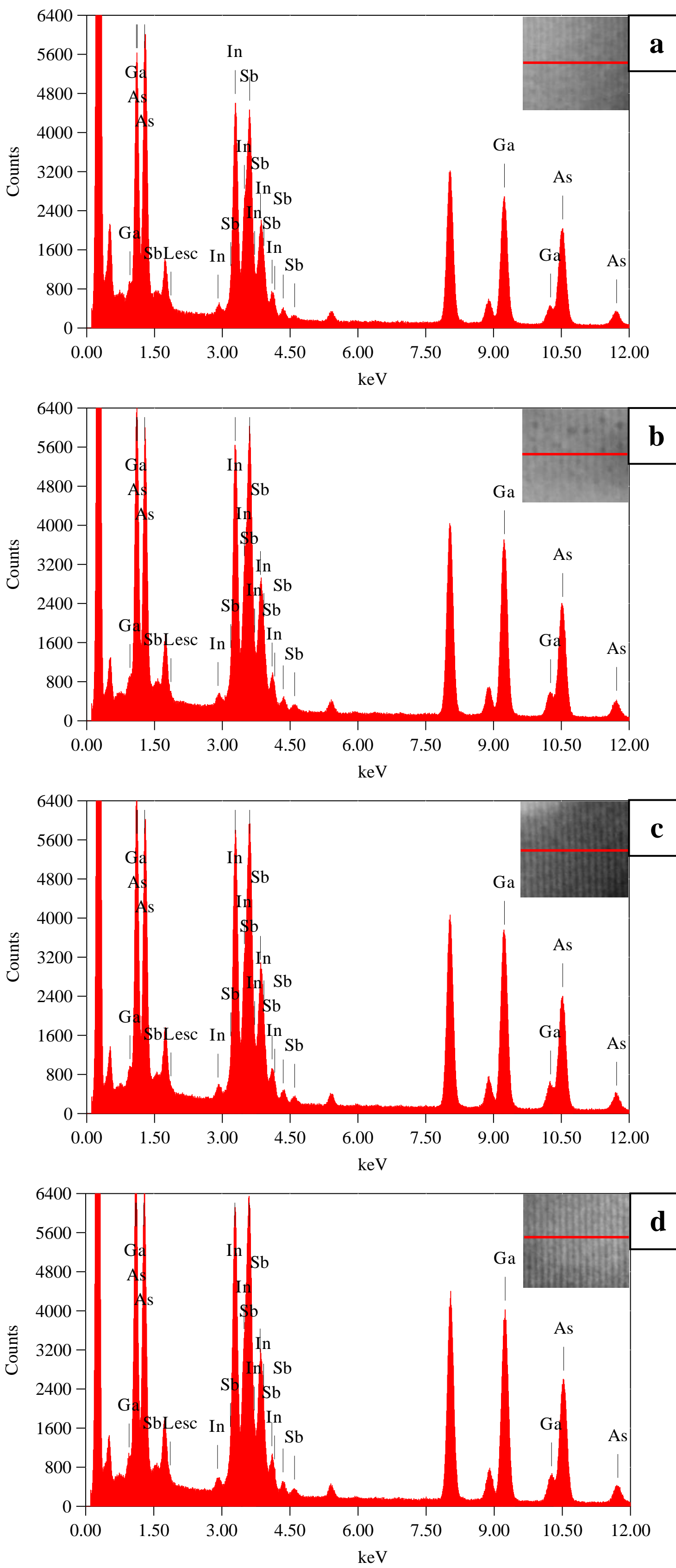

Figure 4.29 STEM-EDX line analysis spectras of a) YES-16 b) YES-15 c) YES-17 d) YES-18

ANADOLU ÜNİVERSİTESİ

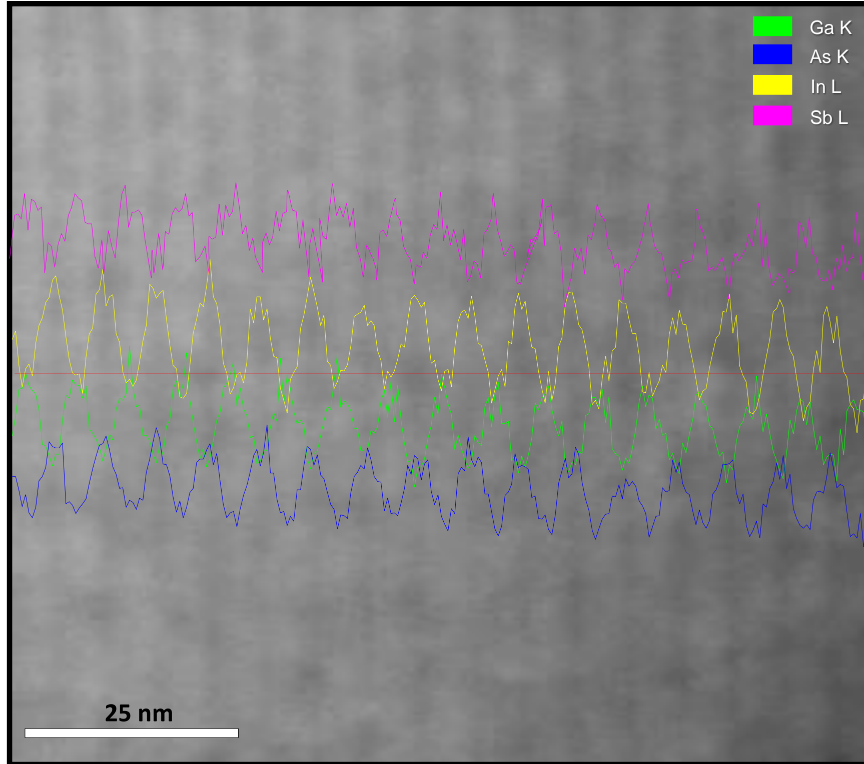

Figure 4.30 STEM-EDX line analysis spectra of sample YES-16

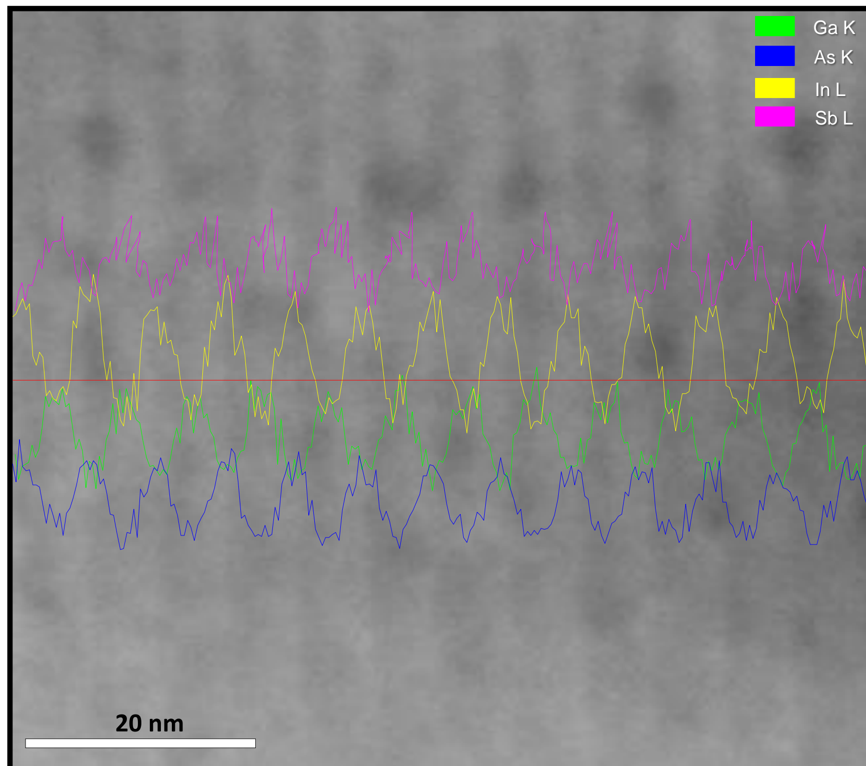

Figure 4.31 STEM-EDX line analysis spectra of sample YES-15

ANADOLU ÜNİVERSİTESİ

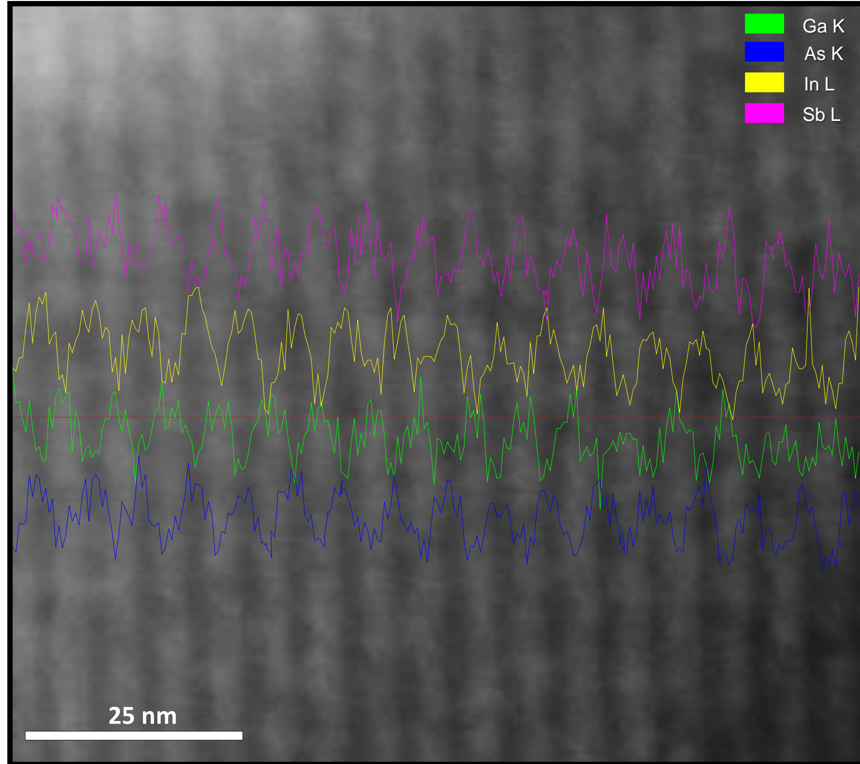

Figure 4.32 STEM-EDX line analysis spectra of sample YES-17

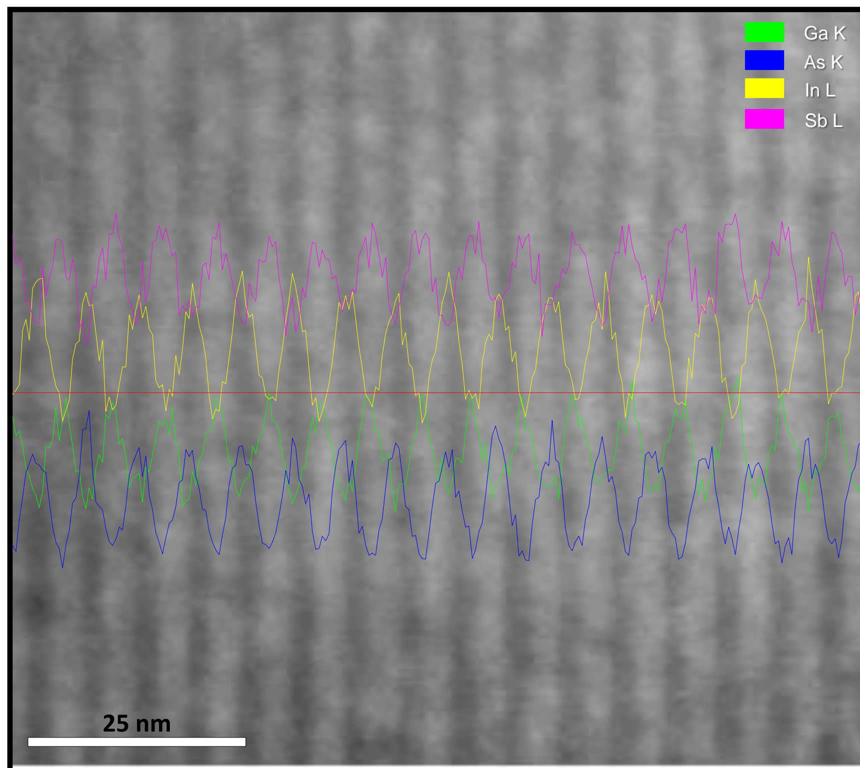

Figure 4.33 STEM-EDX line analysis spectra of sample YES-18

ANADOLU ÜNİVERSİTESİ

In the STEM-EDX analyses, all the peaks associated with the elements Ga, As, In and Sb are clearly resolved. The other peaks seen in the spectras (not labelled) are not related to the SL structures; they come from the TEM sample holder (e.g. Cu) and/or from the contaminations on the sample. Through the STEM-EDX line scan, the elemental distributions of the structures were inspected in detail: The individual InAs and GaSb layers were distinguished according to their elemental differences. The GaSb layers seem brighter and the InAs layers seem darker. After STEM-EDX line analyses were performed for each sample, for one of the samples (YES-17) STEM-EDX point analyses were carried out. The related STEM-HAADF image is given in Figure 4.34 where the analysis points are indicated. The spectras and the table showing the quantitative results are given in Figure 4.35 and Table 4.4, respectively.

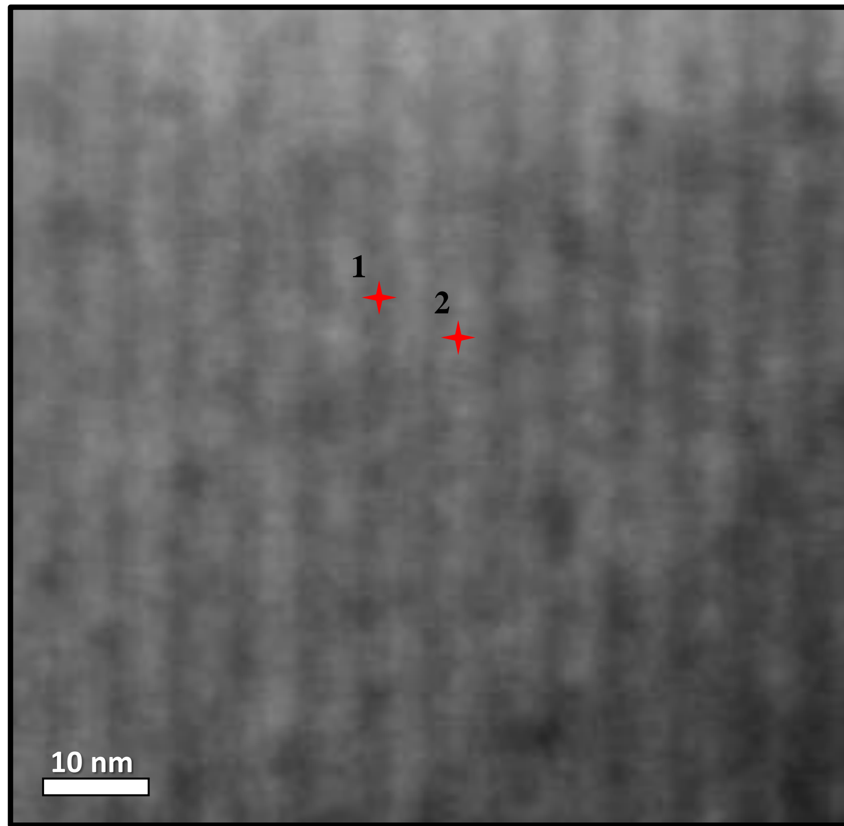

Figure 4.34 STEM-HAADF image of sample YES-17. STEM-EDX spot analyses were performed at the indicated points (YES-17).

ANADOLU ÜNİVERSİTESİ

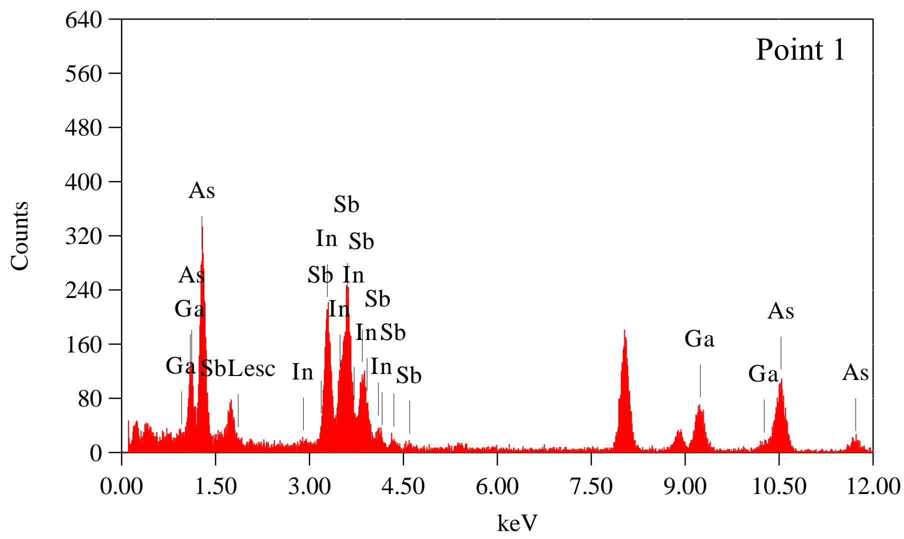

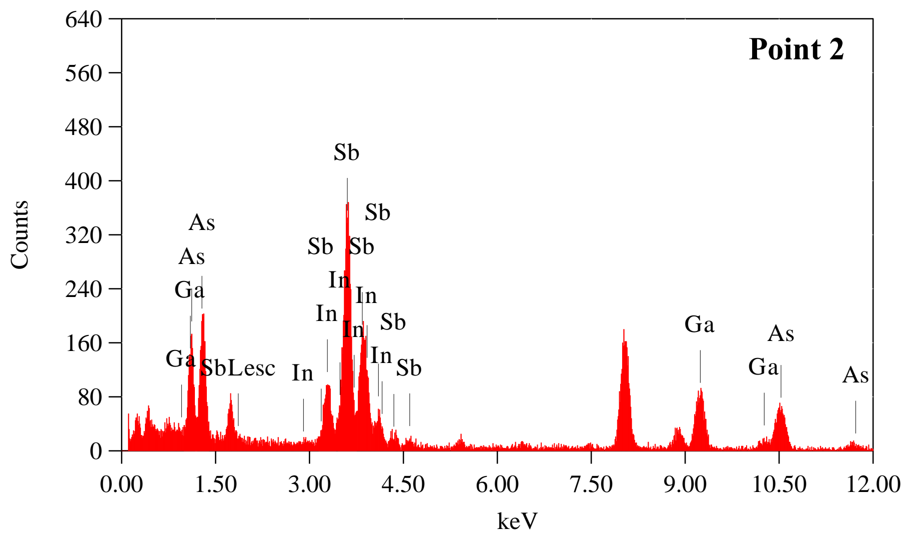

Figure 4.35 STEM-EDX point analyses spectras of Point 1 (top) and Point 2 (bottom)

Table 4.4 Quantitative results of STEM-EDX point analyses from the sample YES-17

	Atomic %	
Elements	**Point 1**	**Point 2**
Ga	14.59	22.02
As	25.36	11.83
In	37.60	25.48
Sb	22.45	40.67

ANADOLU ÜNİVERSİTESİ

Based on the previously identified layers (from STEM-HAADF images and STEM-EDX line analyses), two points were selected on InAs and GaSb layers each. Referring to Figure 4.34, Point 1 corresponds to InAs and Point 2 corresponds to GaSb layers. Theoretical mass percentage of GaSb is (Ga: 69.723, Sb: 121.760) 36.412% for Ga and 63.588% for Sb and the mass percentage of InAs is (As: 74.921, In: 114.818) 39.487% for As and 60.513% for In [69]. However, the obtained values through the quantification are not really close to these theoretically expected values. The reason is the fact that when the GaSb layer was under investigation, signals were collected not only from the GaSb layer itself but also from the surrounding InAs layers because of the relatively large interaction volumes. Nevertheless, the mass percentage ratios of Ga/Sb and As/In were found as only ~5% and ~3% off respectively from the theoretical ratio.

4.3.6. EFTEM Study

In EFTEM technique, inelastically scattered electrons which generate noise in the images are restrained, thus contrast is enhanced. This technique provides high resolution elemental mapping for many materials according to their characteristic energy loses after interacting with the samples, even for light elements [65]. For one of the samples (YES-17), EFTEM three-window elemental mapping was carried out and the results are presented in Figure 4.36: the maps of Sb M4,5 edge with 527 eV energy loss and In M4,5 edge with 443.1 eV energy loss are shown in Figure 4.36a and 4.36b respectively. As in Figure 4.36c the combined map of In and Sb elements are presented.

ANADOLU ÜNİVERSİTESİ

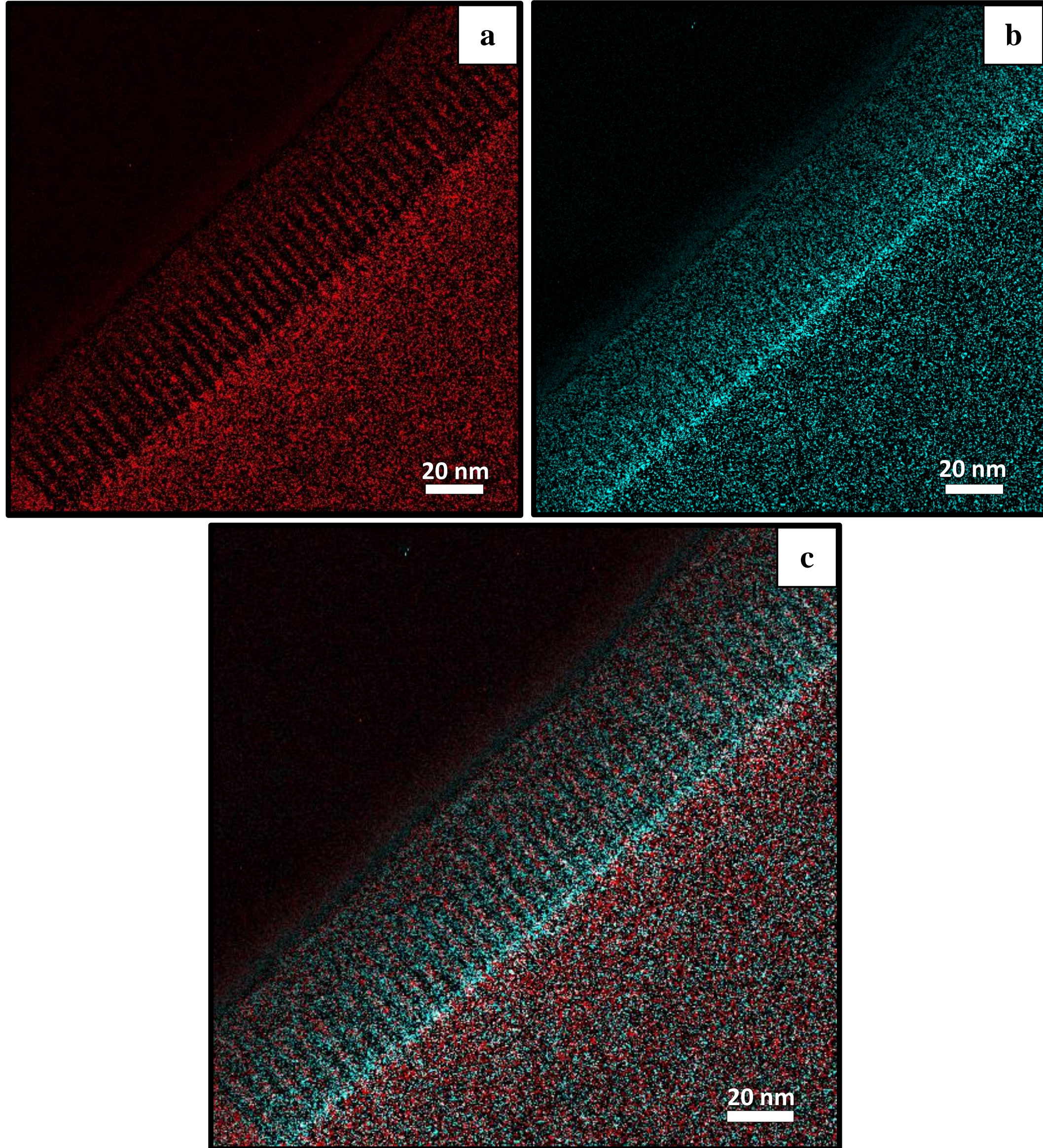

Figure 4.36 Three-window elemental maps: a) the map of Sb $M_{4,5}$ edge with 527 eV energy loss, b) the map of In $M_{4,5}$ edge with 443.1 eV energy loss In c) the unified map of both In and Sb elements

Through the EFTEM analyses the results of the STEM investigations were confirmed and the individual InAs and GaSb layers were compositionally identified. However, the layers could not be distinguished clear enough from each other. One possible reason is the thicknesses of the consecutive layers: each layer is approximately 3 nm thick and the resolution of the technique is not enough to

ANADOLU ÜNİVERSİTESİ

resolve it any better than the presented. The bright band on the images (especially apparent in In map) is believed to be due to the abrupt thickness difference on the sample (see also Figure 4.20).

4.4. Investigation of GaSb Epilayer on GaAs substrate

The use of GaAs substrates for InAs/GaSb SL growth is an alternative approach since GaAs substrates are less expensive and technologically more matured compared to GaSb. But, it is more difficult to grow superlattices on GaAs substrates because of the increased lattice mismatch. One possible way considered to overcome this problem is to use an interface layer so that the lattice mismatch between GaAs and GaSb or alternative layers (InAs or InGaAs) can be reduced. Sample having AlSb QD layer that is proposed as a transition medium between GaAs and GaSb were characterized by TEM-BF and HRTEM techniques. The TEM-BF and HRTEM images manifesting the existence of the quantum dots are shown in Figure 4.37 and Figure 4.38, respectively. The GaAs substrate, interface with AlSb quantum dots and GaSb buffer layer were viewed in different magnifications. It is evidenced that the distribution of AlSb QDs and their sizes are uniform throughout the interface. The existence of the AlSb QDs at the interface is verified by the periodic change of intensity appeared as dark and bright spots on the images. It is however difficult to say which one is the AlSb dot; the appearances can be switched by changing the focus.

ANADOLU ÜNİVERSİTESİ

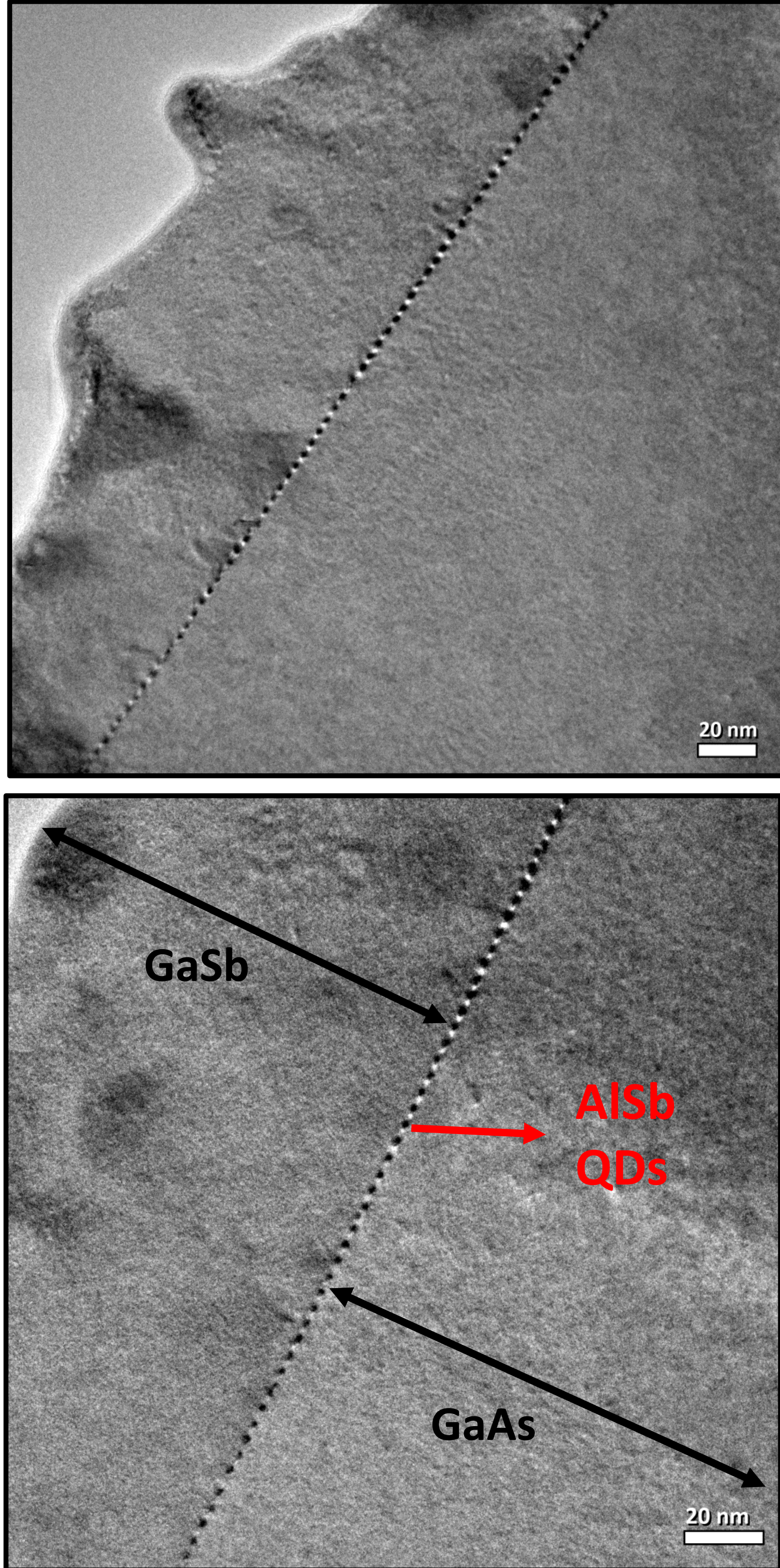

Figure 4.37 TEM-BF images of AlSb QDs with two different magnifications.

ANADOLU ÜNİVERSİTESİ

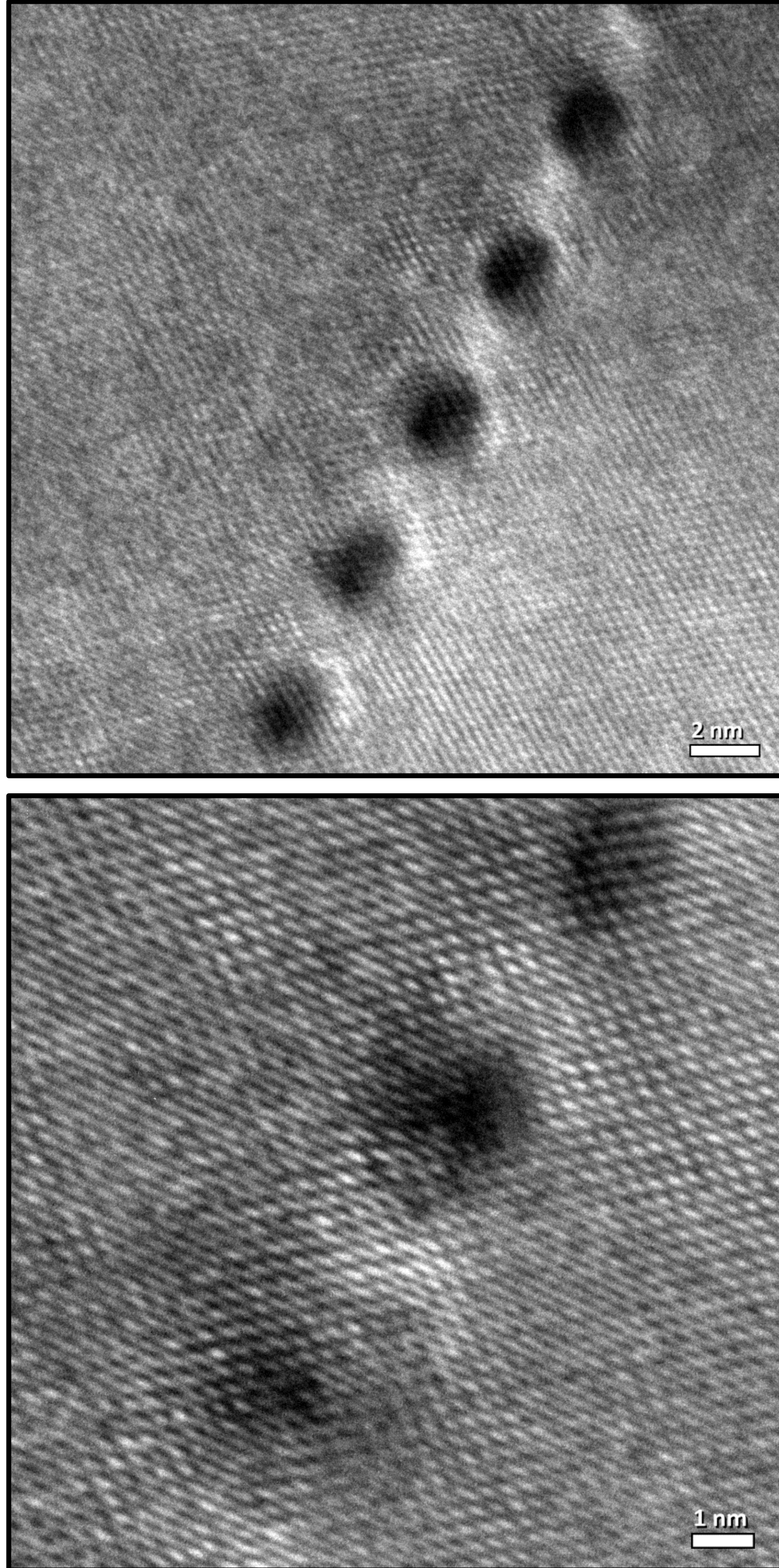

Figure 4.38 HRTEM images of AlSb QDs at different magnifications.

ANADOLU ÜNİVERSİTESİ

The STEM-HAADF images and STEM-EDX line analyses from the same sample are given in Figure 4.39, 4.40 and 4.41, respectively. The compositional difference between the GaAs substrate and the GaSb layer reveal itself in the STEM-HAADF image by a sharp change of contrast: GaSb layer seems brighter while GaAs layer seems darker. The observed gradient in contrast toward the surface for each layer is due to the wedged sample: the thickness of the sample in the investigated region is gradually decreasing towards the surface. Thus, the collected signal is gradually decreasing too. This is also verified by the decreasing nature of the signal lines presented in Figure 4.41. Despite their doubtless observation in TEM-BF and HRTEM images, QDs could not be observed in STEM studies with the existing equipment in our TEM. Consequently, despite its challenging growth, decent GaSb epilayer were grown on GaAs substrate by introducing an AlSb interface. Good surface quality without any defects was visualized by the image presented in Figure 4.42. The image was taken by using in-lens detector.

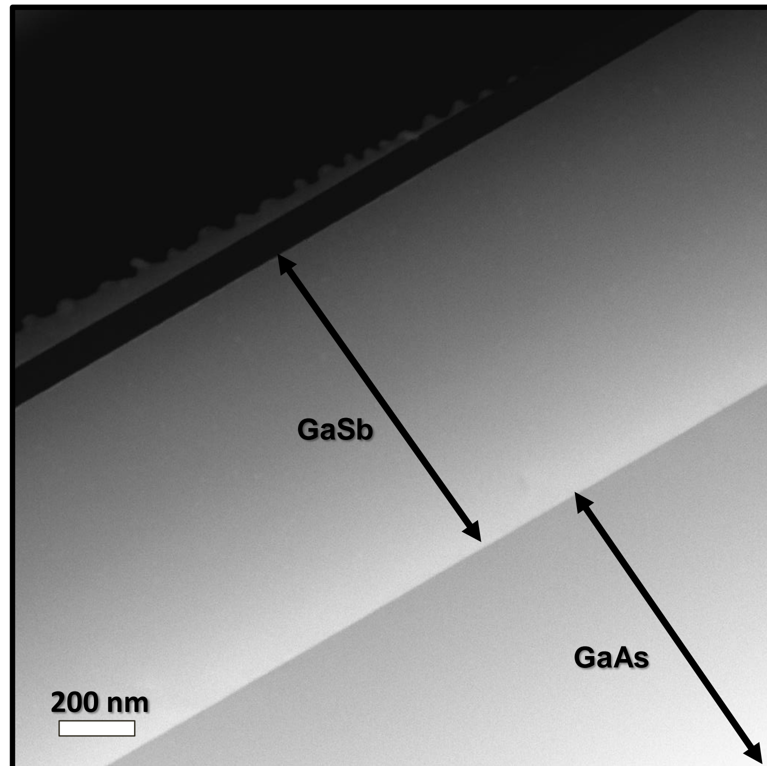

Figure 4.39 STEM-HAADF image of sample YES-19: GaSb epilayer grown on GaAs substrate

ANADOLU ÜNİVERSİTESİ

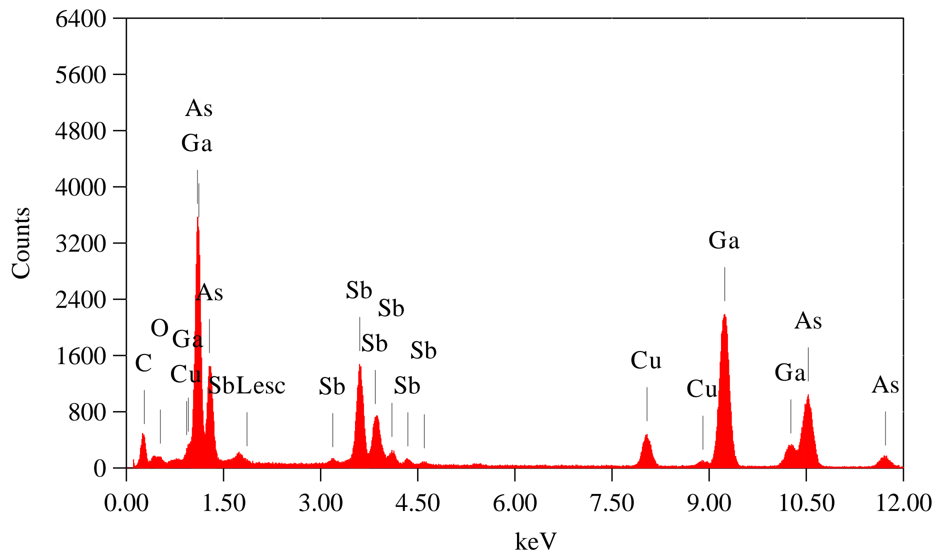

Figure 4.40 STEM-EDX spectra of sample YES-19: GaSb epilayer grown on GaAs substrate

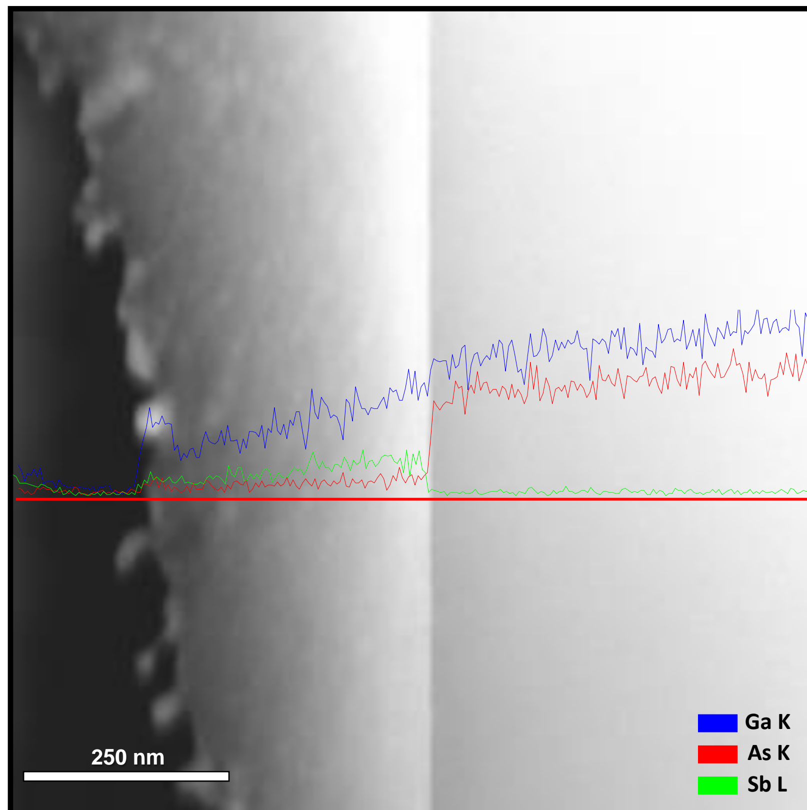

Figure 4.41 STEM-EDX line analysis of sample YES-19: GaSb epilayer grown on GaAs substrate

ANADOLU ÜNİVERSİTESİ

Figure 4.42 The surface images of sample YES-19 taken with in-lens detector. No clear defects observed.

4.5. Observation of InAs Self-assembled Quantum Dots

The shape and size of the QDs, their density (number of QDs per area) and the uniformity throughout the substrate are significant for the device performances [54, 55]. Depending on the ultimate goal their appearance can be altered since they are strongly subject to the growth conditions. In this study, a set of five InAs/GaAs QD samples grown with different parameters were investigated. The samples have two separate QD layers, one is buried in GaAs and the other is left uncapped at the surface. All of the samples were characterized from their surfaces by SEM to determine the size and the density of the quantum dots. One of the samples was then investigated in detail with TEM-BF, HRTEM and STEM techniques.

ANADOLU ÜNİVERSİTESİ

4.5.1. Surface Characterization with Scanning Electron Microscopy

To prove the existence of the surface quantum dots, samples' surfaces were first examined by SE imaging technique. The SEM was operated at an accelerating voltage of 20 kV and the working distance was 8 mm. A SE image taken from one of the samples (YES-21) is shown in Figure 4.43: the image quality is really poor for the purpose and the quantum dots are hardly seen. The surfaces were then investigated with the in-lens detector for better image quality due to the advantages of the in-lens detector mentioned in section 4.2.1. The image taken at accelerating voltage of 20 kV and working distance of 8 mm is presented in Figure 4.44. The formation of the quantum dots are undoubtedly evidenced with this image. Even though it is relatively easier to discern the quantum dots, the image is not good enough for the purpose yet. When the working distance of the in-lens detector was reduced down to nearly 4 mm, QDs were become very clear for the intended characterizations. The images from all of the samples are presented in Figure 4.45.

ANADOLU ÜNİVERSİTESİ

Figure 4.43 Secondary electron image of sample YES-21

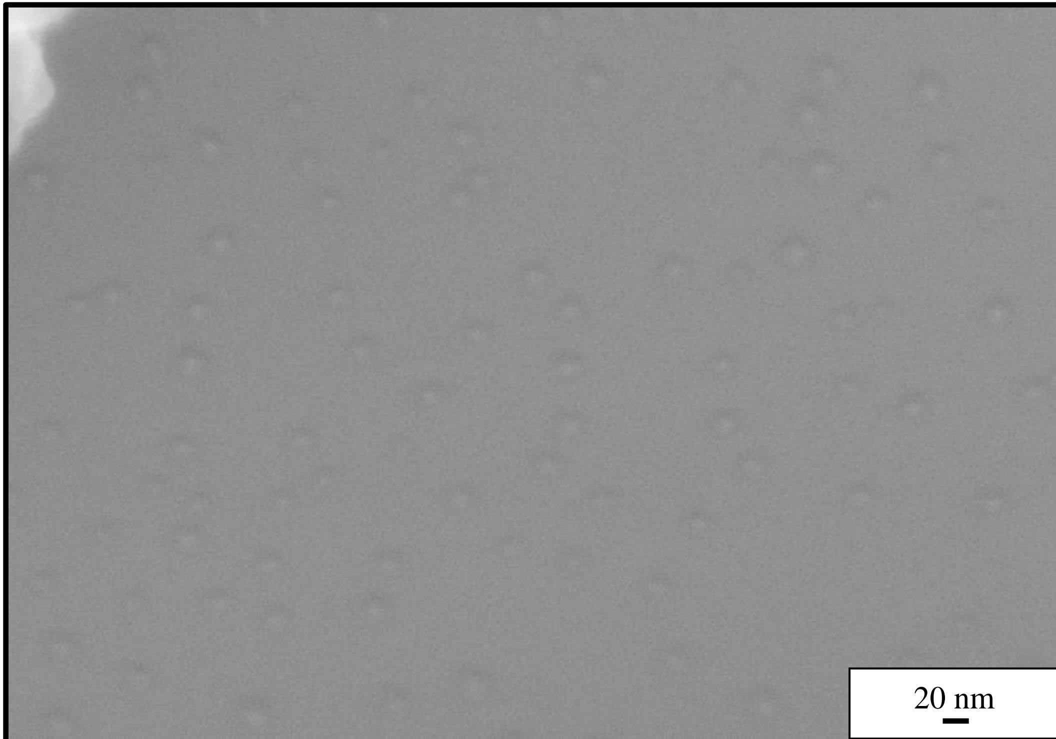

Figure 4.44 Image of sample YES-21 taken with in-lens detector

ANADOLU ÜNİVERSİTESİ

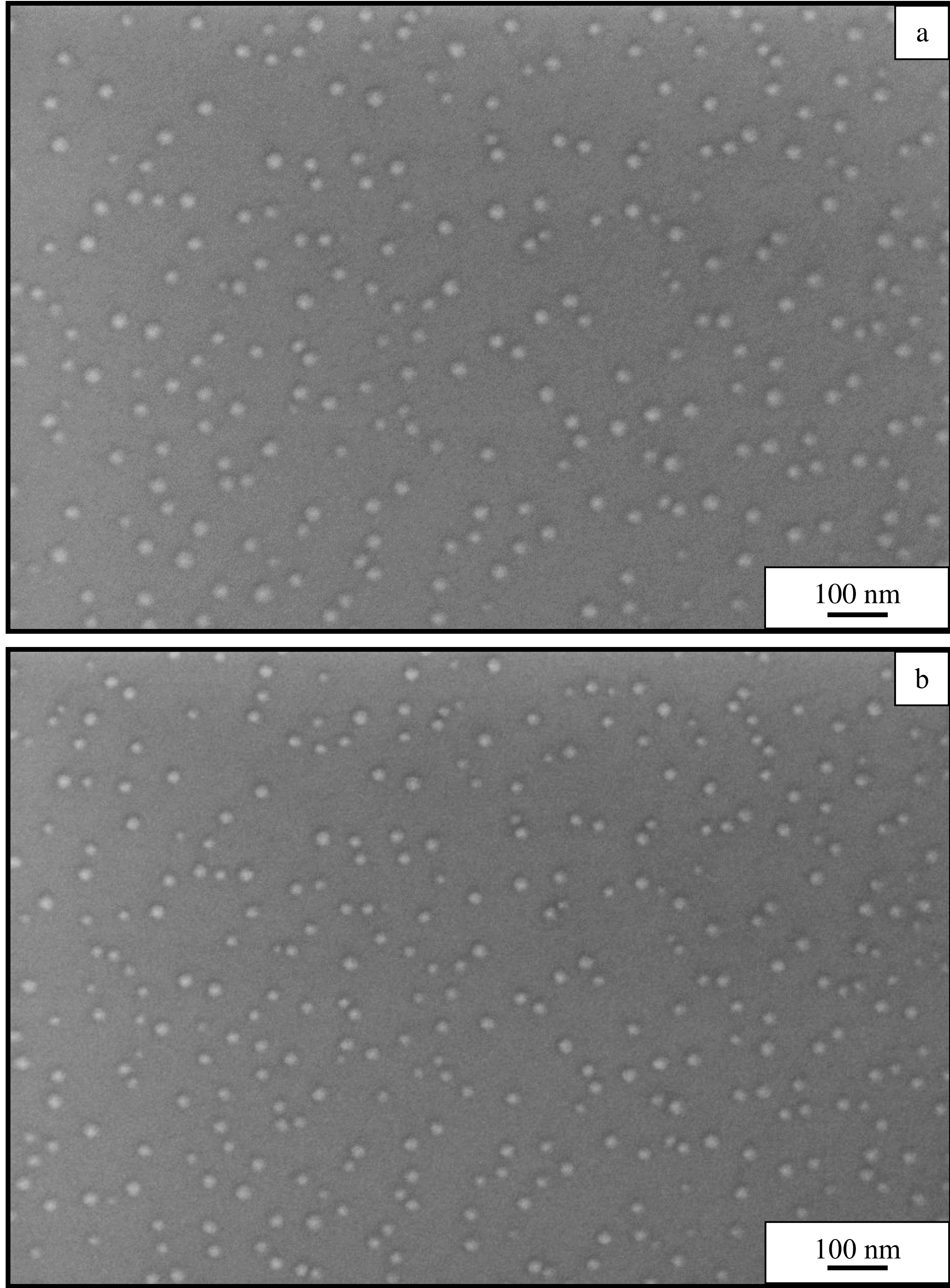

Figure 4.45 SEM images of samples a) YES-20, b) YES-21, c) YES-22, d) YES-23, and e) YES-24 taken with in-lens detector.

ANADOLU ÜNİVERSİTESİ

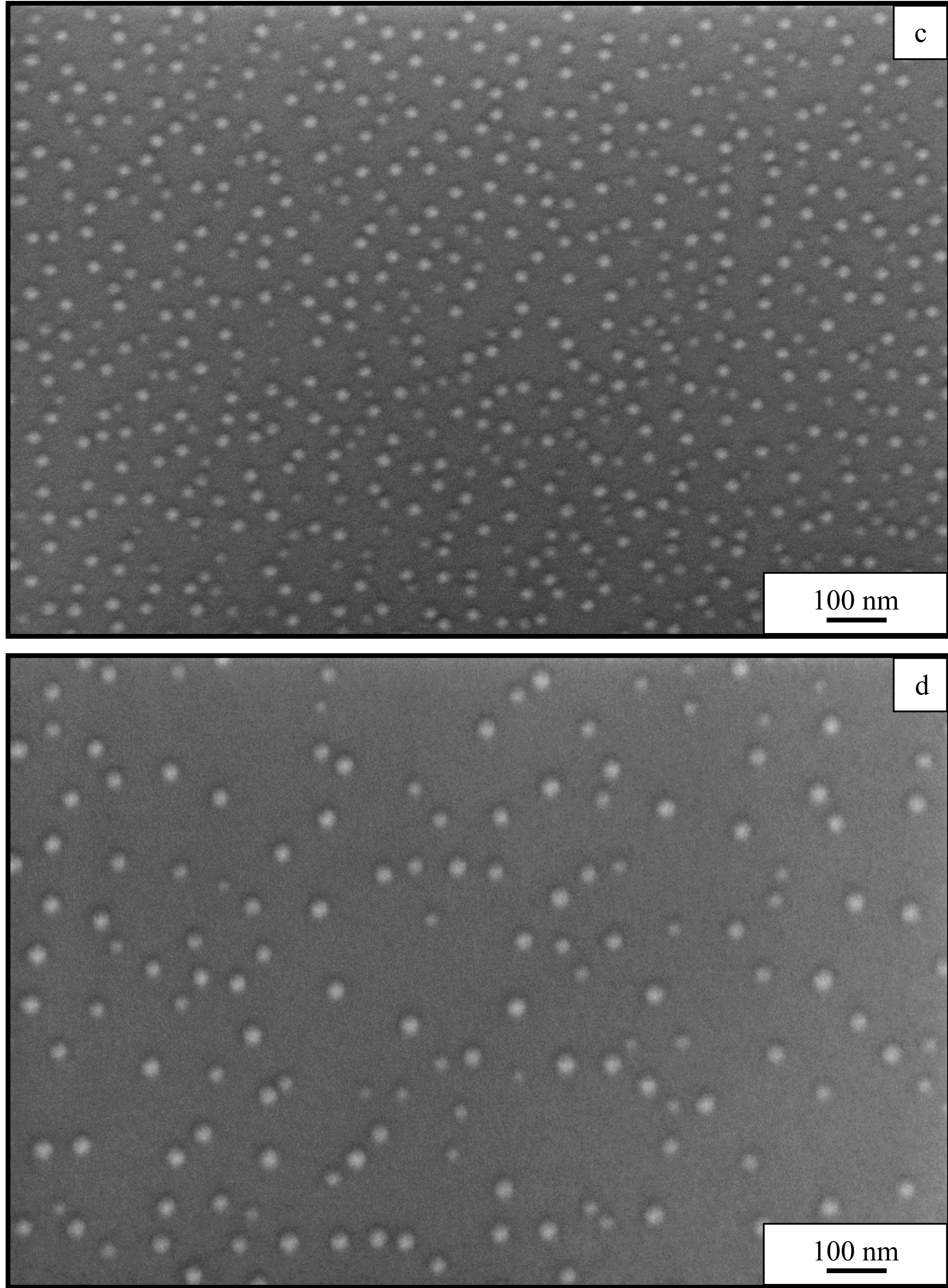

Figure 4.45 (Cont.) SEM images of samples a) YES-20, b) YES-21, c) YES-22, d) YES-23, and e) YES-24 taken with in-lens detector.

ANADOLU ÜNİVERSİTESİ

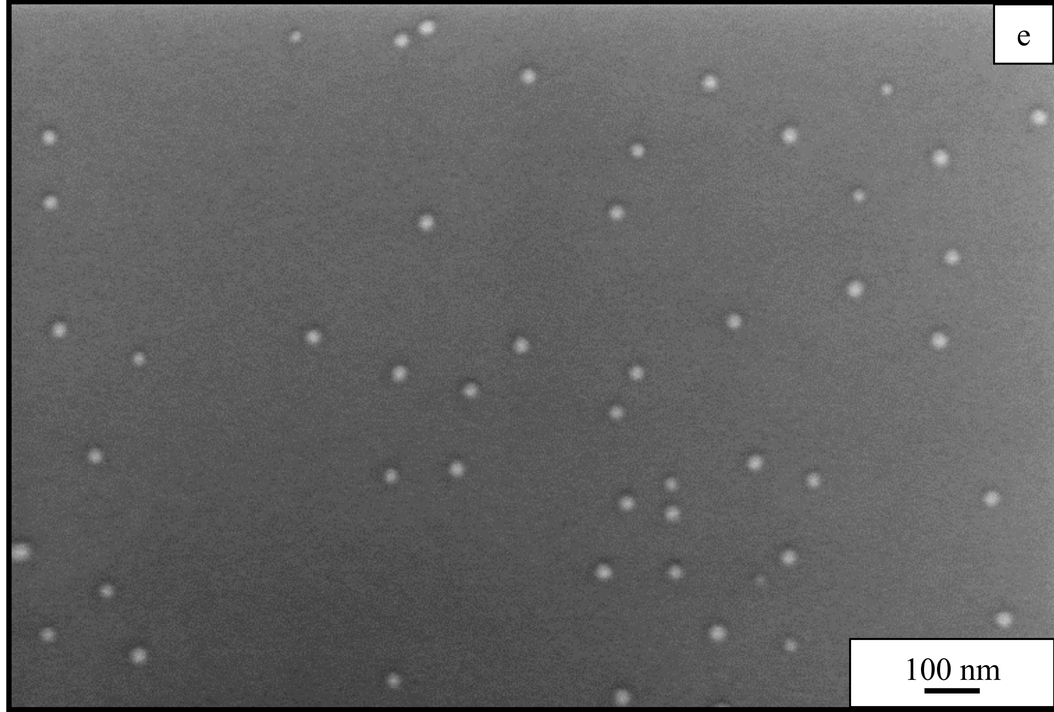

Figure 4.45 (Cont.) SEM images of samples a) YES-20, b) YES-21, c) YES-22, d) YES-23, and e) YES-24 taken with in-lens detector.

Since the sizes of the dots are very small, high magnification values were used during the studies: the images in Figure 4.45a to Figure 4.45d (for samples YES-20, YES-21, YES-22, and YES-23) were taken with 250.000X and the image in Figure 4.45e (for sample YES-24) was taken with 200.000X. From the SEM images, number of QDs per unit area (namely the quantum dot density) is determined for each sample by simply counting the dots for a given area. The obtained values are presented in Table 4.5. The images also revealed that there is a bit of size distribution within each sample. This size distribution also slightly varies among the samples. For the purpose of determining the average QD size, one of the samples (YES-22) was investigated in very high magnification. The image taken by using in-lens detector at very short working distance (3.6 mm) is shown in Figure 4.46. The average base diameter of the QDs is measured as ~20 nm. Consequently, the obtained values of the QD densities and sizes are correlated with the growth conditions and the details can be found elsewhere [70].

ANADOLU ÜNİVERSİTESİ

Table 4.5 Number of QDs per area extracted from the images

Sample	QD Density (dots/cm^2)
YES-20	3.0×10^{10}
YES-21	1.6×10^{10}
YES-22	3.5×10^{10}
YES-23	8.9×10^{9}
YES-24	2.1×10^{9}

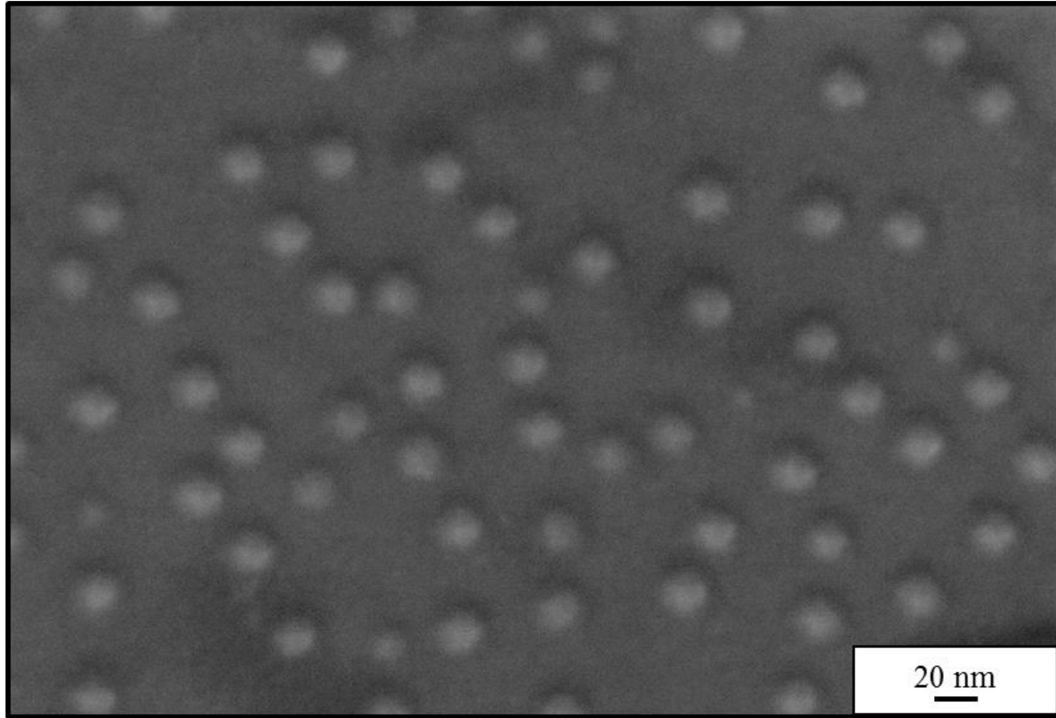

Figure 4.46 SEM image of InAs QDs (YES-22) taken with in-lens detector.

ANADOLU ÜNİVERSİTESİ

4.5.2. TEM-BF and HRTEM Imaging

Both the structural characterizations and the observation of the buried quantum dots were done through the TEM analyses. Thus, a cross-section TEM specimen from sample YES-22 had been prepared to structurally examine the buried QDs. The TEM-BF images are shown in Figure 4.47 and Figure 4.48, and HRTEM images are presented in Figure 4.49 and Figure 4.50.

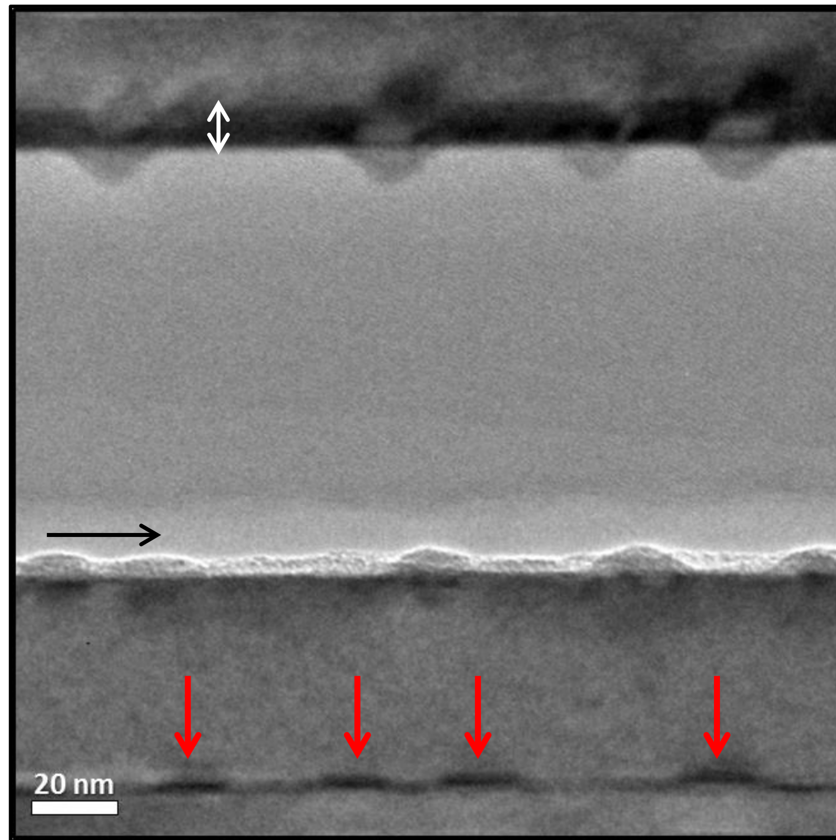

Figure 4.47 TEM-BF image of sample YES-22. The white arrow indicates the out of focus, the black arrow shows the space between the sample and the epoxy, and the red arrows indicate the location of the buried QDs.

ANADOLU ÜNİVERSİTESİ

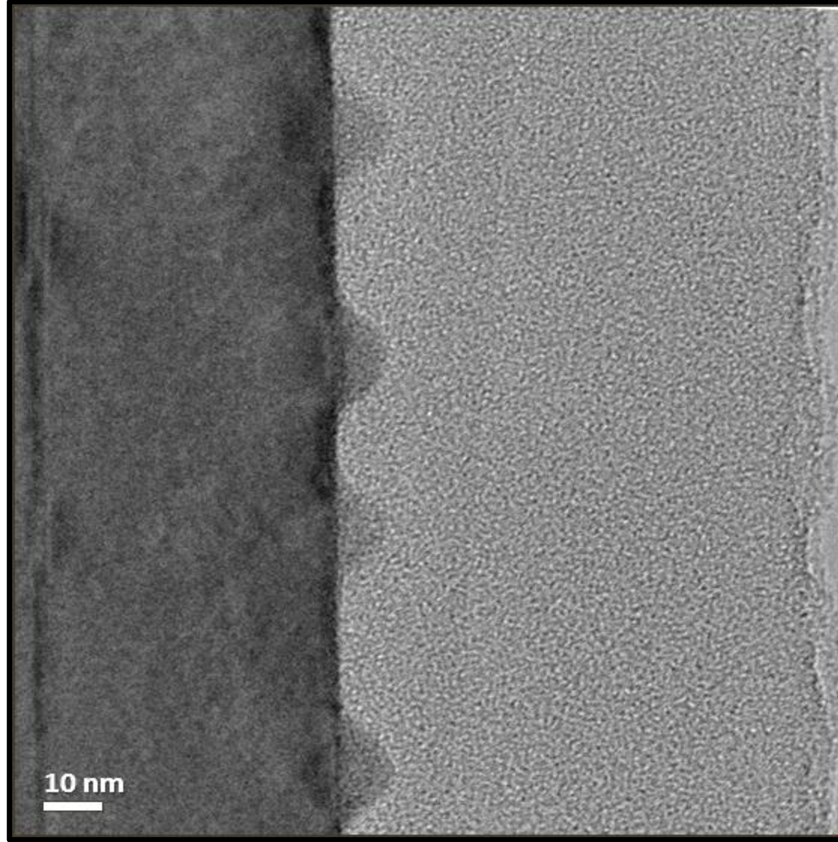

Figure 4.48 TEM-BF image of sample YES-22 showing four uncapped surface QDs.

Both the uncapped surface QDs and the buried layer of QDs in GaAs are seen in TEM-BF images. The buried QDs reveal themselves in the images (see Figure 4.47) as dark contrast due to the strain field around them. The regions that are indicated by white and black arrows on Figure 4.47 are caused by the out of focus of the image and the space between the sample and the epoxy, respectively. Although they contribute to the contrast, it is not possible to verify the exact shape and size of the buried QDs; the surface QDs are relatively more deterministic in this sense. The average diameter and the height of the surface QDs were measured as ~20 nm and ~10 nm, respectively. However, those values are very vague for the buried QDs. The HRTEM images seen in Figure 4.49 and Figure 4.50 provide more detail on both QD layers. The strain field caused by the irregularity of atomic packing has dark contrast and indicated with red arrows (see Figure 4.50). The contrast in the images is created with the contribution of both the phase contrast and the diffraction from unordered atomic planes in the structure.

ANADOLU ÜNİVERSİTESİ

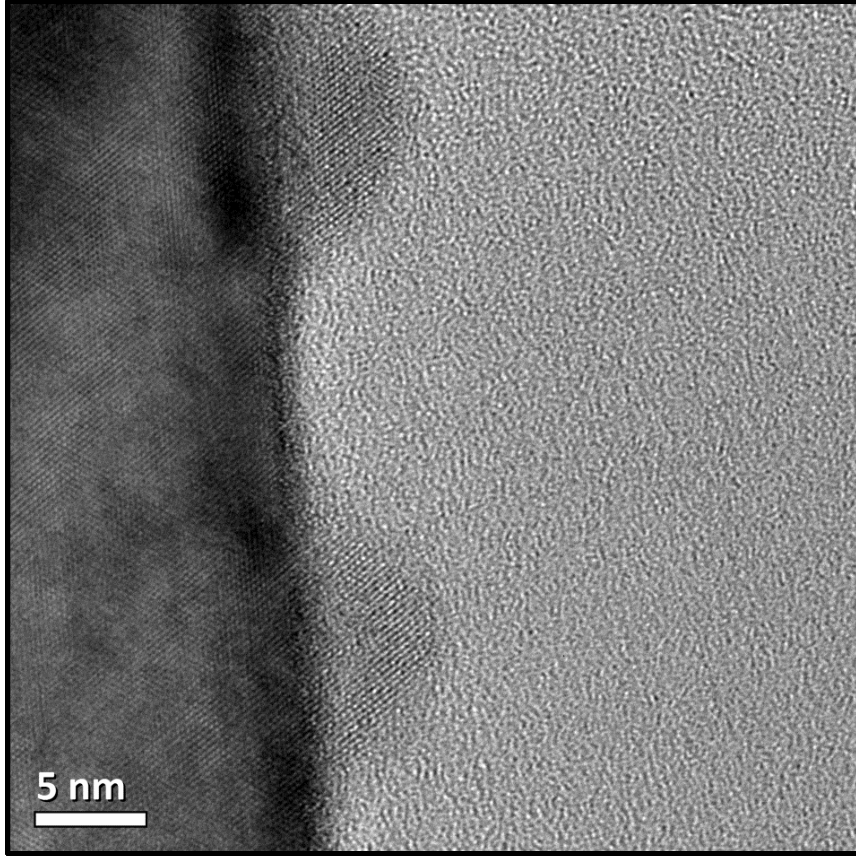

Figure 4.49 Cross sectional HRTEM image shows two uncapped surface InAs QDs (YES-22)

ANADOLU ÜNİVERSİTESİ

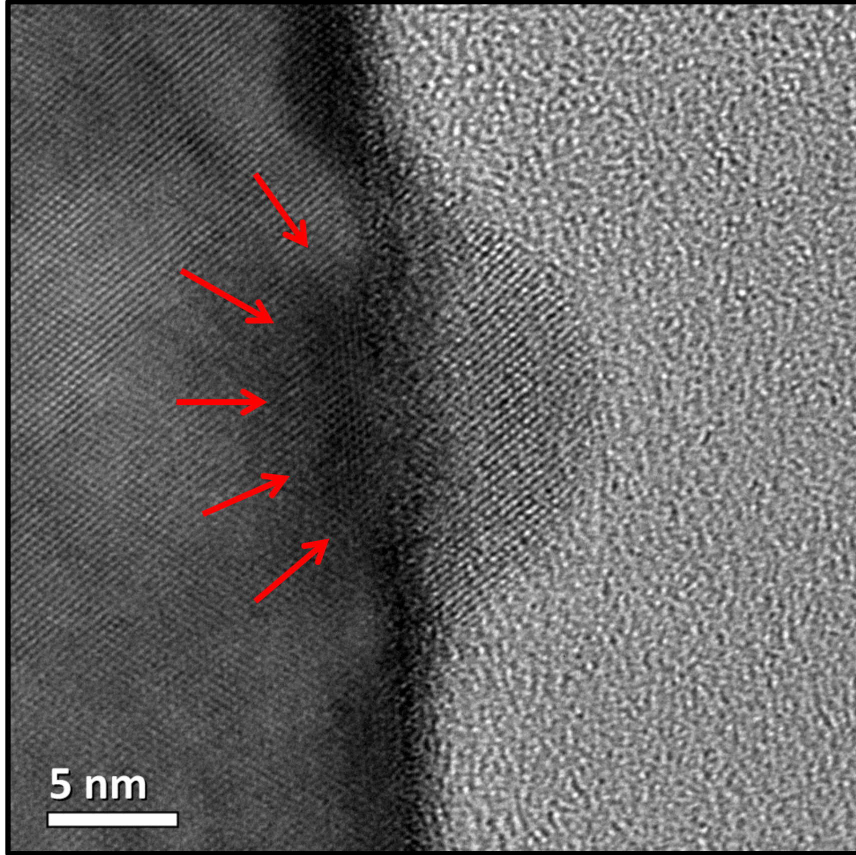

Figure 4.50 Cross sectional HRTEM image of an InAs QD (YES-22). The red arrows indicate the strain field caused by the irregularity of atomic packing.

4.5.3. STEM Imaging

Because of the contrast inadequacy of the previously used imaging techniques (TEM-BF, HRTEM), STEM imaging techniques were used for further examination of the buried QDs. For instance, STEM-BF technique has better contrast but worse resolution in comparison to TEM-BF. Because, the small convergence angle provides strong contrast and the beam size diameter dominates the resolution in STEM [42]. STEM-BF and STEM-ADF images taken from the sample are given in Figure 4.51 and Figure 4.52.

ANADOLU ÜNİVERSİTESİ

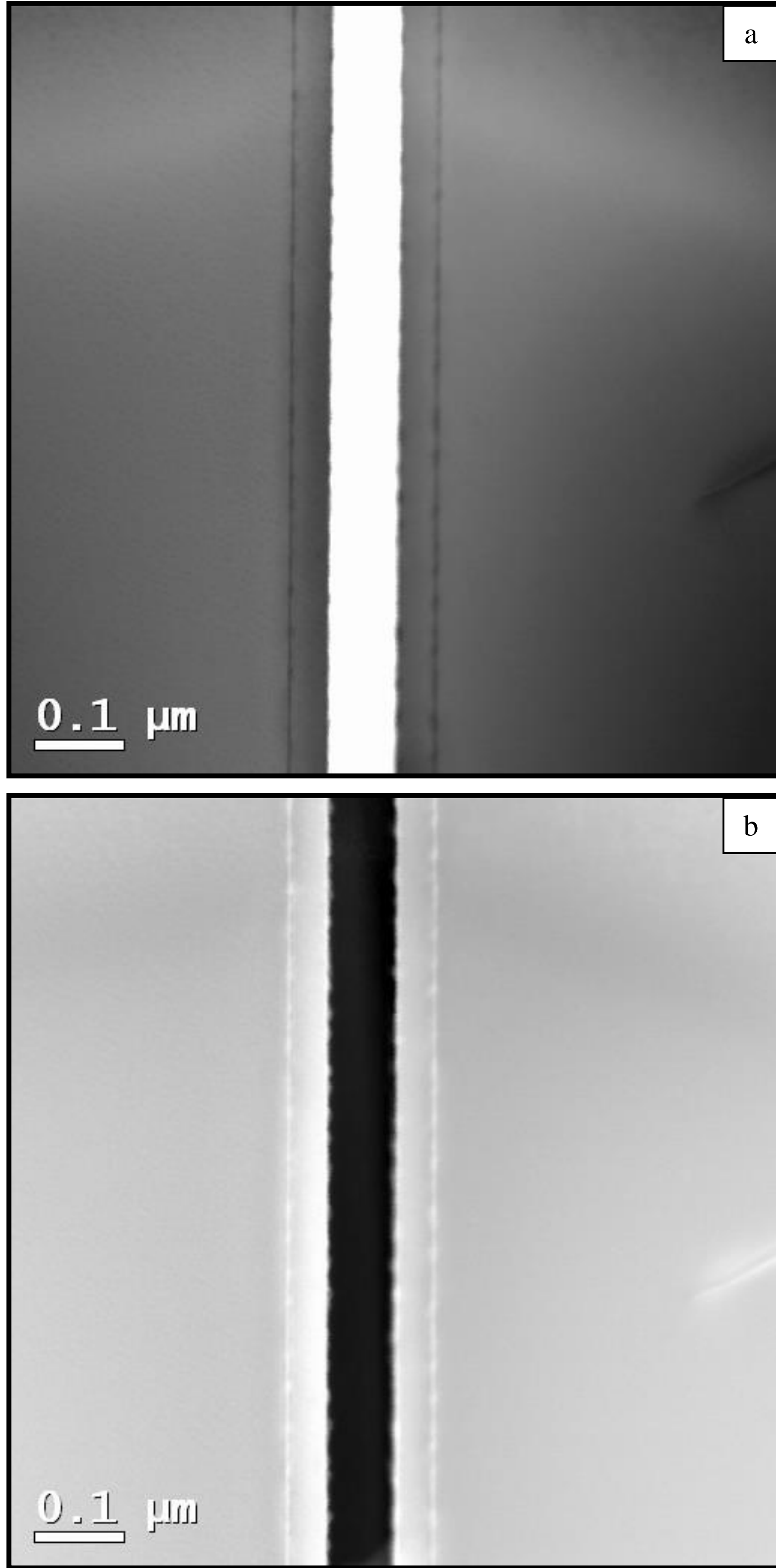

Figure 4.51 a) STEM-BF and b) STEM-ADF images of InAs QDs (YES-22)

ANADOLU ÜNİVERSİTESİ

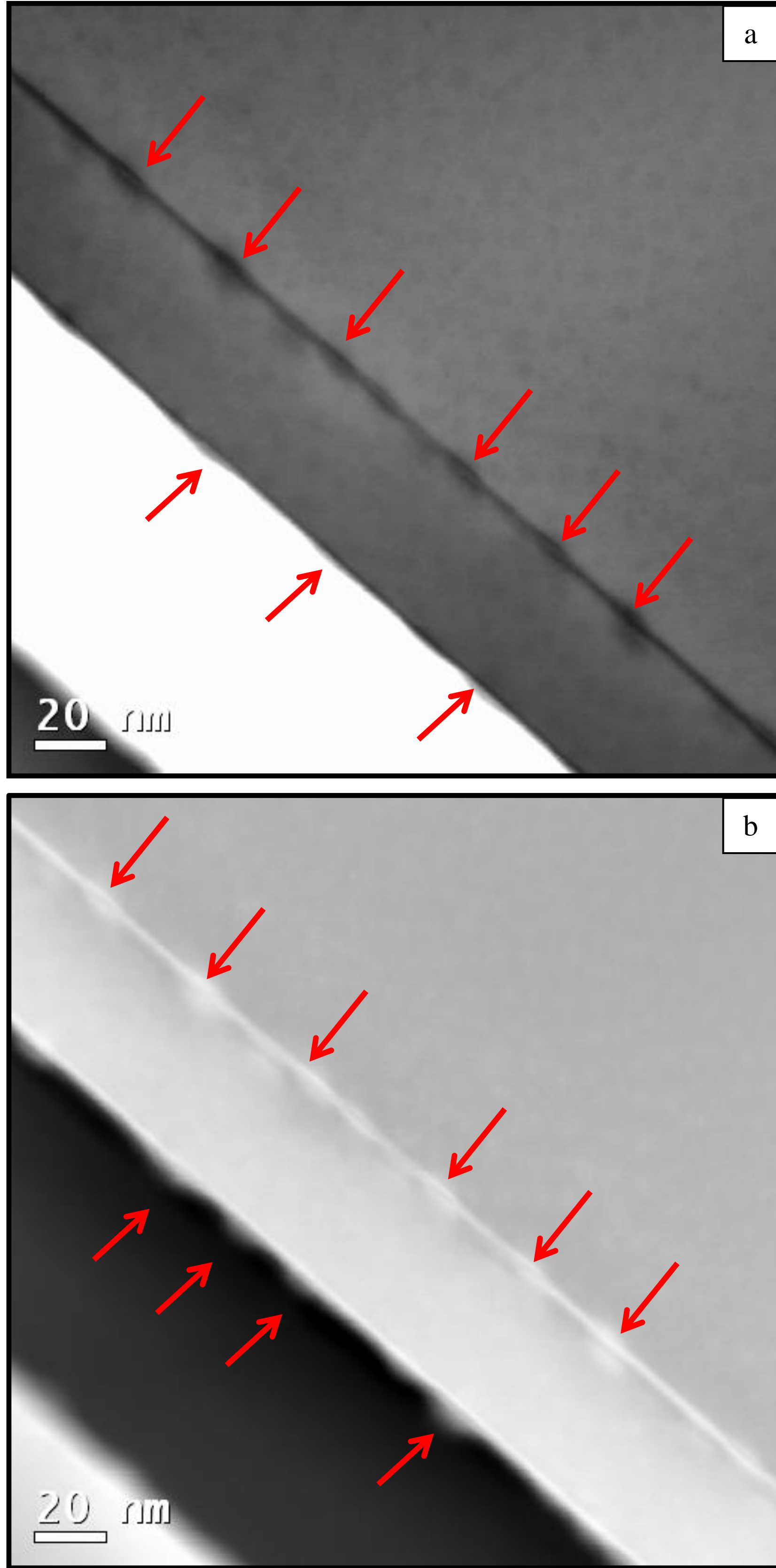

Figure 4.52 a) STEM-BF and b) STEM-ADF images of InAs QDs. The red arrows show the QDs.

ANADOLU ÜNİVERSİTESİ

Figure 4.51 and Figure 4.52 show STEM-BF and STEM-ADF images taken from the sample YES-22. While the resolution is poorer (because the beam size dominates the resolution for thin specimens) in STEM-BF images, the contrast is higher compared to TEM-BF images [42]. Thus, the embedded QDs are pronounced in STEM-BF images. In other respects, in STEM-ADF images the dots were seen more apparently: Bragg diffraction contrast is also effective together with the dominant mass-thickness contrast mechanism. Because of the stress in the QDs, the diffractions from the planes of the stressed structure results in diffraction contrast.

Additionally, STEM images revealed the difference between the embedded QDs and the ones on the surface: size of a buried dot is smaller than that of a surface dot because of a net migration of In atoms away from the InAs QDs during the GaAs capping process [71]. While there is no noteworthy change in the observed lateral dimensions, the measured height is significantly reduced for the embedded QDs. The buried InAs QDs exhibit a lens-shaped cross-section, with a base length and height of ~15 nm and ~5 nm, respectively.

ANADOLU ÜNİVERSİTESİ

5. CONCLUSION

The main aim of this thesis was to investigate the MBE grown nanostructures of III-V group semiconductors by using electron microscopy techniques and to develop an effective sample preparation procedure for reliable analyses. In order to provide a better understanding of the structures and the limitations of the techniques for the studied materials samples have been simultaneously examined with different SEM, TEM and STEM techniques.

A significant amount of time throughout this work has been spent for sample preparation studies for transmission electron microscopy. After many practices an efficient cross-section sample preparation recipe has been established for structures grown on GaSb and GaAs substrates of soft and brittle character. Some of the important points and optimized parameters to prepare the best sample with high success rate can be itemized as follows:

-- Thickness of the sliced pieces should be around 450 μm for lower chance of damaging and for the time efficiency for the consequent steps.

-- Pieces should not be mechanically thinned down to less than ~250 μm before the disc cutting process for better results.

-- Once the sample is less than ~150 μm thick, the lapping films of particle size smaller than 9 μm should be used for polishing.

-- It was concluded that the dimpling process increases the risk of damaging the pieces; therefore, it has been removed from the final recipe and the parameters used in ion milling has been optimized accordingly.

Electron microscopy studies performed during this thesis can roughly be grouped as (i) thickness determination, (ii) surface characterization, and (iii) high resolution structural and compositional/elemental analyses. Major studies and their outcomes accomplished in this thesis can be summarized as below:

The systematically changed InAs and GaSb layer thicknesses in multiple-repeat sample were measured by using SEM imaging techniques from their cross-

ANADOLU ÜNİVERSİTESİ

sections; this provided quantitative feedback to epitaxial growth processes for future growths. Similarly the same imaging techniques were used for surface characterization of GaSb epilayers grown on both GaSb and GaAs substrates. Different types of defects and features were evidenced on the surfaces of the epilayers grown under different conditions. Particularly, EDX analyses proved that for some of the samples there is an Sb condensation layer at the surface with different thicknesses. Investigation of a set of samples revealed that these are related with the growth conditions and can be avoided once the proper actions are taken.

A group of InAs/GaSb type-II SL structures were studied with TEM-BF and HRTEM imaging techniques for structural quality, microstructural consistency and thickness determination of individual layers. Even though the abrupt transition between the layers were observed, the interfaces as one of the most important features of such systems could not be examined in detail because of the technical limitations of the microscope operated. InAs and GaSb layers were also investigated with STEM-HAADF imaging to distinguish the compositionally different consecutive layers. The elemental distributions were then quantified with STEM-EDX line and point analyses. The EFTEM analyses showed that the resolution of the method is not enough for clear differentiation of very thin (~3 nm) layers in our structures.

A sample of GaSb epilayer grown on GaAs substrate with AlSb QD layer as a transition region to reduce the lattice mismatch GaAs and GaSb were characterized by TEM, STEM and SEM techniques. TEM-BF and HRTEM images showed that the distribution and the size of AlSb QDs are uniform. The STEM-HAADF and STEM-EDX techniques were incapable of detecting the AlSb QDs.

InAs/GaAs self-assembled QDs left uncapped on the surface of a GaAs layer were first investigated by SEM to acquire the information about the density and distribution of the dots. Observation of the surface dots was only possible when the in-lens detector is used at very short working distance of 4 mm. Through the TEM-BF and HRTEM both physical dimensions and the structural quality of

ANADOLU ÜNİVERSİTESİ

the dots were examined. Additionally, the contrast superiority of STEM-BF and STEM-ADF images is used to reveal the shape and size differences between the surface dots and buried dots. The surface dots were found to be dome-shaped while the buried ones were more like in lens-shape.

Some of the studies conducted during this thesis serve as complimentary results for several projects targeting different subjects. The projects that are directly related to the studies presented in this thesis are as follows;

-- Characterization of Epitaxially Grown GaSb/InAs Superlattice Structures by Electron Microscopy, Anadolu University Scientific Research Projects with project number BAP-1205F083.

-- Growth and Characterization of GaSb and InAs layers on GaAs Substrate by Molecular Beam Epitaxy, The Scientific and Technological Research Council of Turkey (TÜBİTAK) with project number 111T335.

-- Development of GaSb/InAs Infrared Photodetector Technology (KOFDE), Undersecretariat for Defense Industries (SSM).

-- Growth and Characterization of Self-assembled InAs/GaAs Quantum Dot Structures Used in Infrared Detection, Anadolu University Scientific Research Projects with project number BAP-1205F086.

ANADOLU ÜNİVERSİTESİ

REFERENCES

[1] Blakemore, J.S., *Solid State Physics*, W.B. Sounders Company, Philadelphia, A.B.D., 1969.

[2] Ashcroft, N.W. and Mermin, N.M., "Solid State Physics", Int. Ed., Saunders College Publishing, Philadelphia, A.B.D., 1976.

[3] T. Nishinaga and S. Naritsuka.: "Epitaxial Growth of III-V Compounds" *Crystal Growth Technology*, Edited by K. Bayrappa and T. Ohachi: Berlin, Heidelberg, New York, Springer, 55-92, 2003

[4] Sadao Adachi.: "III-V Ternary and Quaternary Compounds", *Handbook of Electronic and Photonic Materials*, Edited by Safa Kasap and Peter Capper: New York, Springer Science + Business Media; 735-752, 2007.

[5] M. Razeghi, Overview of antimonide based III-V semiconductor epitaxial layers and their applications at the center for quantum devices", *Eur. Phys. J. AP*, **23**, 149-205, 2003.

[6] Razeghi, M., "Technology of Quantum Devices", Springer, 2010.

[7] Ting Z. Y. David, Soibel, A., Höglund, L., Ngyuen, J., Hill, C. J., Khoshakhlagh, A., Gunapala S. D., "Chapter 1- Type-II Superlattice Infrared Detectors", *Semiconductors and Semimetals*, **84**, 1-50, 2011.

[8] Haugan H.J., Szmulowicz F., Brown G.J., Mahalingam K., "Bandgap tuning of InAs/GaSb type-II superlattices for mid-infrared detection", *Journal of Applied Physics*, **96**, 2580, 2004.

[9] Sai-Halasz, G.A., Tsu, R., Esaki, L., "A New Semiconductor Superlattice", *Appl. Phys. Lett.*, **30**, 651, 1977.

[10] Arikan, B., Korkmaz, G., Suyolcu, Y.E., Aslan, B., Serincan, U., "On the structural characterization of InAs/GaSb type-II superlattices: The effect of interfaces for fixed layer thicknesses", *Thin Solid Films*, **548**, 288, 2013.

[11] Wei, Y., Hood, A., Yau, H., Yazdanpanah, V., Razeghi, M., Tidrow, M.Z., Nathan, V., "High-performance type-II InAs/GaSb superlattice photodiodes with cutoff wacelength around 7 μm" *Appl. Phys. Lett.*, **86**, 091109, 2005.

ANADOLU ÜNİVERSİTESİ

[12] R. Rehm, M. Walther, F. Rutz, J. Schmitz, A. Wörl, J.-M. Masur, R. Scheibner, J. Wendler, J. Ziegler, “Dual-Color InAs/GaSb Superlattice Focal-Plane Array Technology”, *J. Electron. Mater.* **40**, 1738, 2011.

[13] Plis, E.A., Krishna, S.S., Gautam, N., Myers, S.,Krishna, S., “Bias Switchable Dual-Band InAs/GaSb Superlattice Detector With pBp Architechure”, *IEEE Photonics*, **3**, 234, 2011.

[14] Plis E., Rodriquez J.B., Krishna S.: “InAs/(In)GaSb Type-II Strain Layer Superlattice Dedectors” *Comprehensive Semiconductor Science and Technology*, Edited by Bhattacharya P., Fornari R., Kamimura H.: UK: Elsevier; 229-264, 2011.

[15] Plis E., Annamalai S., Posani K.T., Krishna S., “Midwave infrared type-II InAs/GaSb superlattice detectors with mixed interfaces”, *Journal of Applied Physics*, **100**, 014510, 2006.

[16] Rodriquez J.B., Christol P., Cerutti L., Chevrier F., Joullie A., “MBE growth and characterization of type-II InAs/GaSb superlattices for mid-infrared detection”, *Journal of Crystal Growth*, **274**, 6, 2005.

[17] Nguyen, B.M., Hoffman, D., Huang, E. K., Delaunay, P.-Y., Razeghi, M., “High performance Antimony-based Type-II Superlattice Photodiodes on GaAs Substrate”, *Proc. of SPIE*, **7298**, 72981T-13-72981T-1, 2009.

[18] Haugan H.J., Grazulis L., Brown G.J., Mahalingam K., Tomich D.H., “Exploring optimum growth for high quality InAs/GaSb type-II superlattices”, *Journal of Crystal Growth*, **261**, 471-478, 2004.

[19] Wei Y, and Razeghi M, “Modeling of type-II InAs/GaSb superlattices using an empirical tight-binding method and interface engineering”, *Physical Review B*, **69,** 085316, 2004.

[20] Walther, M., Rehm, R., Schmitz, J., Rutz, F., Fleissner, J., Ziegler, J., “Antimony-based Superlattices for High-performance Infrared Imagers”, *Proc. of SPIE*, **6940**, 69400A-8-69400A-1, 2008.

[21] Guo J., Sun W-G., Peng Z-Y., Zhou Z-Q., Xu Y-Q., Niu Z-C., “Interfaces in InAs/GaSb Superlattices Grown by Molecular Beam Epitaxy”, *Chinese Physics Letters*, **26**, 047802, 2009.

ANADOLU ÜNİVERSİTESİ

[22] Rehm R., Walther M., Schmitz J., Fleiβner J., Fuchs F., Ziegler J., Cabanski W., "InAs/GaSb superlattice focal plane arrays for high-resolution thermal imaging", *Proc SPIE*, **5957**, 595707-1-8, 2005.

[23] Chen, Z.B., Lei, W., Chen, B., Wang, Y.B., Liao, X.Z., Tan, H.H., Zou, J., Ringer, S.P., Jagadish, C., "Preferential nucleation and growth of InAs/GaAs (001) quantum dots on defected sites by droplet epitaxy", Scripta Materialia, 69, 638-641, 2013.

[24] Ajit V. Barve and Sanjay Krishna, "Chapter 3- Quantum Dot Infrared Detectors", *Semiconductors and Semimetals*, **84**, 153-194, 2011.

[25] Plis, E., Klein, B., Myers, S., Gautam, N., Rotter, T.J., Dawson, R.L., Krishna, S., Lee, S.J., Kim, Y.H., "Type-II InAs/GaSb strained layer superlattices grown on GaSb (111)B substrate", *J. Vac. Sci. Technol. B*, **31**, 03C123, 2013.

[26] Quan, M., Wang, L., Wang, K., Guo, F., Han, X., Zhao, L., "Interfacial structure of InAs/$Ga_{1-x}In_xSb$ superlattices", *Applied Physics Letters*, **95**, 012111, 2009.

[27] Hill, C.J., Soibel, A., Keo, S.A., Mumolo, J.M., Ting, D.Z., Gunapala, S.D., "Demonstration of large format mid-wavelength infrared focal plane arrays based on superlattice and BIRD detector structures", *Infrared Physics & Technology*, **52**, 348–352, 2009.

[28] Tournie E. and Trampert A, "MBE growth and interface formation of compound semiconductor heterostructures for optoelectronics", *physica status solidi (b),* **244**, 2683-2696, 2007.

[29] Satpati, B., Rodriguez, J.B., Trampert, A., Tournie, E., Joullie, A., Christol, P., Interface analysis of InAs/GaSb superlattice grown by MBE, *Journal of Crystal Growth*, **301-302**, 889-892, 2007.

[30] BROWN, G. J., Houston, S., Szmulowicz, F., Mahalingam, K., Haugan, H., Wei, Y., Gin, A., Razeghi, M., "Type-II Superlattice Photodiodes: an Alternative for VLWIR Detection", *The Society of Photo-Optical Instrumentation Engineers*, **507**, 191-198, 2003.

ANADOLU ÜNİVERSİTESİ

[31] Gong, Q., Li, J., Li, S.G., Li, A.Z., Lin, C., "Growth of InAs/GaSb Type-II Superlattices by Gas-source Molecular Beam Epitaxy" , *Journal of Crystal Growth*, **311**, 1703-1706, 2009.

[32] Ashuach, Y., Kauffmann, Y., Lakin, E., Zolotoyabko, E., Grossman, S., Klin, O., Weiss, E., "Investigation of InAs/GaSb-based superlattices by diffraction methods", *Nuclear Instruments and Methods in Physics Research B*, **268**, 231-235, 2010.

[33] Twigg, M. E., Bennett, B. R., Thibado, P. M., Shanabrook, B. V., Whitman, L. J., "Interfacial disorder in InAs/GaSb superlattices", *Philosophical Magazine A*, **7**, 7-30, 1998.

[34] Khoshakhlagh, A., Plis, E., Myers, S., Sharma, Y.D., Dawson, L.R., Krishna, S., "Optimization of InAs/GaSb type-II superlattice interfaces for long-wave (~8 µm) infrared detection", *Journal of Crystal Growth,* **311**, 1901-1904, 2009.

[35] Khoshakhlagh, A., Myers, S., Kim, H., Plis, E., Gautam, N., Lee, S.J., Noh, S.K., Dawson, L.R., Krishna, S., "Long-Wave InAs/GaSb Superlattice Detectors Based on nBn and Pin Designs", IEEE *Journal of Quantum Electronics,* **46**, 959-964, 2010.

[36] Ryou J-H., Huang, Y., Dupuis R.D., Zuo, D., Kesler, B., Chuang, S-L., Hu, H., Kim, K-H., Lu, Y.T., Hsieh, K.C., Zuo, J-M., "Strain-balanced InAs/GaSb type-II superlattice structures and photodiodes grown on InAs substrates by metal organic chemical vapor deposition" *Applied Physics Letters*, **99**, 011109, 2011.

[37] Mahalingam, K., Haugan, H. J., Brown, G. J., Eyink, K. G., Jiang, B., "Quantitative strain analysis of interfaces in InAs/GaSb Superlattices by aberration-corrected HAADF-STEM", *Proc. Of SPIE*, **8268**, 826831-1, 2012.

[38] Ashuach, Y., Kauffmann, Y., Saguy, C., Grossman, S., Klin, O., Weiss, E., Zolotoyabko, E., "Quantification of atomic intermixing in short-period InAs/GaSb superlattices for infrared photodetectors", *Journal of Applied Physics*, **113**, 184305, 2013.

ANADOLU ÜNİVERSİTESİ

[39] Jung, H., Pinsukanjana, P., Dutta, M., Choi, K.-K., Tidrow, M.Z., "Structural and optical characterization of infrared hot electron transistor", *Journal of Applied Physics,* **108**, 034515, 2010.

[40] Siverns, P.D., Malik, S., Childs, D., Roberts, C., Murray, R., Joyce, B.A., Davock, H., "Scanning transmission-electron microscopy study of InAs/GaAs quantum dots", *Physical Review B*, **58**, R10 127, 1998.

[41] Zhi, D., Davock, H., Murray, R., Roberts, C., Jones, T.S., Pashley, D.W., Goodhew, P.J., Joyce, B.A., "Quantitative compositional analysis of InAs/GaAs quantum dots by scanning transmission electron microscopy", *Journal of Applied Physics,* **89**, 2079-2083, 2001.

[42] Williams, D.B. and Carter, B.C., *Transmission Electron Microscopy: A Textbook for Materials Science*, Springer, 2009.

[43] E.C. Larkins, J.S. Harris Jr., "Molecular Beam Epitaxy: Applications to Key Materials", Noyes Publications, Parkridge, New Jersey, pp. 176-181, 1995.

[44] Liu Amy, W.K., Lubyshev, D., Qiu, Y., Fastenau J.M., Koerperik, E.J., Olesberg, J.T., Norton, D.Jr., "Manufacturable MBE Growth Process for Sb-based Photodetector Materials on Large Diameter Substrates", *Proc. Of SPIE*, **8268**, 82681A-1 – 82681A-10, 2012.

[45] Koerperick, E.J., Murray L.M., Norton, D.T., Boggess, T.F., Prineas, J.P., "Optimization of MBE-grown GaSb buffer layers and surface effects of antimony stabilization flux", *Journal of Crystal Growth*, **312**, 185-191, 2010.

[46] L. Esaki and R. Tsu "Superlattice and Negative Differential Conductivity in Semiconductors", *IBM J. Res. Develop.*, **14**:61-5, 1970.

[47] Kroemer, H., "The 6.1 Å family (InAs,GaSb,AlSb) and its heterostructures: a selective review", *Physica E*, **20**, 196-203, 2003.

[48] Smith, D.L., and Mailhiot, C., "Proposal for strained type II superlattice infrared detectors," *Journal of Applied Physics,* **62**, 2545-2548, 1987.

[49] Grein, C. H., Young, P. M., and Ehrenreich, H., "Minority carrier lifetimes in ideal InGaSb/InAs superlattices", *Appl. Phys. Lett.* **61** (24), 2905, 1992.

[50] Ariyawansa G., Duran J.M., Grupen M., Scheihing J.E., Nelson T.R., Eismann M.T, "Multispectral Imaging with Type II Superlattice Detectors", *Proc of SPIE* , **8353**, 83530E-1-14, 2012.

ANADOLU ÜNİVERSİTESİ

[51] Li, L.L., Xu, W., Zhang, J., Shi, Y.L., "Midinfrared absorption by InAs/GaSb type-II superlattices", *Journal of Applied Physics*, **105**, 013115, 2012.

[52] ROGALSKI, A., "Competitive Technologies and Third Generation Infrared Photon Detectors", *Opto-Electron. Rev.*, **14**, 98-84, 2006.

[53] Razeghi, M., "Type-II InAs/GaSb superlattices for high-performance photodiodes and FPAs", *Proc. of SPIE*, **5246**, 501-511, 2003.

[54] Adrienne Diarra Stiff-Roberts, "Design, fabrication, and characterization of In(Ga,Al)As/(Ga,Al)As quantum dot infrared photodetectors for high-temperature operation", Philosophy of Doctorate Thesis, The University of Michigan, 2004.

[55] Tetsuya Asano, "Growth Control And Design Principles Of Self-Assembled Quantum Dot Multiple Layer Structures For Photodetector Applications", Philosophy of Doctorate Thesis, Faculty Of The USC Graduate School, University Of Southern California, 2010.

[56] Aslan, B., Liu, H.C., Korkusinski, M., Cheng, S.-J., Hawrylak, P., "Response spectra from mid- to far-infrared, polarization behaviors, and effects of electron numbers in quantum-dot photodetectors", *Appl. Phys. Lett.*, **82**, 630, 2003.

[57] Fafard, S., Wasilewski, Z.R., Ni Allen, C., Picard, D., Spanner, M., McCaffrey, J.P., Piva, P.G., "Manipulating the energy levels of semiconductor quantum dots", *Physical Review B*, **59,** 15368-15373, 1999.

[58] Hawrylak, P., Fafard, S., Wasilewski, Z.R., "Engineering Quantum States in Self-Assembled Quantum Dots for Quantum Information Processing", *Condensed Matter News*, **7**, 16, 1999.

[59] Jacak, L., Hawrylak, P., Wójs A., *Quantum Dots*, Springer-Verlag, Berlin, 1998.

[60] Ryzhii, V., "The theory of quantum-dot infrared phototransistors", *Semiconductor Science and Technology*, **11**, 759-765, 1996.

[61] Ayache, J., Beaunier, L., Boumendil, J., Ehret, G., Laub, D., *Sample preparation handbook for transmission electron microscopy,* Springer, New York, 2010.

ANADOLU ÜNİVERSİTESİ

[62] Fultz, B. and Howe, J. M., *Transmission Electron Microscopy and Diffractometry of Materials*, Springer, Berlin, Heidelberg, New York, 2008.

[63] Karakulak, T., “Characterization of GaAs/AlGaAs Quantum Wells with TEM (Transmission Electron Microscopy)”, Master of Science Thesis, Anadolu University, Graduate School of Science, Eskişehir, 2010.

[64] Leng, Y., “Materials Characterization: Introduction to Microscopic and Spectroscopic Methods”, Wiley, 2008.

[65] Kaya, P., “Characterization of Boron Carbide – Aluminium Composites With Transmission Electron Microscopy Techniques”, Master of Science Thesis, Anadolu University, Graduate School of Science, Eskişehir, 2010.

[66] Joseph Goldstein, *Scanning Electron Microscopy and X-Ray Microanalysis*, New York, Springer Science + Business Media, 2003.

[67] Şahin, S., “GaSb Alttaş Üzerine Kaliteli GaSb Epi-Katmanların Büyütülmesi ve Karakterizasyonu”, Master of Science Thesis, Anadolu University, Graduate School of Science, Eskişehir, 2014.

[68] Goodhew, P.J., Humphreys J., Beanland, R., *Electron Microscopy and Analysis*, Taylor &Francis, London and New York, 2001.

[69] De Laeter, J.R., Böhlke, J.K., De Bievre, P., Hidaka, H., Pesiser, H.S., Rosman, K.J.R., Taylor, P.D.P., “Atomic Weights of the Elements: Review 2000”, *Pure Appl. Chem.*, **75** (6), 683-800, 2003.

[70] Ozdemir, S., “Kızılötesi algılamada kullanılan kendiliğinden oluşan InAs/GaAs kuantum nokta yapıların üretimi ve karakterizasyonu”, Master of Science Thesis, Anadolu University, Graduate School of Science, Eskişehir, 2014.

[71] Songmuang, R., Kiravittaya, S., Schmidt, O.G., “Shape evolution of InAs quantum dots during overgrowth”, *Journal of Crystal Growth*, **249**, 416-421, 2003.

ANADOLU ÜNİVERSİTESİ